MATERIALS CHEMISTRY
FRONTIERS

REVIEW

View Article Online
View Journal | View Issue

Cite this: *Mater. Chem. Front.*, 2023, **7**, 1520

Progress of layered double hydroxide-based materials for supercapacitors

Xue Li,[a] Jianning Ren,[a] Deepak Sridhar,[b] Ben Bin Xu,[c] Hassan Algadi,[de] Zeinhom M. El-Bahy,[f] Yong Ma,*[a] Tingxi Li*[a] and Zhanhu Guo*[g]

Nowadays, supercapacitors are receiving widespread attention because of their large specific capacitance, excellent cycle life, high power density and energy density, and wide operating temperature range. Electrode materials as an important component of supercapacitors directly determine their electrochemical performances. Layered double hydroxides (LDHs) are emerging in the field of electrode materials because of their unique 2D layer morphology, simple preparation method, large specific surface area and high theoretical specific capacitance. In this paper, the methods for the preparation of LDHs in recent years are reviewed, while different methods resulting in different properties are presented. In addition, some recent methods for the modification of LDHs are demonstrated, from content composition to structural changes giving rise to different properties. Furthermore, various types of LDHs used for supercapacitors are presented, their electrochemical performances are displayed, and their energy storage mechanisms are meanwhile illuminated in detail. This article aims to elucidate the usage of LDHs for supercapacitors, as well as hopes to provide a reference for further research based on these promising materials.

Received 23rd December 2022,
Accepted 19th January 2023

DOI: 10.1039/d2qm01346k

rsc.li/frontiers-materials

1 Introduction

With the development of society, the use of non-renewable fossil fuels such as coal, oil and natural gas is increasing, leading to more and more serious environmental pollution.[1] The development of new energy can effectively solve this problem.[2] Therefore, scientists have devoted themselves to the field of new energy, which is also a research hotspot today.

[a] *School of Material Science and Engineering, Shandong University of Science and Technology, Qingdao 266590, China. E-mail: mayong@sdust.edu.cn, litx@sdust.edu.cn*
[b] *Zentek Ltd., 24 Corporate Crt, Guelph, Ontario, N1G 5G5, Canada*
[c] *Mechanical and Construction Engineering, Faculty of Engineering and Environment, Northumbria University, Newcastle Upon Tyne, NE1 8ST, UK*
[d] *Department of Electrical Engineering, Faculty of Engineering, Najran University, Najran, 11001, Saudi Arabia*
[e] *College of Materials Science and Engineering, Taiyuan University of Science and Technology, Taiyuan, 030024, China*
[f] *Department of Chemistry, Faculty of Science, Al-Azhar University, Nasr City 11884, Cairo, Egypt*
[g] *Integrated Composites Laboratory (ICL), Mechanical and Construction Engineering, Faculty of Engineering and Environment, Northumbria University, Newcastle Upon Tyne, NE1 8ST, UK. E-mail: nanomaterials2000@gmail.com, zhanhu.guo@northumbria.ac.uk*

Xue Li

Xue Li is pursuing a master's degree at the Shandong University of Science and Technology, majoring in Materials and Chemical Engineering.

Jianning Ren

Jianning Ren is pursuing a bachelor's degree at the Shandong University of Science and Technology, majoring in Polymer Materials and Engineering.

Green renewable energy, mainly including solar energy,[3] tidal energy,[4] wind energy,[5,6] hydrogen energy,[7,8] *etc.*, has the advantages of being sustainable, renewable[9] and easy to obtain. It has shown broad prospects in replacing one-time energy and has been developed rapidly.[10–12] However, these energy sources are unstable and have contingency and other shortcomings that limit their large-scale practical applications. For example, solar energy cannot work at night, and wind energy is affected by wind speed and is intermittent. Therefore, in the search for clean, efficient and renewable energy sources,[13] the development of energy conversion and storage must also keep in pace. The need to provide high-capacity and portable power supplies[14–16] for various technological products and equipment has attracted widespread attention, and for the above reasons, supercapacitors have emerged as the times require.[17]

So far, supercapacitors have been developed for more than forty years since their birth, but the history of development in China is only about twenty years.[18] At the beginning, supercapacitors were only applied to small devices like tape recorders and water heaters,[19,20] but with the development of technology, supercapacitors were applied to large devices such as tanks and electric starting systems of cars,[21] and their role has been increasingly highlighted. It can be predicted that supercapacitors have great development and application potential in the future development of society,[22–25] therefore, the current research on supercapacitors attracts researchers in various fields.[26–28] Supercapacitors, as a type of energy storage device between traditional capacitors and rechargeable batteries, have the characteristics of fast charging and discharging of a capacitor and energy storage of a battery at the same time.[29,30] Because of non-pollution to the environment, long cycle life,[31,32] high power density[33] and high safety,[34–36] they have received more and more attention from scientific researchers. At present, people are optimistic about supercapacitors and expect that they can provide services for more aspects of human life in the future.[37–39] A supercapacitor is mainly composed of several parts including a current collector, electrode, electrolyte and diaphragm, where the diaphragm plays a role in separating the two electrodes, preventing a short circuit between the electrodes, and allowing ions to pass through.[40–43] Electrolytes are homogeneous mixtures of acids, alkaline or salts with specific solvents and can be mainly classified as liquid electrolytes and solid electrolytes. Among them, solid electrolytes can be divided into all-solid electrolytes and quasi-solid electrolytes.[44,45] The latter, also called gel-polyelectrolyte, consists of a polymer network dissolved in a solvent containing active ions. It has both high transport properties similar to liquid electrolytes and mechanical stability like solid electrolytes, which is essential for enhancing the flexibility, stretchability and temperature resistance of supercapacitors. During charging and discharging, the ions migrating at the interface originate from the electrolyte.[46,47] Jin *et al.* obtained polyaniline by *in situ* growth on an organic hydrogel polymer electrolyte and acquired a low-temperature resistant, externally stretched supercapacitor with excellent rate performance and cycling performance at −30 °C.[48] In addition, they developed an aqueous phase freeze-proof and heat-resistant symmetric micro-supercapacitor with a 2.3 V voltage window, using aqueous polyacrylamide polyelectrolytes and carbon nanotube electrodes, which shows good cycling stability in both high and low temperature environments.[49] Not coincidentally, Song *et al.* developed high-performance carbon nanotube–MnO_2 microelectrodes and excellent temperature-resistant aqueous

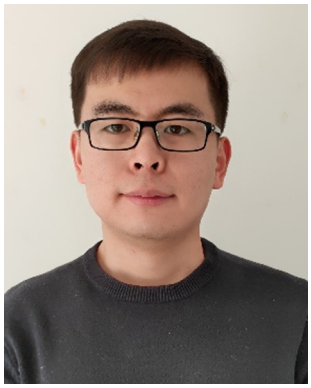

Yong Ma

Yong Ma received his PhD from Northwestern Polytechnical University in 2017 and is currently an academic associate professor at the Shandong University of Science and Technology in Qingdao, China.

Tingxi Li

Tingxi Li received his PhD from Yamagata University in 2002 and is currently a professor at the Shandong University of Science and Technology in Qingdao, China.

Zhanhu Guo

Zhanhu Guo is a Professor in Mechanical & Construction Engineering at Northumbria University. Prof. Guo earned his PhD degree in Chemical Engineering from Louisiana State University in 2005. He received his three-year postdoctoral training in Mechanical and Aerospace Engineering at the University of California Los Angeles. His current research interests are in the areas of optoelectronic, electric, and magnetic materials for solar cells, catalysis, sensing, electronics, environmental remediation and education.

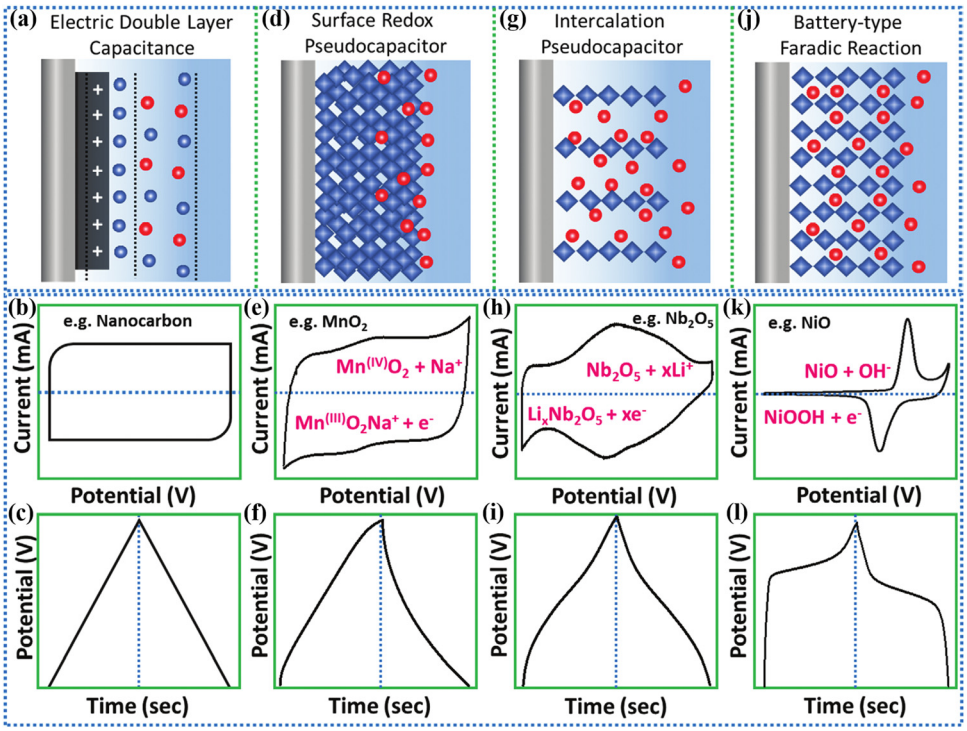

Fig. 1 Schematic diagram of the storage mechanism and the corresponding electrochemical characteristics of several capacitors (representative shapes of CV and GCD curves): (a–c) electrical double layer capacitance, (d–f) surface redox pseudocapacitance, (g–i) intercalated pseudocapacitance, and (j–l) battery-type. Adapted with permission from ref. 71 Copyright 2020, Wiley-VCH GmbH.

polyacrylamide polyelectrolytes. The device reached a voltage window of 2 V at temperatures ranging from −15 °C to 100 °C and had good cycling stability.[50]

Due to the difference in the energy storage mechanism, supercapacitors can be divided into double layer supercapacitors,[51,52] Faraday pseudo supercapacitors and hybrid supercapacitors.[53,54] Fig. 1 shows the schematic diagram of the storage mechanism and the corresponding electrochemical characteristics of several capacitors. An electric double layer capacitor uses an electric double layer between the electrolyte and the electrode to store the charges.[55] In the working process, no charge transfer occurs between the electrode and the electrolyte.[56] Storing charges is a physical adsorption process without a redox reaction. Carbon materials mainly use this mechanism to store charge.[57] Faraday pseudo supercapacitors are electrochemically active substances that undergo rapid and reversible chemical adsorption or desorption on electrodes and electrochemical redox reactions for charge storage.[58,59] The transfer of electrons in the energy storage process causes a change in the valence state of an element in the electrode material,[60] which is commonly used in conducting polymers,[61–63] metal oxides,[64–66] *etc.* Hybrid supercapacitors generally exhibit both mechanisms,[67,68] but the proportion of double layer capacitance and Faraday pseudo capacitance in supercapacitors is different.[69] Hybrid supercapacitors can be divided into asymmetric supercapacitors and symmetric supercapacitors. The two electrodes of the asymmetric supercapacitor are different materials, which can make full use of the different voltage windows to maximize the operating voltage of the whole device to the extent of providing higher energy density.[70] However, issues such as matching the capacitance of the two electrodes need to be considered. The two electrodes of symmetrical supercapacitors are of the same material, which requires less consideration, and they are easy to assemble and are less costly. The poor thing is that it can only rely on the conductivity of the electrode material and its own structure to provide electrochemical performances, so its usage performances are somewhat limited.

As the reaction proceeds, the electrode material undergoes a series of structural changes due to its own involvement in the reaction.[72,73] Problems such as corrosion of the electrode surface and shrinkage of the material volume can lead to a serious degradation of the electrode material performances.[74–76] Most of the problems in supercapacitors can be attributed to the presence of significant material defects that prevent the electrochemical reaction.[77] Currently, energy storage devices with low energy density cannot meet the demand in many applications, limiting their commercial applications.[78] The energy density can be increased through designing and fabricating electrode materials.[79–82]

2D layered double hydroxides (LDHs)[83,84] have a high specific surface area and abundant ion insertion sites and have received focus because of high theoretical specific capacitance,[85–89] showing good prospects for applications in supercapacitors. There are mainly metal cations (M^{2+}, M^{3+}) and interlayer anions (A^{n-}) and solvent molecules (H_2O) in the hydroxide layer. Metal cations are located in the center and hydroxide ions are six-coordinated through chemical bonds to form an octahedron to form the main layer of the layered structure,[90,91] anions are filled in the interlayer gaps to balance the charges, and solvent molecules fill the

remaining gaps.[92] It is usually expressed by the following chemical general formula: $[M_{1-x}^{2+}M_x^{3+}(OH)_2]^{x+}[A^{n-}]_{x/n}\cdot zH_2O$. M^{2+} (Fe^{2+}, Ni^{2+}, Zn^{2+}, Mn^{2+}, Co^{2+} and Mg^{2+}) are the +2 valence cations in the main layer structure. M^{3+} (Co^{3+}, Al^{3+}, Fe^{3+}, Mn^{3+}, Cr^{3+}, Ga^{3+}, *etc.*) are the +3 valence cations alternating with M^{2+}, and two metal cations are arranged alternately in the main layer in the laminar structure in addition to the more special monovalent Li^+ and tetravalent Ti^{4+} ions that constitute the LDH of the laminar structure. A^{n-} denotes the interlayer anions, mainly NO_3^-, CO_3^{2-}, SO_4^{2-}, Cl^-, *etc.*[93] In recent years, researchers have improved the level of research on LDHs and found that some +1-valent and +2-valent cations can exist in the molecule, and this discovery makes the structural composition of layered bimetallic hydroxides more complex and variable. The changes that can be brought about based on its structure are also more varied.[94–96] Fig. 2 shows the carbonate-intercalated LDHs in various M^{2+}/M^{3+} molar ratios, declaring that the metal hydroxide octahedra stack along the crystallographic *c*-axis. Due to the unique layer structure of LDHs, the composition and ratio of their metal cations can be adjusted, the type and number of interlayer anions can be controlled, and the number of layers and layer spacing can be easily changed, making them easy to be compounded with other materials to realize functionalization, *etc.*[97–99]

Pristine LDHs are also considered superior supercapacitor electrodes, thanks to their layered structure and adjustable interlayer spacing, providing large specific surface area and adequate ion transport rates.[101–103] However, pristine LDHs suffer from severe refilling, which can reduce their overall exposed surface area and make electrolyte ion transport difficult.[104–106] Besides, the poor conductivity can affect the transfer of electrons and full utilization of active sites.[107–109] The ultrathin nanosheet structure of LDHs usually leads to rapid structural deterioration under harsh electrochemical conditions, which eventually affects the usage performance.[110] To overcome these limitations, hybridized LDH-based nanostructures have been developed as potential multifunctional nanomaterials, and the fabrication of these materials with large specific surface area and more active sites is the key to improve their electrical conductivity and multiplicative properties.[111–114] The use of LDH materials as electrode materials for supercapacitors is mainly based on their special lamellar-pore structure, which can provide a large specific surface area and a large number of reactive sites required for supercapacitors. It has gradually developed into a new generation of environmentally friendly and efficient electrochemical functional materials.

Chen *et al.*[115] provided a systematic review of the synthesis methods of 2D LDH materials, focusing on the characteristics possessed by different synthesis methods. A comprehensive review of the properties and synthesis methods of LDHs, carbon nanomaterials and composite nanomaterials is presented by Khorshidi *et al.*[116] Kim *et al.*[117] reviewed the standard synthesis methods for LDHs, analyzed the design and improvement of typical exemplary LDHs and LDH composites, and focused on the performance of LDH-based sensors for key biomarkers and contaminants, including glucose and metal ions. However, the systematic introduction of LDH material preparation and modification methods, as well as the application in the field of supercapacitors are rarely reviewed. Herein, this paper focus on the preparation of heterogeneous LDHs including co-precipitation, hydrothermal and solvothermal methods, electrodeposition and some other methods, as well as the modification of heterogeneous LDHs including the addition of components, the construction of defects and the generation of heterostructures.[19,24,54,118,119] The prospects of the usage of LDHs for supercapacitors are foreseen, as well as it is

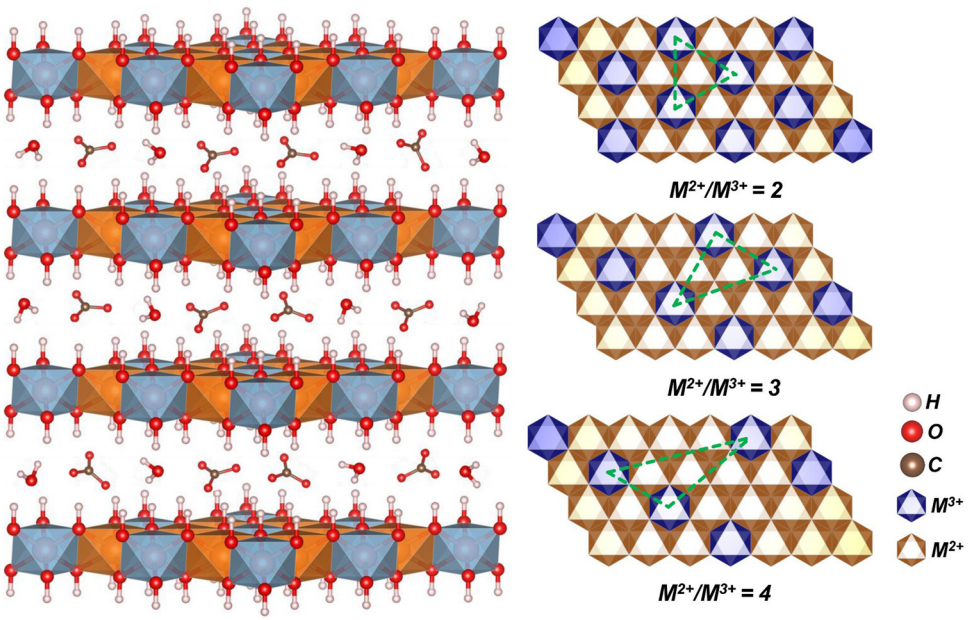

Fig. 2 The idealized structure of carbonate-intercalated LDHs with different M^{2+}/M^{3+} molar ratios showing the metal hydroxide octahedra stacked along the crystallographic *c*-axis. Adapted with permission from ref. 100 Copyright 2020, Zhengzhou University.

hoped that they will provide assistance for the later research of this material.

2. Preparation methods

There are various methods for the synthesis of pristine LDH nanostructures, while the synthesis of hybrid LDHs is often more complex than that of pristine LDHs, usually requiring two or more steps to synthesize them. In this chapter, a variety of methods for the synthesis of LDH nanostructures are reviewed, including co-precipitation, hydrothermal and solvothermal methods, electrodeposition, electrostatic interlayer interaction and some other methods. Different methods require different conditions, and the structure and the morphology of the synthesized materials also differ, but ultimately, they all aim to synthesize materials with better properties.[120]

2.1 Co-Precipitation method

The co-precipitation method is one of the most common preparation methods for LDHs, which mainly involves adding mixed salt solution and mixed base solution dropwise to distilled water at a certain temperature and a certain rate, then accelerating the reaction by stirring, and finally filtering and drying to obtain LDHs with uniform size and regular structure. Since strong alkali solutions cause rapid precipitation of metal ions and make it difficult to regulate and control the reaction process, a certain concentration of sodium hydroxide and sodium carbonate is often formulated into a mixed alkali solution as a precipitant.[121–124] This method has been widely used in practice because of its simplicity, cheapness and stability of the product. However, the addition of a precipitating agent during the preparation process may cause local concentration too high and lead to agglomeration of the product. Selecting a suitable precipitant, controlling the addition method of the precipitant and reasonably controlling the reaction time in the synthesis process are beneficial to the LDH materials with excellent performances. Wen *et al.*[125] prepared $Zn_6Al_2(OH)_{16}CO_3{\cdot}4H_2O$ LDH by the co-precipitation method using NaOH and Na_2CO_3 as the base alkaline sources. The obtained samples were nanosheet powders with a thickness of about 80 nm. Its specific capacitance was 37.0 F g^{-1} at 1.0 A g^{-1}. Besides, Wiston *et al.*[126] used a co-precipitation method to couple two highly electroactive metal ions together to form a nanoflower-like array in the presence of urea. The synthesis schematic is shown in Fig. 3(a). At 1 A g^{-1}, the obtained NiFe-LDH has a specific capacitance of 381 C g^{-1} (1368 F g^{-1}) and retains 87.5% after 5000 consecutive cycles (Fig. 3(b)). At a power density of 1483 W kg^{-1}, the prepared symmetric supercapacitor has an energy density of 66.13 W h kg^{-1}, showing excellent application prospects.

Pure LDHs have poor electrical conductivity and structural instability. The introduction of other anions during the synthesis process can facilitate better performance. Xiao *et al.*[127] prepared NiCo-LDH/CO_3-*x* by a facile chemical co-precipitation method, and the flow chart is shown in Fig. 3(c). CO_3^{2-} was introduced into the LDH in a controlled manner by the addition of $NaHCO_3$. The doping of CO_3^{2-} can cause the original nanosheet structure to bend and interconnect, increasing the contact between the electrolyte and the electrode. By analyzing the TEM images of Fig. 3(d) and (e), it can be inferred that the carbonate-doped samples are more dispersed and the thickness of the nanosheets is smaller than that of the undoped samples. This indicates that more active sites will be exposed to the electrolyte, enhancing the energy storage properties of the material and effectively increasing the specific capacitance. When the doping ratio of carbonate is 5% (Ni, Co-LDH/CO_3-5%), 1970 F g^{-1} of specific capacitance is realized at 1 A g^{-1} as well as 82.8% of specific capacitance is still maintained at 20 A g^{-1}. At a power density of 374.9 W kg^{-1}, the asymmetric supercapacitor assembled with NiCo-LDH/CO_3-5% as the positive electrode has an energy density of 54.8 W h kg^{-1} and maintains 80.8% after 10 000 cycles at 10 A g^{-1}.

Inevitably, in a range of materials synthesized by co-precipitation, there will be instances of poor performances, in which the synthesized materials need to be further treated to achieve even better performance. Wang *et al.*[128] synthesized NiCo-LDHs and at 1 A g^{-1} the specific capacitance was 285.8 C g^{-1}, but the material has poor electrical conductivity and the obtained capacitance is lower than that of the theoretical value. Based on this, NiCo-LDHs were subsequently phosphorylated and P@NiCo-LDH cabbage-like spheres were successfully synthesized, as shown in Fig. 3(f). At 1 A g^{-1}, its specific capacitance reached 536 C g^{-1} due to the generation of metal phosphide having good electron conduction ability (Fig. 3(g) and (h)). In addition, the prepared electrodes show good cycling performance, and at 10 A g^{-1} the capacitance after 5000 cycles is almost constant. The prepared symmetric supercapacitor devices have 7.83 W h kg^{-1} energy density at 300 W kg^{-1}, as well as show excellent cycle performance (Fig. 3(i)), which indicates that phosphorylation can be as an effective route to enhance the performance of LDH-based supercapacitor composites.

The properties of materials are inextricably linked to factors such as the structure, and variations in the synthesis methods can affect the structure of materials, and therefore their properties.[129] Further modifications can be made to the material based on co-precipitation to give it superior properties. Li *et al.*[130] synthesized $Zn_{0.25}Ni_{0.75}Co$-LDH-BA^- inserted with benzoate anions by the zeolitic imidazolate framework-L (ZIF-L) assisted co-precipitation process, as displayed in Fig. 4(a). The specific capacitance was 1378 mA h g^{-1} at 1 A g^{-1}, presenting good capacitance performance (Fig. 4(b) and (c)). This electrode can maintain 91.2% after 10 000 cycles at 10 A g^{-1} (Fig. 4(d)). The asymmetric supercapacitor has a high energy density of 51.8 W h kg^{-1} at a power density of 789 W kg^{-1} and a 94.6% capacitance retention after 10 000 cycles. Wang *et al.*[131] prepared S-NiCoAl-LDH electrode materials by surface sulfidation. From TEM image in Fig. 4(e), it could be inferred that S-NiCoAl-LDH exhibits a tiny flake morphology and aggregates in micron size. It had a 727.1 C g^{-1} specific capacitance at 1 A g^{-1} and still reached 556 C g^{-1} at 20 A g^{-1} (Fig. 4(f) and (g)). The surface sulfide enhances conductivity and improves multiplicative performance. The capacity retention rate was 95.1%

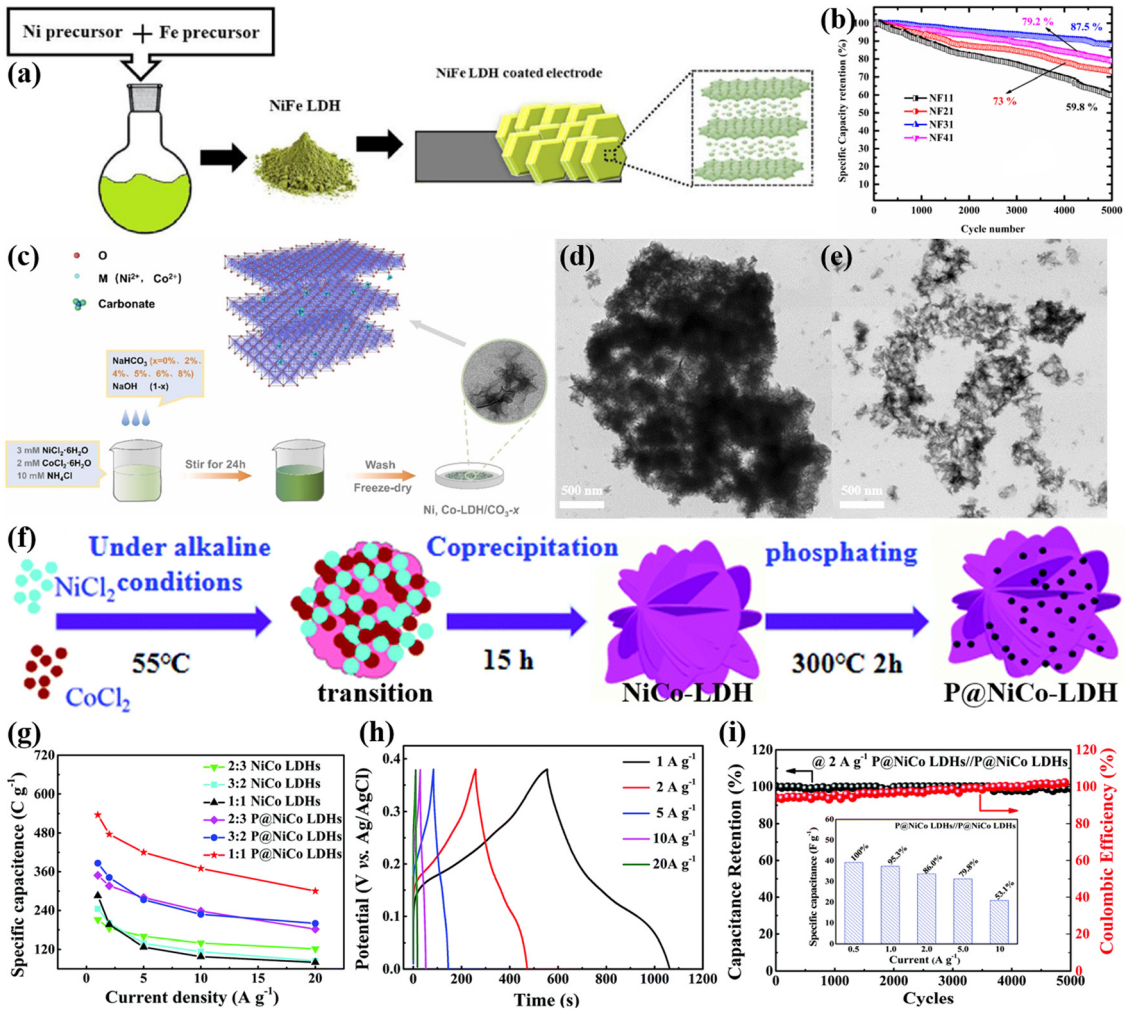

Fig. 3 (a) Schematic diagram of the synthesis of NiFe-LDH, (b) cycling stability of NF11, NF21, NF31 and NF41. Adapted with permission from ref. 126 Copyright 2022, Elsevier Ltd. (c) Flow chart of Ni, Co-LDH/CO_3-x. (d and e) TEM images of Ni, Co-LDH/CO_3-x when (e) x = 0% and (f) x = 5%. Adapted with permission from ref. 127 Copyright 2022, Elsevier B.V. (f) Schematic illustration of fabrication procedures of P@NiCo LDHs, (g) charge results of the 1 : 1 P@NiCo LDHs under various current specific capacitances of different obtained electrodes at various current densities, (h) GCD results of the 1 : 1 P@NiCo LDHs under various current densities, (i) capacitance retention and coulombic efficiency at 2 A g^{-1} and the specific capacitance of the device. Adapted with permission from ref. 128 Copyright 2021, Royal Society of Chemistry.

after 10 000 cycles (Fig. 4(h)). The Al doping stabilizes the crystal form of S-NiCoAl-LDH and make it exhibit high cycling performance. The assembled S-NiCoAl-LDH//AC device has a specific capacitance of 182.6 F g^{-1} at 0.5 A g^{-1} and a high energy density of 82.2 W h kg^{-1} at 450 W kg^{-1}.

The co-precipitation method also allows the synthesis of composites of LDHs with other materials, resulting in unique structures with excellent properties. The hydrangea-like HC@NiCo-LDHs were prepared by applying a chemical co-precipitation without the addition of additional alkaline reagents.[132] The synthesis processes are shown in Fig. 4(i). The high Ni concentration allows the less crystalline NiCo-LDHs to grow uniformly and be in close contact with the hollow carbon shell, forming an embroidered spherical structure (Fig. 4(j)). This unique structure and crystalline phase expose abundant active sites and promote diffusion of ions. At 2 A g^{-1}, its specific capacitance was 758 C g^{-1}, and the capacity retention was 79% at 20 A g^{-1}, demonstrating good multiplicative properties (Fig. 4(k and l)). The assembled HC@NiCo-LDHs//AC asymmetric supercapacitor maintained 70.2% capacitance after 4000 cycles.

2.2 Hydrothermal and solvothermal methods

The hydrothermal and the solvothermal methods involve confining the reactants in a reactor where the reaction process is accomplished by chemical transfer.[133] Liquid or gaseous water is the medium for transferring pressure at high temperatures and pressures, and most of the reactants can be partially dissolved in water,[134] allowing the reaction to take place at a critical level (coexistence of gas and liquid phases).[135] The hydrothermal method involves first mixing a certain proportion and concentration of a mixed metal salt solution and alkali solution quickly,[136] and then the mixture is immediately transferred to a stainless-steel high-pressure reaction kettle, where the reaction takes place at a certain temperature for 6–24 h, and

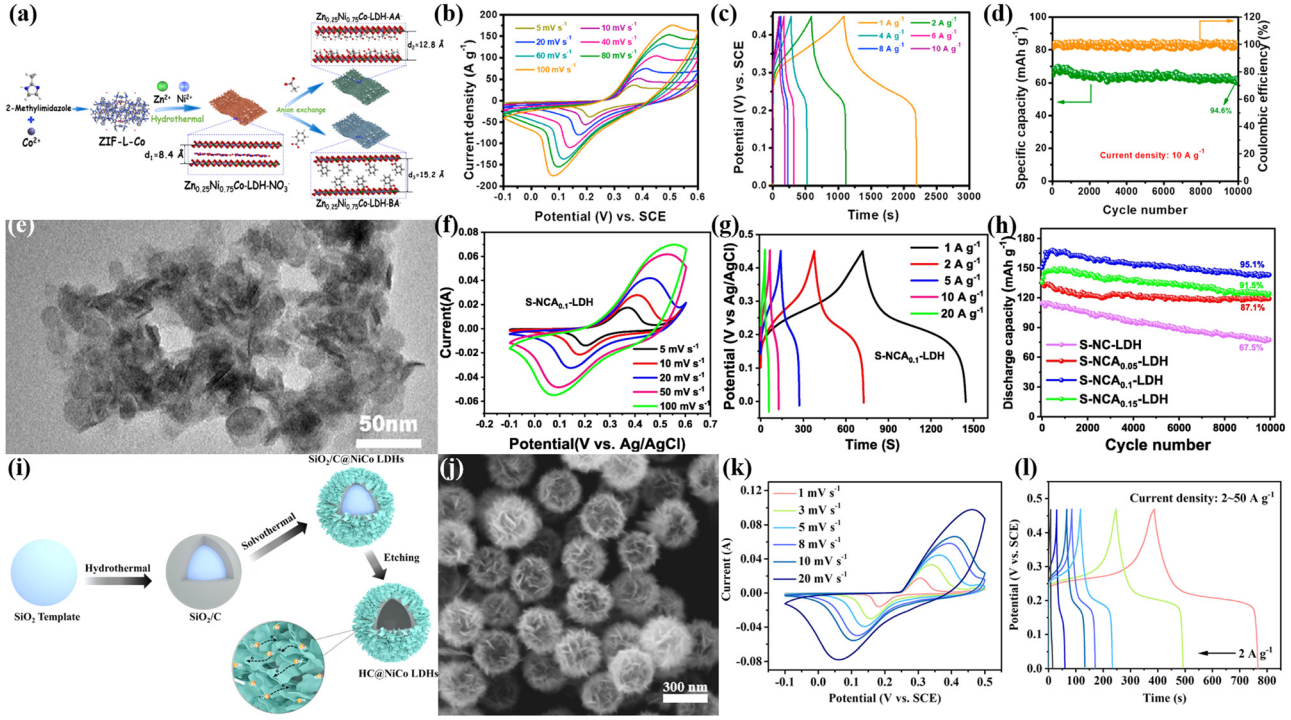

Fig. 4 (a) Schematic illustration of formation processes for $Zn_{0.25}Ni_{0.75}Co$-LDH-BA^-, (b) CV curves of $Zn_{0.25}Ni_{0.75}Co$-LDH-BA^- with the potential sweep rate varied from 5 to 100 mV s^{-1}, (c) fraction of the capacitive contribution of $Zn_{0.25}Ni_{0.75}Co$-LDH-$BA^-/AA^-/NO_3^-$ at different scan rates, (d) cycling life properties and coulombic efficiency of $Zn_{0.25}Ni_{0.75}Co$-LDH-BA^- at 10 A g^{-1}. Adapted with permission from ref. 130 Copyright 2022 Elsevier B.V. (e) TEM image of the S-$NiCoAl_{0.1}$-LDH, (f and g) CV and GCD curves of the S-$NiCoAl_{0.1}$-LDH at different scan rates and current densities, respectively, and (h) cycling stability of S-NiCoAl-LDH after 10 000 cycles at 10 A g^{-1}. Adapted with permission from ref. 131 Copyright 2022 Elsevier Inc. (i) Diagram of the synthesis of HC@NiCo LDH microspheres, (j) SEM image of HC@NiCo LDH spheres, and (k and l) CV and GCD curves of the optimized HC@NiCo LDHs (with the initial ratio of Ni/Co = 4 : 1) at different scan rates and current densities. Adapted with permission from ref. 132 Copyright 2021 Elsevier Ltd.

finally after through washing, drying, grinding, powder products are obtained.[137] The reaction environment is closed and stable with strong controllability, and the prepared product has crystal structure integrity and narrow particle size distribution.[138] It is found that the concentration of the solution can affect the resulting morphology and properties of the synthesized material. When the concentration is too low, the thickness of the nanosheet is uneven, while when the concentration is too high, the impurity phase is generated[139] The solvothermal method is developed on the basis of the hydrothermal method,[140] in which the water is replaced by organic solvents or non-aqueous solvents (organic amines, alcohols, ammonia, carbon tetrachloride, benzene, *etc.*). The principle of this method is similar to that of hydrothermal method, in aqueous solution cannot grow, easy oxidation, easy hydrolysis or water sensitive materials are synthesized, such as III–V group semiconductor compounds, nitride, chalcogenide, new phosphorus (arsenic) molecular sieve 3D framework structure, *etc.*[141,142] In the process of preparation, products with different sizes and morphologies can be obtained by adjusting the reaction temperature, reaction time, and concentration of metal ions and surfactants. However, the high-pressure reactor can only adjust the external environment temperature, and the internal temperature and pressure are difficult to monitor. A reasonable control of reaction temperature and reaction time is beneficial for the synthesis of high performance LDH materials.

By using ethanol as the solvent, NiCoAl-LDHNs were prepared with the aid of a one-step solvothermal method (Fig. 5(a)) by Meng *et al.*[143] As can be seen in Fig. 5(b), the sample exhibits 3D nanoflower clusters. NiCoAl-LDHN-9 had a specific capacitance of 1228.5 F g^{-1} at 1 A g^{-1}. In the case of 20 A g^{-1}, the value was 1001.8 F g^{-1}, which still had an 81.6% capacitance retention (Fig. 5(c)). The specific capacitance of the NiCoAl-LDHN-9//AC device was 102.1 F g^{-1} at 0.5 A g^{-1} (Fig. 5(d)). The energy density was 35.9 W h kg^{-1} at 225.8 W kg^{-1}, and the capacitance retention rate was 87.1% after 10 000 cycles.

LDHs are produced on the surface of different substrates by hydrothermal and solvothermal methods, and after reasonable regulation of the reaction time and other factors it is possible to obtain electrode materials with more satisfactory properties.[144] Li *et al.*[145] prepared a layered hybrid structure of $NiCo_2S_4$ and NiCoAl-LDHs on binder less carbon cloth (CC) by a series of hydrothermal reactions (Fig. 5(e)). Fig. 5(f) shows the regular and uniformly grown nanosheet structure. The NiCoAl-LDHs@$NiCo_2S_4$@CC electrode exhibited 1775 F g^{-1} at 1 A g^{-1} (Fig. 5(g)). At 10 A g^{-1}, the value was 79.6% when the number of cycles reached 10 000. Flexible solid-state asymmetric supercapacitors were assembled using NiCoAl-LDHs@$NiCo_2S_4$@CC as the positive electrodes, with an energy density of 33.13 W h kg^{-1} at 750 W kg^{-1} and a cycle performance of 71.4% after 10 000 cycles (Fig. 5(h)). By using a solvothermal way, Nguyen *et al.*[146]

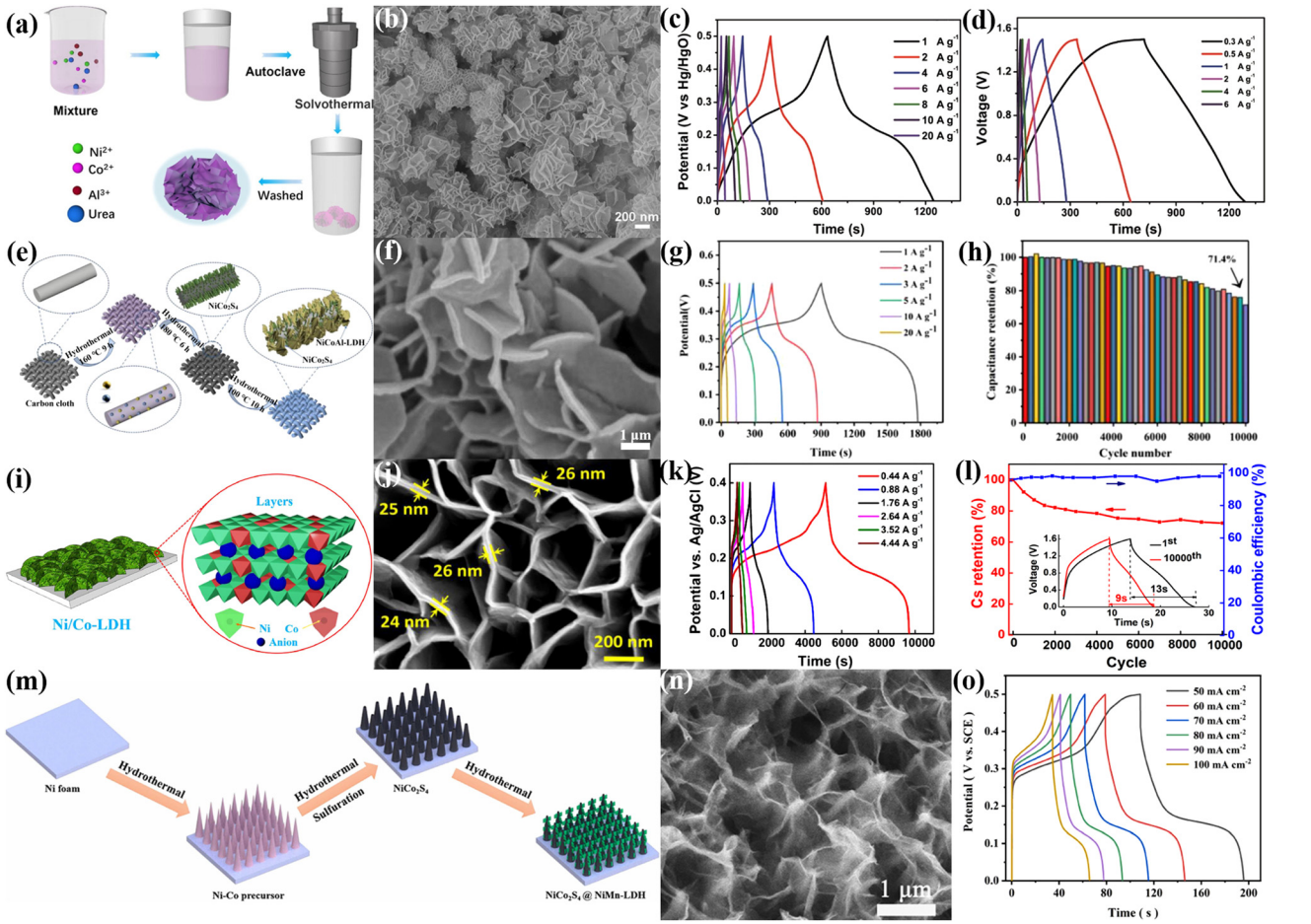

Fig. 5 (a) Schematic representation of the synthesis of NiCoAl LDH nanosheets, (b) SEM image of NiCoAl-LDHN-9, (c) GCD curves of the NiCoAl-LDHN-9 electrode at various current densities, (d) GCD curves of the device at different current densities. Adapted with permission from ref. 143 Copyright 2021, Elsevier B.V. (e) Schematic illustration of the synthesis processes of hierarchical NiCoAl-LDHs@$NiCo_2S_4$@CC, (f) SEM image of NiCoAl-LDHs@$NiCo_2S_4$@CC, (g) GCD curves of NiCoAl-LDHs@$NiCo_2S_4$@CC at various current densities, and (h) cycling stability performance of device at 1 A g^{-1}. Adapted with permission from ref. 145 Copyright 2021 Elsevier B.V. (i) Schematic diagram of the structural growth of NiCo LDHs on an NF substrate, (j) SEM image of NiCo LDHs, (k) GCD curves at different current densities, and (l) cycling stability and coulombic efficiency of the NiCo LDHs//AC with the inset showing the first and 10 000th GCD curves. Adapted with permission from ref. 146 Copyright 2020, Elsevier Ltd. (m) Schematic illustration of the synthesis processes of $NiCo_2S_4$@NiMn-LDHs core–shell hybrid arrays on NF, (n) SEM image of $NiCo_2S_4$-NM-6, and (o) GCD curves at different current densities. Adapted with permission from ref. 147 Copyright 2021, Elsevier B.V.

grew NiCo-LDHs in layers on nickel foam (NF) without using any binder to obtain NF@NiCo-LDH material as shown in Fig. 5(i). The SEM image in Fig. 5(j) shows that the nanosheets are interwoven with 25 nm thickness. This material achieved a 4392 F g^{-1} specific capacitance at 0.44 A g^{-1} (Fig. 5(k)). The energy density of the prepared NF@NiCo-LDHs//AC device was 51.1 W h kg^{-1} at 777 W kg^{-1}. The electrochemical stability was 72.2% after 10 000 cycles at 10 mA cm^{-2} (Fig. 5(l)), demonstrating its potential for energy storage applications. Xue *et al.*[147] successfully synthesized core–shell $NiCo_2S_4$@NiMn-LDH nanosheet hybrids on the surface of NF by a controlled three-step hydrothermal method, and NiMn-LDH nanosheets of different thicknesses were attached to the outer layer of $NiCo_2S_4$ nanotubes by adjusting the heating time of the hydrothermal reaction in Fig. 5(m). NiMn-LDH nanosheets were uniformly grown on $NiCo_2S_4$ hollow nanotubes with complete connection and moderate thickness forming a stable core–shell system, which can provide more porous channels. The SEM image is shown in Fig. 5(n). The optimized $NiCo_2S_4$@NiMn-LDH electrode exhibited a specific capacitance of 822.64 C g^{-1} at 50 mA cm^{-2} (Fig. 5(o)), and the specific capacitance was maintained at 92.7% after 5000 cycles. In addition, the asymmetric supercapacitor prepared with $NiCo_2S_4$@NiMn-LDHs has a maximum energy density of 53.10 W h kg^{-1} at 370.82 W kg^{-1} and an 94.3% capacitance retention after 10 000 cycles at 20 mA cm^{-2}.

A number of hybrids based on LDHs with superior properties can also be obtained by hydrothermal and solvothermal methods. NiMn-LDHs/hrGO hybrids were fabricated by a solvothermal route by Yan *et al.*[148] The incorporation of hrGO improved the conductivity and specific surface area. At 1 A g^{-1}, the capacitance was up to 302.0 C g^{-1}. The asymmetric supercapacitor achieved a specific capacitance of 237.6 C g^{-1} at 1 A g^{-1}, a cycling stability of 80.5% after 2000 cycles, and an energy density of 59.9 W h kg^{-1} 901.5 W kg^{-1}. Wang *et al.*[149]

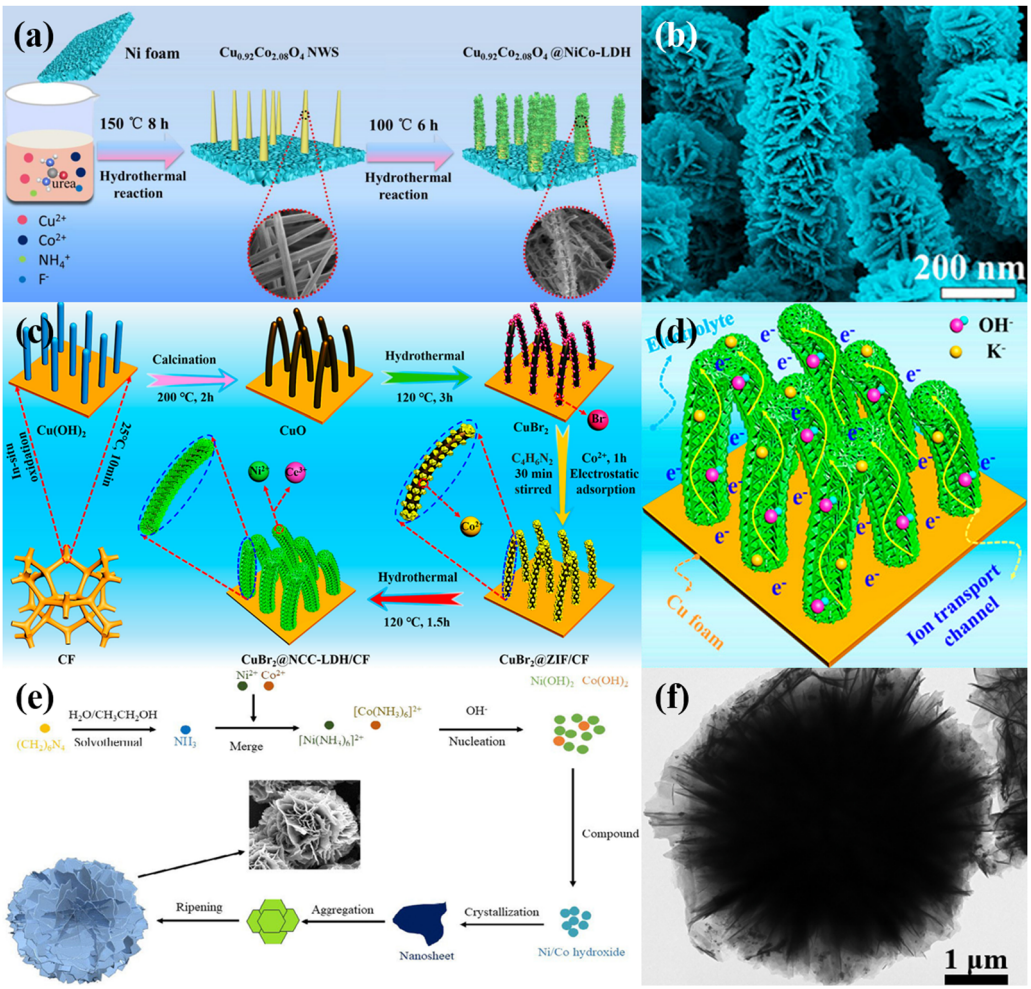

Fig. 6 (a) Synthetic schematic of $Cu_{0.92}Co_{2.08}O_4$@NiCo-LDHs. Adapted with permission from ref. 149 Copyright 2021, Elsevier Ltd. (b) SEM images of the $CuBr_2$@NiCeCo-LDH core–shell nanorod, (c) schematic illustration of the $CuBr_2$@NiCeCo-LDH core–shell nanorod, and (d) schematic diagram of electron and ion transfer across the surface of the active component. Adapted with permission from ref. 150 Copyright 2022, American Chemical Society. (e) Synthetic schematic of NiCo-LDH synthesis, and (f) TEM image of NiCo-LDHs/S-15. Adapted with permission from ref. 151 Copyright 2022, Elsevier Ltd.

fabricated uniform NiCo-LDH nanosheet arrays on $Cu_{0.92}Co_{2.08}O_4$ (CCO) nanowires using a two-step solvothermal method as shown in Fig. 6(a). The non-homogeneous core–shell structure consists of a highly conductive core layer and a highly capacitive shell layer, and CCO can slow down the agglomeration of NiCo-LDH nanosheets. The CCO@NiCo-LDH electrode provided a specific capacitance of 1652 F g^{-1} at 1 A g^{-1}. The flexible asymmetric supercapacitor has an energy density of 42.38 W h kg^{-1} at 1350 W kg^{-1}.

LDHs have certain drawbacks in terms of performances and still need to be used in conjunction with other methods to prepare ideal electrode materials. Fu *et al.*[150] fabricated NiCeCo LDHs on copper bromide nanowire arrays ($CuBr_2$@NiCeCo-LDHs) by hydrothermal and calcination methods, and a visual representation of the preparation is illustrated in Fig. 6(c). The $CuBr_2$@NiCeCo-LDH electrode exhibited excellent electrochemical performances with a 5460 mF cm^{-2} area capacitance at 2 mA cm^{-2} and 88% capacitance retention at 50 mA cm^{-2} due to the unique top entangled structure (Fig. 6(d)) and the complex assembly of different active components. The asymmetric supercapacitor with $CuBr_2$@NiCeCo-LDHs and AC electrodes has an energy density of 118 W h kg^{-1} at 1013 W kg^{-1}. Besides, Wang *et al.*[151] synthesized a hydrophobic-like NiCo-LDH precursor (Fig. 6(e)) by a hydrothermal method. Based on this precursor, highly conductive sulfide nanoparticles were constructed on NiCo-LDH nanosheets (Fig. 6(f)) by an ion-exchange strategy. The newly formed heterojunction between NiCo-LDHs and sulfide nanoparticles enabled them to provide ion or electron transfer paths to each other, significantly improving the conductivity. Through the adjustment of the thioacetamide amount, the optimized NiCo-LDH/S-15 material has a 267.8 mA h g^{-1} specific capacitance at 1 A g^{-1}. The assembled supercapacitor has a specific capacitance of 126.76 F g^{-1} at 1 A g^{-1}, a reasonable energy density and power density (43.6 W h kg^{-1}, 375 W kg^{-1}), and a 83% capacitance retention after 5000 cycles.

Liu *et al.*[152] successfully synthesized a nano-flowery NiAl-LDHs-S electrode material by a pre-synthetic solvothermal reaction using a sulfide modification procedure, as shown in Fig. 7(a).

tThe obtained NiAl-LDHs-S electrode material has a 1680 F g^{-1} specific capacitance at 1 A g^{-1} because of the generation of sulfide on the surface of LDHs. The energy density of the assembled NiAl-LDHs-S//AC asymmetric supercapacitor reaches 35.78 W h kg^{-1} at 1127.03 W kg^{-1}. In Fig. 7(b), Liu *et al.*[153] synthesized an Se-NiAl-LDH electrode material by a pre-synthetic solvothermal reaction and selenide modification. It is worth noting that some new selenide crystals were generated, and the obtained material has a 1098 F g^{-1} specific capacitance at 1 A g^{-1}. The energy density of the Se-NiAl-LDHs// AC device is 29 W h kg^{-1} at 1593.17 W kg^{-1}. Besides, Liu *et al.*[154] decorated Ag nanoparticles on CoAl-LDH flower-like hollow microspheres as shown in Fig. 7(c) by a simple one-step solvothermal reaction and chemical plating solution deposition reaction. The modification of Ag nanoparticles can promote the fast diffusion kinetics and electrochemical reactivity of electrolyte ions. The prepared Ag/CoAl-2 LDHs had a 1214 C g^{-1} specific capacitance at 3 A g^{-1} and a 91% capacity retention at 10 A g^{-1} for 10 000 cycles. Moreover, the assembled device using Ag/CoAl-LDHs and N-doped carbon nanotubes (N-CNTs), respectively as electrodes, exhibited an energy density of 61.2 W h kg^{-1} at 800 W kg^{-1}, declaring the great promise of engineered conductive nanoparticle modified LDH-based active materials for high-performance supercapacitors.

2.3 Electrodeposition method

The electrodeposition method is a technique in which an electric current is passed through the electrolyte solution and a redox reaction takes place at the electrode to fabricate a coating.[155,156] The reduction of metal ions at the cathode to produce a metallic coating is called electroplating.[157,158] It requires the use of a conductive substrate as the working electrode. Typically, a three-electrode system is worked in an electrolyte containing a metal precursor, and then LDH nanostructures are synthesized on the working electrode at or within a certain potential range.[159] The advantage of this method is that, in most cases, no additional reagents are required to induce the formation of hydroxides other than the metal precursors.[160] During the electrodeposition process, water molecules are electrolyzed to produce oxygen and hydroxide ions, which facilitate the formation of metal hydroxides.[161,162] The main difference between electrochemical deposition and chemical plating is that although both redox reactions are carried out in solution, the former occurs at the electrode through the migration of ions in the presence of an

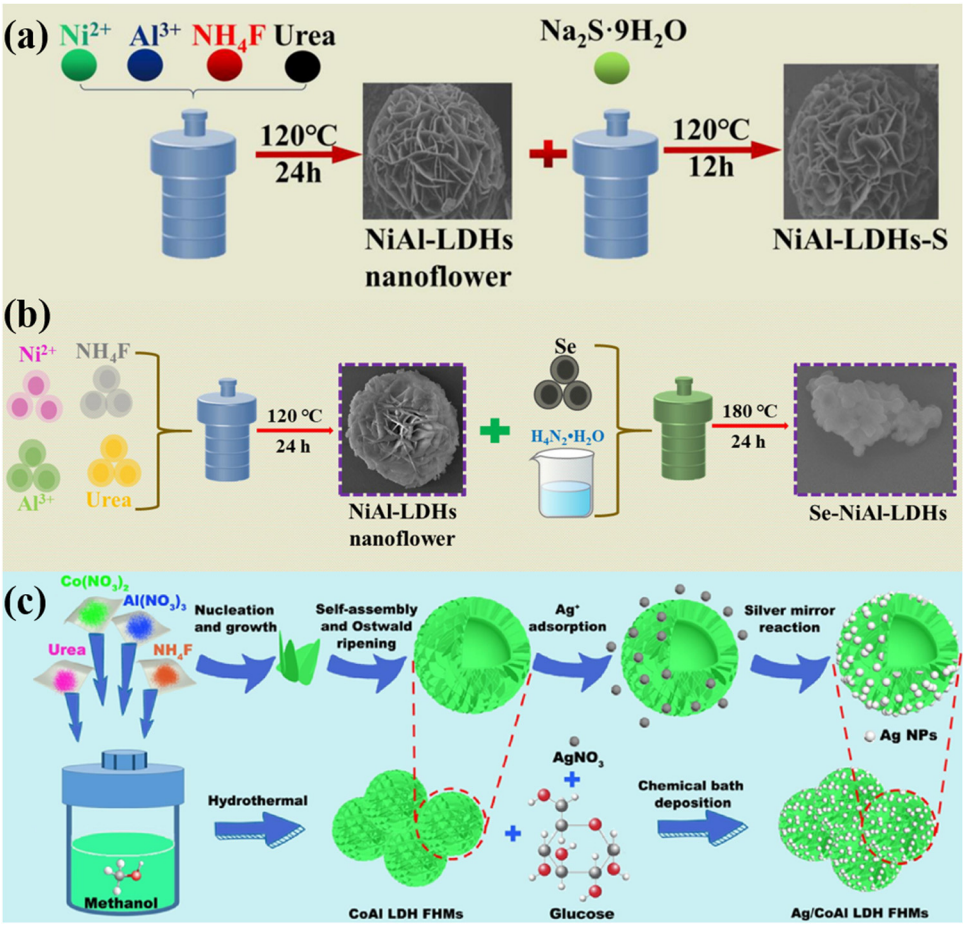

Fig. 7 (a) The preparation process route of the NiAl-LDHs and NiAl-LDHs-S. Adapted with permission from ref. 152 Copyright 2022, Elsevier B.V. (b) Roadmap for the synthesis of NiAl-LDHs and Se-NiAl-LDHs. Adapted with permission from ref. 153 Copyright 2022, Elsevier Ltd. (c) Schematic illustration of the preparation of Ag/CoAl-LDHs. Adapted with permission from ref. 154 Copyright 2020, Elsevier Inc.

electric field, while the latter is formed directly on the surface of the workpiece through the autocatalytic action of the chemical plating solution.[163] This method can be applied to obtain LDH materials with various grain sizes. However, the generation and growth rate of nuclei on the substrate surface cannot be controlled. LDH materials with excellent performances can be obtained by selecting suitable electrodeposition conditions and choosing a reasonable electrolyte and matrix. Huang *et al.*[164] obtained a unique array of LDH nanosheets with intercalated pseudocapacitive properties and battery-type electrode materials using a simple and pollution-free two-step electrodeposition technique. The electrode material consists of MoO_3 and NiCo-LDHs grown directly on a 3D conductive NF substrate to form a binder-free 2D ultrathin cross-layered heterostructure (NiCo-LDHs@MoO_3/NF) (Fig. 8(a)). At 1 A g^{-1}, the specific capacitance of this heterogeneous nanomaterial was 952.2 C g^{-1} at 1 A g^{-1}, Fig. 8(b) clearly shows that this composite outperforms the other two individual materials produced directly on the substrate, and the capacity retention was 86.42% after 10 000 cycles. The NiCo-LDHs@MoO_3/NF//AC device (Fig. 8(c)) has an energy density of 58.06 W h kg^{-1} at 800 W kg^{-1}, as well as a 84.57% capacity retention after 10 000 cycles. Zhang *et al.*[165] used MoO_3 nanorod arrays as a matrix to encapsulate NiCo-LDHs by electrodeposition to obtain layered MoO_{3-x}@NiCo-LDHs containing oxygen vacancies. The MoO_{3-x}@NiCo-LDHs-15 electrode exhibited a capacitance of 3.49 F cm^{-2} at 5 mA cm^{-2} (Fig. 8(e)), and the capacitance retention was 94.9% after 3000 cycles in a neutral electrolyte (Fig. 8(d)). The corresponding symmetric flexible solid-state supercapacitor exhibits good flexibility and an energy density of 0.047 mW h cm^{-2} at 0.865 mW cm^{-2}. In this work, the layered structure changes the microenvironment of the electrode surface, shortening the ion transport path and accelerating the reaction kinetics. Moreover, the NiCo-LDH nanosheets tightly packed on the surface of the MoO_3 nanorod arrays slow down the structural collapse during potassium ion removal. In addition, the formation of oxygen vacancies enhances the structural stability

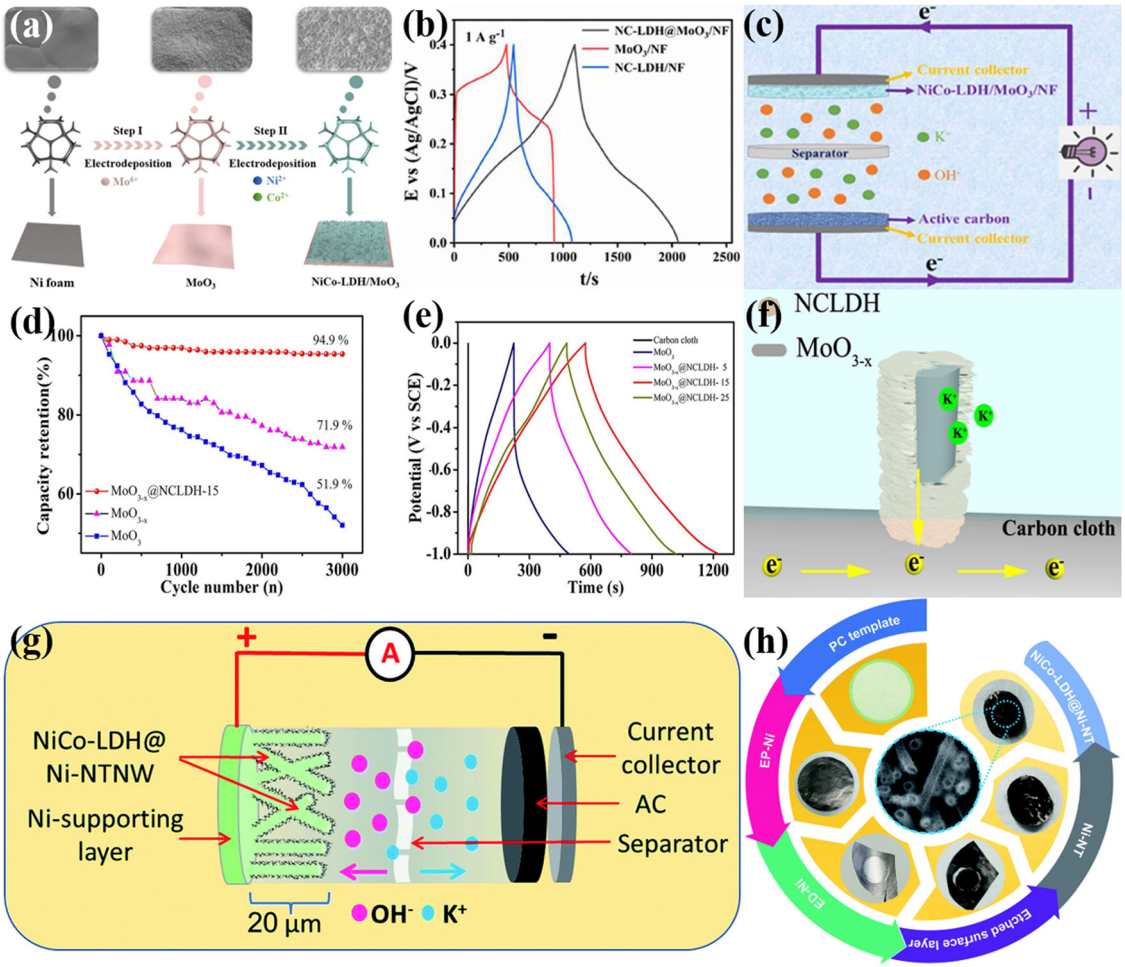

Fig. 8 (a) Schematic illustration of the preparation procedures for NiCo-LDHs@MoO_3/NF, (b) GCD curves of MoO_3/NF, NiCo-LDHs/NF and NiCo-LDHs@MoO_3/NF electrodes, and (c) schematic diagram of the assembled device. Adapted with permission from ref. 164 Copyright 2021, Elsevier Ltd. (d) Cycle performance of MoO_3, MoO_{3-x} and MoO_{3-x}@NiCo-LDHs-15 at 10 mA cm^{-2}, and (e) GCD curves at 5 mA cm^{-2}, (f) schematic transportation process of electrons and ions in MoO_{3-x}@NiCo-LDHs. Adapted with permission from ref. 165 Copyright 2021, Elsevier B.V. (g) Schematic illustration of the assembled NiCo-LDHs@Ni-NTNW//AC device. (h) Schematic illustration presenting photographs of the self-supported NiCo-LDHs@Ni-NTNW electrode through the fabrication process. Adapted with permission from ref. 166 Copyright 2022, Royal Society of Chemistry.

and electrical conductivity of MoO_3. Therefore, this study provides a new strategy for constructing flexible electrode materials with high electrochemical performance, which is of great value in subsequent applications. Amin *et al.*[166] used an electrodeposition method to directly grow NiCo layered double hydroxide nanosheets on Ni nanotube (Ni-NTNW) networks to obtain a 3D self-supporting layered electrode. The electrode utilizes the large interface and high redox activity of the 2D coated nanosheets, and the highly porous network structure of the 1D Ni-NTNW support enhances its performance, enables fast mass transfer, and acts as a "highway for fast electron transfer". At 0.2 mA cm^{-2} the as-prepared NiCo-LDHs@Ni-NTNW structure exhibits an ultrahigh capacity of 126.4 C cm^{-3}. Furthermore, the assembled NiCo-LDHs@Ni-NTNW//AC asymmetric supercapacitor (Fig. 8(g)) can provide a 76.7 F cm^{-3} capacitance at 1 mA cm^{-2}. Meanwhile, its energy density of 14.7 mW h cm^{-2} at 4769 mW cm^{-2} exceeds those of most state-of-the-art supercapacitors. Thus, hybrid core–shell nanotube networks represent an emerging design paradigm for high-performance devices in portable devices.

In Fig. 9(a), Zhao *et al.*[167] successfully prepared NiCoFe-LDH nanosheet electrodes with high specific capacitance and electrical conductivity by electrodeposition on CC. More importantly, the multiplicative performance and the cycling stability were better compared with the NiCo-LDH electrode, which reached 145% stability after 4000 cycles. Moreover, the NiCoFe-LDHs//AC device has a 207 F g^{-1} specific capacitance at 1 mA cm^{-2} and an energy density of 65 W h kg^{-1} at 83 W kg^{-1}. Moreover, the device has an excellent cycling stability of 126% after 5000 cycles. Wang *et al.*[168] used electrochemical deposition to synthesize NiCo-LDHs on a graphite paper-derived 3D electrode substrate (called EGP, with partially exfoliated graphite sheets and expanded lateral graphite layers on the surface), resulting in an EGP@NiCo-LDH electrode material (Fig. 9(b)). Due to the simultaneous 3D electrode structure and the high capacitance of NiCo-LDHs, EGP@NiCo-LDHs exhibit ultrahigh capacitance (1650 F g^{-1} at 1 A g^{-1}) and excellent rate capability. In addition, the asymmetric device achieves an energy density of 44.31 W h kg^{-1} at 799.98 W kg^{-1} and a 92.8% retention rate after 5000 cycles.

The use of electrodeposition in conjunction with other methods results in improved electrode materials with better performances. Wang *et al.*[169] prepared oxygen-rich NiCo-LDHs with excellent supercapacitor performance on NF substrates by electrodeposition and *in situ* oxidation. The oxygen vacancies can be adjusted by hydrogen peroxide treatment to remarkably enhance electrical conductivity and electrochemical properties of the materials. The NiCo-LDHs containing oxygen vacancies (O_v-NiCo-LDHs) reached a 1160 C g^{-1} specific capacitance at 1 A g^{-1} as well as showed 61% retention at 20 A g^{-1}.

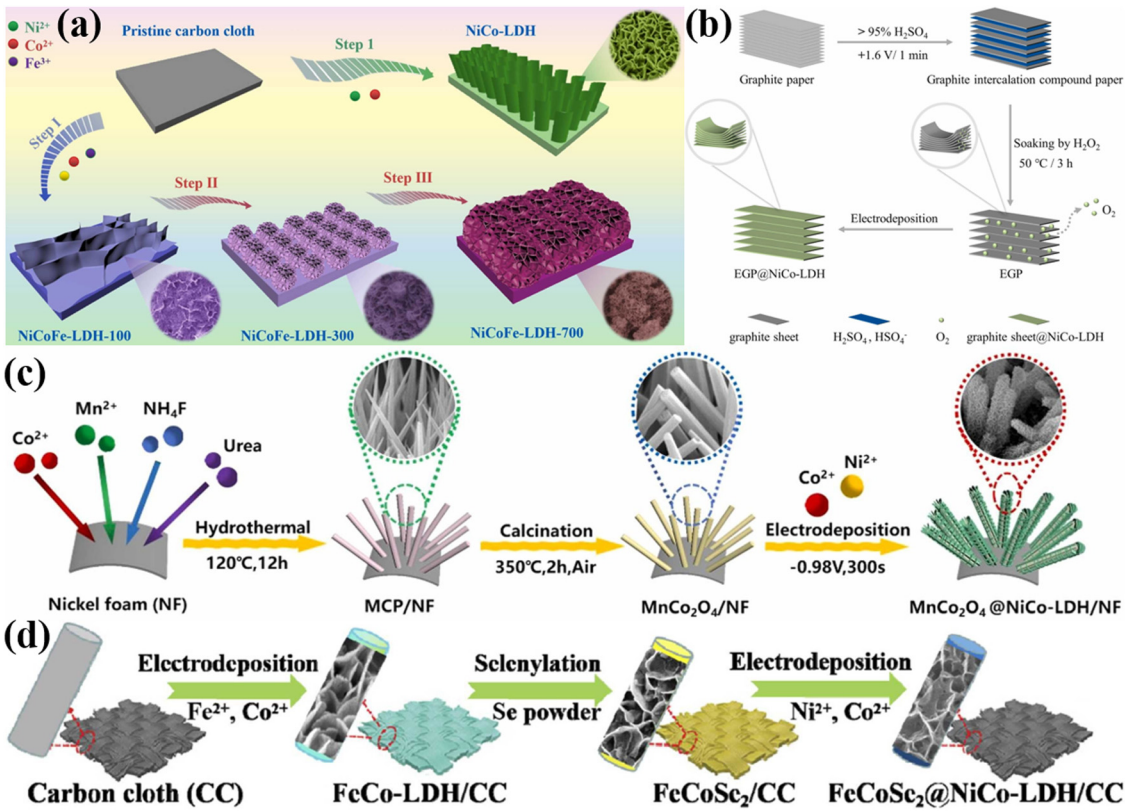

Fig. 9 (a) Schematic illustration of the synthesis processes of the as-made NiCoFe-LDH electrode. Adapted with permission from ref. 167 Copyright 2021, Elsevier B.V. (b) Schematic illustration of the fabrication processed of the EGP@NiCo-LDH electrode. Adapted with permission from ref. 168 Copyright 2022, Elsevier B.V. (c) Schematic illustration of the fabrication of the $MnCo_2O_4$@NiCo-LDHs/NF core-sheath heterostructure. Adapted with permission from ref. 170 Copyright 2022, Elsevier B.V. (d) Schematic illustration of the fabrication steps of the $FeCoSe_2$@NiCo-LDH nanosheet arrays on CC. Adapted with permission from ref. 171 Copyright 2022, Elsevier B.V.

The tsymmetrical device has an energy density of 216.19 W h kg^{-1} at 1.75 kW kg^{-1}. Wang *et al.*[170] prepared a core-sheath heterostructure ($MnCo_2O_4$@NiCo-LDHs/NF) (Fig. 9(c)) consisting of $MnCo_2O_4$ nanowires encapsulated by NiCo-LDH nanosheets using a combination of hydrothermal preparation and electrochemical deposition. The material achieved a 4555.0 F g^{-1} specific capacitance at 1 A g^{-1}. Furthermore, the $MnCo_2O_4$@NiCo-LDHs/NF//AC asymmetric device has an energy density of 21.3 W h kg^{-1} at 160.0 W kg^{-1} and can be able to light up a green LED indicator for more than 30 min. Wan *et al.*[171] *in situ* modified highly porous $FeCoSe_2$@NiCo-LDH core–shell nanosheet arrays on the surface of CC by an electrodeposition method and salinization treatment, as displayed in Fig. 9(d). These hierarchical heterostructures composed of two vertically aligned interconnected 2D nanosheets not only provide a huge surface area and efficient diffusion pathways for fast electron/ion transport, but also generate abundant electronically altered heterointerfaces, resulting in a synergistic effect between the two components. The obtained $FeCoSe_2$@NiCo-LDH electrode achieves a 220.9 mA h g^{-1} specific capacitance at 1 A g^{-1}, as well as the cycling stability is better than that of the single component. Furthermore, the device assembled using the $FeCoSe_2$@NiCo-LDH electrode and layered porous carbon electrode exhibits an energy density of 1.248 kW kg^{-1} at 65.9 W h kg^{-1}, and the capacity retention after 10 000 cycles is 87.6%.

2.4 Electrostatic interstratification

Due to the large distance between the layers of LDHs, it is difficult to contact the inserted anions to increase the electrical conductivity, lowering the electrochemical properties. In order to solve this problem, various methods have been tried to spin out the LDHs into thin layers, such as mechanical agitation and with larger anion exchange reactions.[172,173] However, the re-stacking of these shed layers is a thermodynamically driven process to stabilize the high surface area of these layers. To this end, sandwiching the positively charged LDHs with the negatively charged 2D thin material between the layers is an effective method to obtain better electrical conductivity and higher electrochemical performances.[174–177] MXene is a 2D layered material with excellent properties[178] and has a wide range of applications[179] in the synthesis of LDHs using electrostatic interlayer interaction.[10,180–182] This method can generate a sandwich-like electrostatic layer between LDHs with positive charges and 2D thin materials with negative charges, which can achieve better conductivity and superior electrochemical properties. However, two materials with different charges need to be carefully searched. If the properties of various materials are widely understood, suitable materials are selected, and suitable intercalators are introduced in the synthesis process, and the performances of the materials can be obviously enhanced. Zhao *et al.*[183] prepared a surface covalently functionalized MXene based $Ti_3C_2Cl_2$ nanodot-dotted MXene@NiAl-LDHs

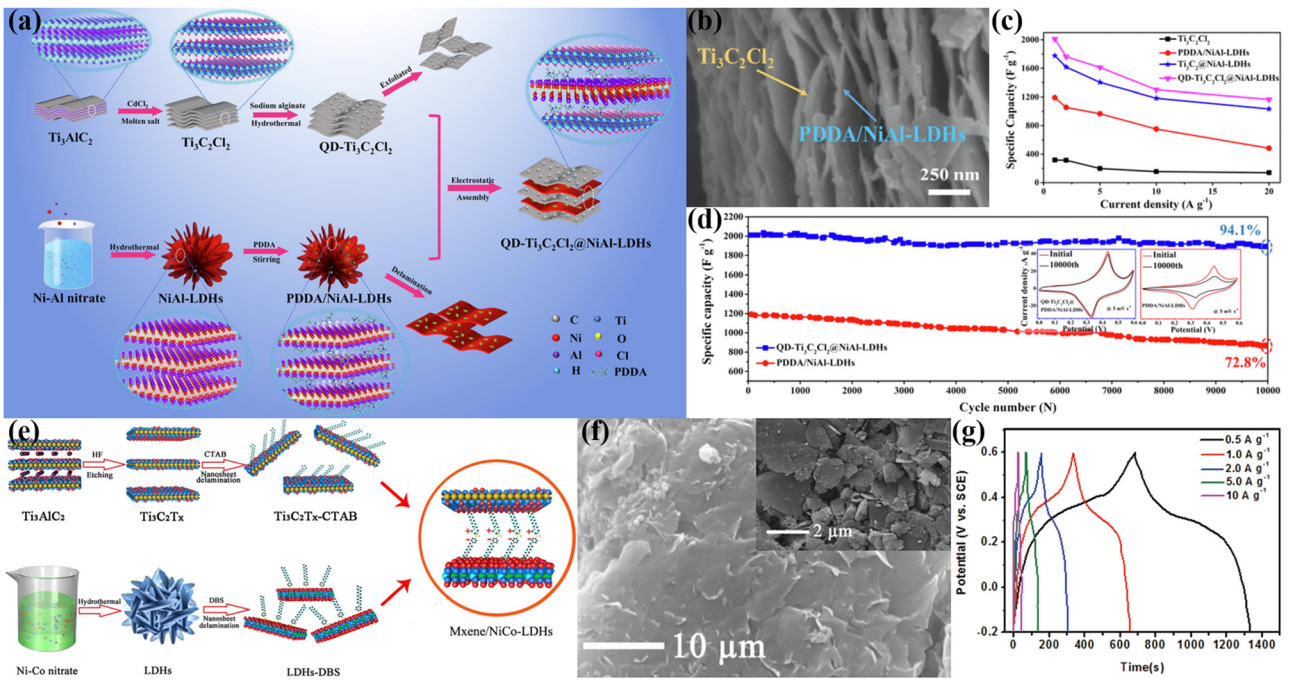

Fig. 10 (a) Schematic diagram of the processes for synthesizing the QD-$Ti_3C_2Cl_2$@NiAl-LDH electrode by electrostatic attraction and self-assembly and (b) the corresponding cross-sectional SEM image, (c) specific capacitances of the $Ti_3C_2Cl_2$ MXene, PDDA/NiAl-LDHs, Ti_3C_2@NiAl-LDHs and QD-$Ti_3C_2Cl_2$@PDDA/NiAl-LDHs at different current densities, (d) the cycling stability of the PDDA/NiAl-LDHs and QD-$Ti_3C_2Cl_2$@PDDA/NiAl-LDHs at 1.0 A g^{-1}, the inset of the CV curves of the above electrodes before and after 10 000 cycles. Adapted with permission from ref. 183 Copyright 2021, Elsevier Inc. (e) Schematic illustration of the fabrication of 2D MXene/NiCo-LDHs by electrostatic adsorption of anions–cations, and (f) the corresponding cross-sectional SEM images, (g) GCD curves of the MXene/NiCo-LDH electrode at different current densities. Adapted with permission from ref. 184 Copyright 2019, Elsevier B.V.

(QD-$Ti_3C_2Cl_2$@NiAl-LDHs) composite electrode (Fig. 10(a)) and the SEM image is shown in Fig. 10(b). The QD-$Ti_3C_2Cl_2$@NiAl-LDH electrode displayed a 2010.8 F g^{-1} specific capacitance at 1.0 A g^{-1}. (Fig. 10(c)). The capacitance retention reached 94.1% after 10 000 cycles at 1.0 A g^{-1} (Fig. 10(d)). Wu *et al.*[184] used an electrostatic assembly method to establish a 2D structure between MXene modified with the cetyltrimethylammonium bromide cation (CTAB) and NiCo-LDHs modified with the dodecyl benzenesulfonic acid anion. Composite electrodes are assembled with each other (Fig. 10(e)). In this case, the self-stacking of MXene and NiCo-LDHs nanosheets is effectively prevented, resulting in a regular interlayer structure and large interlayer spacing, accelerating the movement of electrolyte ions. Fig. 10(f) shows the SEM image of the MXene/NiCo-LDHs. At 0.5 A g^{-1}, the specific capacitance of the electrode is 1207 F g^{-1} (Fig. 10(g)), and the capacitance retention is 93% after 5000 cycles. In addition, its maximum energy density is 107.3 W h kg^{-1} (98.5 mW h cm^{-3}), and its power density is 571 W kg^{-1} (524 mW cm^{-3}). This remarkable electrochemical performance is mainly attributed to the hydration of 2D electrodes and the exchange or adsorption of anions between layers.

2.5 Miscellaneous methods

In addition to the conventional methods, there are a variety of other methods used to synthesize LDHs. The exfoliative recombination method has the advantages of being a simple process with mild conditions and the disadvantage of its parameters being very hard to control. LDHs with better performances can be obtained by regulating the experimental parameters reasonably. NiCr LDHs and polyoxotungstate nanoclusters (NiCr-LDHs-POW) were fabricated by Padalkar *et al.*[185] using an exfoliative recombination method, as shown in Fig. 11(a). The intercalation of POW nanoclusters forms a stacked framework layer by layer, obtaining a high specific surface area interconnected lamellar morphology, increasing ion transport channels and facilitating the diffusion of electrolyte ions between the layers. Alkaline etching is another simple and efficient method to increase the porosity of aluminum-containing layered double hydroxyl talc. Wang *et al.*[186] synthesized NiTiAl-LDHs by adding a trace amount of Al to the NiTi-LDHs substrate layer and then etching some Al with a sodium hydroxide solution, resulting in higher specific surface area, specific capacitance and rate performance of supercapacitor electrodes. The microwave synthesis method has the advantages of high heating rate, high thermal energy utilization, and good crystallinity and dispersion of the synthesized materials. However, this method has high requirements for equipment. Considering the condition of using this method fully, it can be combined with other methods. Wang *et al.*[187] synthesized 3D hollow NiCo-LDHs with interlaced nanosheets in the shell layer using ZIF-67 as a template by microwave treatment (Fig. 11(b)). As an electrode material, NiCo-LDHs have a 2369.0 F g^{-1} specific capacitance at 0.5 A g^{-1}, as well as multiplicative performance, more exposed active sites and synergistic interaction between the Ni-Co ions facilitating ion transport and diffusion. In addition, the assembled NiCo LDHs//AC device has 83.6% capacitance retention after 10 000 cycles. Besides, Chu *et al.*[188] integrated CuCo-LDH nanoarrays onto NF by an *in situ* hydrolysis approach (Fig. 11(c)). The resulting CuCo-LDHs//AC asymmetric supercapacitor exhibits an energy density of 22 W h kg^{-1}. This approach provides a new idea for the preparation of superior supercapacitor electrode materials in the future.

In order to more visually demonstrate the properties of LDHs and their corresponding composites prepared by different preparation methods, the advantages and disadvantages of different preparation methods are shown in Table 1. Concurrently, the properties of LDHs and their composite electrodes mentioned in this manuscript are exhibited in Table 2, and the properties of devices consisting of LDHs and their composites mentioned in this manuscript are shown in Table 3.

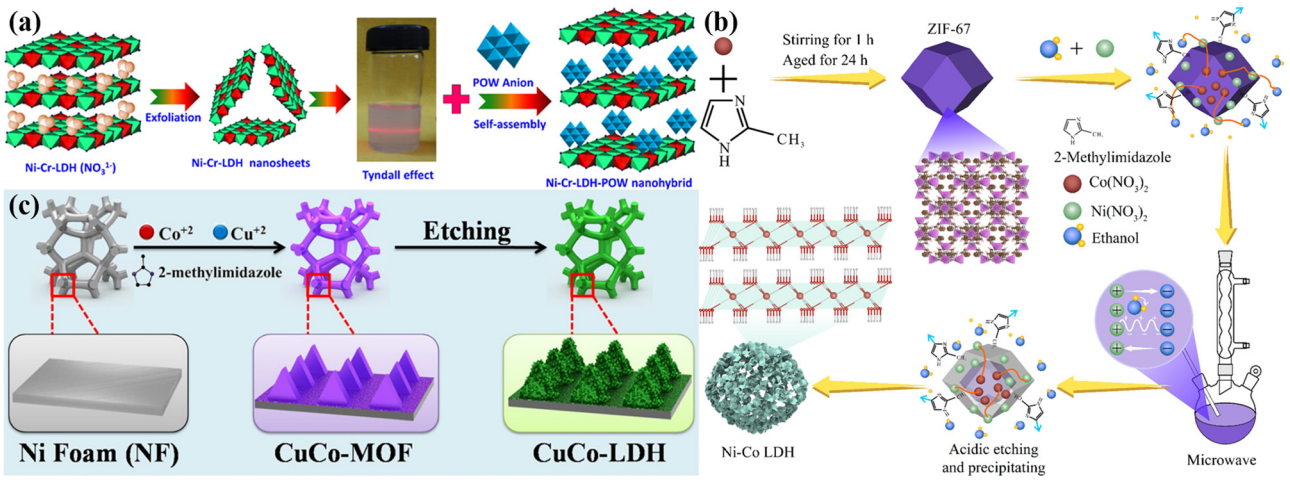

Fig. 11 (a) Schematic diagram of the exfoliation-reassembling route to NiCr-LDH nanohybrids. Adapted with permission from ref. 185 Copyright 2022, Elsevier Inc (b). Schematic illustration of the synthesis procedures of NiCo-LDH nanocages. Adapted with permission from ref. 187 Copyright 2022, Elsevier B.V. (c) Schematic illustration of the synthesis strategy and morphological characterization of CuCo-LDHs. Adapted with permission from ref. 188 Copyright 2022, American Chemical Society.

Table 1 Comparison of the advantages and disadvantages of different preparation methods

Preparation methods	Advantage	Disadvantage
Co-precipitation	This method has been widely used in practice because of its simplicity, cheapness and stability of the product.	The addition of the precipitating agent during the preparation process may cause local concentration too high and lead to the agglomeration of product.
Hydrothermal and solvothermal	The reaction environment is closed and stable with strong controllability, and the prepared product has crystal structure integrity and narrow particle size distribution.	The high-pressure reactor can only adjust the external environment temperature, and the internal temperature and pressure are difficult to monitor.
Electrodeposition	This method can be applied to obtain LDH materials with various grain sizes.	The generation and growth rate of nuclei on the substrate surface cannot be controlled.
Electrostatic interstratification	This method can generate a sandwich-like electrostatic layer between LDHs with positive charges and 2D thin materials with negative charges, which can achieve better conductivity and superior electrochemical properties.	Two materials with different charges need to be carefully searched.
Exfoliative recombination	It is a simple process with mild conditions.	The parameters are very hard to control.
Alkaline etching	Improve the sample porosity.	Strict control of experimental conditions.
Microwave synthesis	High heating rate, high thermal energy utilization, and good crystallinity and dispersion of the synthesized materials.	High requirements for equipment.
In situ hydrolysis	Simple and easy to use.	Longer time consumption.

3. Modification method of hybrid LDHs

The modification of LDHs is particularly important for overcoming disadvantages including low specific capacitance and poor cycling stability, which can be carried out based on the various synthetic methods described earlier, starting from the basic properties of the material and modifying it compositionally and structurally to improve their performances in electrochemical applications.[189–192] Since LDHs have a 2D layered structure, compounding with various 1D and 2D nanomaterials such as carbon nanotubes, graphene and MoS_2 is highly feasible, and the addition of polymerase also enhances the conductivity.[193–195] In hybridized LDH nanostructures, the construction of ionic vacancy defects[196,197] and porous structures can alter the crystalline shape and increase the active sites, allowing for a superior level of electrochemical performances. In addition, metal sapphires and

Table 2 The properties of LDHs and their composite electrodes mentioned in this manuscript

Method	Electrode	Electrolyte	Capacitance	Condition	Cycles	Ref.
Co-Precipitation	Zn Al-LDHs	6 M KOH	37.0 F g^{-1}	1 A g^{-1}	—	125
Co-Precipitation	Ni Fe-LDHs	2 M KOH	1368 F g^{-1}	1 A g^{-1}	5000, 87.5%	126
Co-Precipitation	Ni Co-LDHs	2 M KOH	1970 F g^{-1}	1 A g^{-1}	—	127
Co-Precipitation	P@NiCo-LDHs	6 M KOH	536 C g^{-1}	1 A g^{-1}	5000, Rarely decrease	128
Co-Precipitation	$Zn_{0.25}Ni_{0.75}Co$-LDHs-BA^-	2 M KOH	1378 mA h g^{-1}	1 A g^{-1}	10 000, 91.2%	130
Co-Precipitation	S-NiCoAl-LDHs	1 M KOH	727.1 C g^{-1}	1 A g^{-1}	10 000, 95.1%	131
Co-Precipitation	HC@NiCo-LDHs	2 M KOH	758 C g^{-1}	2 A g^{-1}	—	132
Hydrothermal	NiCoAl-LDHs@$NiCo_2S_4$@CC	6 M KOH	1775 F g^{-1}	1 A g^{-1}	10 000, 79.6%	145
Solvothermal	$CuBr_2$@NCC-LDHs/CF	6 M KOH	5460 mF cm^{-2}	2 mA cm^{-2}	5000, 88%	150
Hydrothermal	NC/S-15	2 M KOH	267.8 mA h g^{-1}	1 A g^{-1}	2000, 70.4%	151
Hydrothermal	$NiCo_2S_4$@NiMn-LDHs	2 M KOH	822.64 C g^{-1}	50 mA cm^{-2}	5000, 92.7%	147
Solvothermal	NiAl-LDHs-S	6 M KOH	1680 F g^{-1}	1 A g^{-1}	—	152
Solvothermal	NiMn-LDHs/hrGO	2 M KOH	302 C g^{-1}	1 A g^{-1}	2000, 89.6%	148
Solvothermal	CCO@NiCo-LDHs	3 M KOH	1652 F g^{-1}	1 A g^{-1}	10 000, 72.5%	149
Solvothermal	Se-NiAl-LDHs	6 M KOH	1098 F g^{-1}	1 A g^{-1}	—	153
Solvothermal	NiCoAl-LDHN-9	6 M KOH	1228.5 F g^{-1}	1 A g^{-1}	—	143
Solvothermal	NF@NiCo-LDHs	3 M KOH	4392 F g^{-1}	0.44 A g^{-1}	10 000, 64.2%	146
Solvothermal	Ag/CoAl-LDHs	2 M KOH	1214 C g^{-1}	3 A g^{-1}	10 000, 91%	154
Electrodeposition	NiCo-LDHs@MoO_3/NF	2 M KOH	952.2 C g^{-1}	1 A g^{-1}	10 000, 86.42%	164
Electrodeposition	NiCoFe-LDHs	3 M KOH	3800 mC cm^{-2}	4 mA cm^{-2}	4000, 149%	167
Electrodeposition	EGP@NiCo-LDHs	2 M KOH	1650 F g^{-1}	1 A g^{-1}	—	168
Electrodeposition	O_v-NiCo-LDHs	3 M KOH	1160 C g^{-1}	1 A g^{-1}	5000, 73.5%	169
Electrodeposition	MoO_{3-x}@NiCo-LDHs	0.5 M K_2SO_4	3.49 F cm^{-2}	5 mA cm^{-2}	3000, 94.5%	165
Electrodeposition	$MnCo_2O_4$@NiCo-LDHs/NF	6 M KOH	4555 F g^{-1}	1 A g^{-1}	5000, 78.7%	170
Electrodeposition	NiCo-LDHs@Ni-NTNW	1 M KOH	1202.2 F g^{-1}	0.2 mA cm^{-2}	4000, 106%	166
Electrodeposition	$FeCoSe_2$@NiCo-LDHs	2 M KOH	220.9 mA h g^{-1}	1 A g^{-1}	5000, 82.8%	171
Electrostatic interstratification	QD-$Ti_3C_2Cl_2$@NiAl-LDHs	1 M KOH	2010.8 F g^{-1}	1 A g^{-1}	10 000, 94.1%	183
Electrostatic interstratification	MXene/NiCo-LDHs	1 M $(NH_4)_2SO_4$	1207 F g^{-1}	0.5 A g^{-1}	5000, 93%	184
Exfoliative recombination	NCW-2	2 M KOH	736 C g^{-1}	1 A g^{-1}	5000, 86%	185
Alkaline etching	NTA18	1 M KOH	3483 mF cm^{-2}	5 mA cm^{-2}	3000, 37.9%	186
Microwave treatment	Ni-Co LDHs	1 M KOH	2369.0 F g^{-1}	0.5 A g^{-1}	—	187
In situ hydrolysis	CuCo-LDHs	1 M KOH	433 C g^{-1}	1 A g^{-1}	10 000, 82.46%	188

Table 3 Properties of devices consisting of LDHs and their composites mentioned in this manuscript

Devices	Electrolyte	Capacitance	Energy density at power density	Cycles	Ref.
NiFe-LDHs//NiFe-LDHs	2 M KOH	186 F g^{-1}, 1 A g^{-1}	66.13 W h kg^{-1} at 1483 W kg^{-1}	—	126
NiCo-LDHs//AC	2 M KOH	186 F g^{-1}, 1 A g^{-1}	54.8 W h kg^{-1} at 374.9 W kg^{-1}	10 000, 80.8%	127
P@NiCo-LDHs//P@NiCo-LDHs	PBI-KOH	—	7.83 W h kg^{-1} at 300 W kg^{-1}	10 000, 80%	128
$Zn_{0.25}Ni_{0.75}Co$-LDHs-BA^{-}//AC	2 M KOH	65 mA h g^{-1}, 1 A g^{-1}	51.8 W h kg^{-1} at 789 W kg^{-1}	10 000, 94.6%	130
S-NiCoAl-LDHs//AC	PBI-KOH	182.6 F g^{-1}, 0.5 A g^{-1}	82.2 W h kg^{-1} at 450 W kg^{-1}	10 000, 92.5%	131
HC@NiCo-LDHs//AC	2 M KOH	148 C g^{-1}, 0.4 A g^{-1}	32.8 W h kg^{-1} at 320 W kg^{-1}	4000, 70.2%	132
NiCoAl-LDHs@$NiCo_2S_4$@CC//AC	PVA-KOH	106 F g^{-1}, 1 A g^{-1}	33.13 W h kg^{-1} at 750 W kg^{-1}	10 000, 71.4%	145
$CuBr_2$@NCC-LDHs/CF//AC	6 M KOH	118 F g^{-1}, 0.4 A g^{-1}	118 W h kg^{-1} at 1013 W kg^{-1}	5000, 86.7%	150
NC/S-15//AC	2 M KOH	126.76 F g^{-1}, 1 A g^{-1}	43.6 W h kg^{-1} at 375 W kg^{-1}	5000, 83%	151
$NiCo_2S_4$@NiMn-LDHs//AC	2 M KOH	96.23 F g^{-1}, 50 mA cm^{-2}	53.10 W h kg^{-1} at 370.82 W kg^{-1}	10 000, 94.3%	147
NiAl-LDHs-S//AC	6 M KOH	100.64 F g^{-1}, 2 A g^{-1}	35.78 W h kg^{-1} at 1127.03 W kg^{-1}	10 000, 104.37%	152
NiMn-LDHs/hrGO//$Bi(OH)_3$/hrGO	2 M KOH	237.6 C g^{-1}, 1 A g^{-1}	59.9 W h kg^{-1} at 901.5 W kg^{-1}	2000, 80.51%	148
CCO@NiCo-LDHs//AC	3 M KOH	37.67 F g^{-1}, 0.5 A g^{-1}	42.38 W h kg^{-1} at 1350 W kg^{-1}	10 000, 80%	149
Se-NiAI-LDHs//AC	6 M KOH	80 F g^{-1}, 2 A g^{-1}	29 W h kg^{-1} at 1593.17 W kg^{-1}	5000, 95.24%	153
NiCoAl-LDHsN-9//AC	PVA-KOH	102.1 F g^{-1}, 0.5 A g^{-1}	35.9 W h kg^{-1} at 225.8 W kg^{-1}	10 000, 87.1%	143
NF@NiCo-LDHs//AC	3 M KOH	152.3 F g^{-1}, 1 A g^{-1}	51.1 W h kg^{-1} at 777 W kg^{-1}	10 000, 72.2%	146
Ag/CoAl-LDHs//N-CNTs	2 M KOH	275 C g^{-1}, 1 A g^{-1}	61.2 W h kg^{-1} at 800 W kg^{-1}	10 000, 92%	154
NiCo-LDHs@MoO_3/NF//AC	2 M KOH	261.3 C g^{-1}, 1 A g^{-1}	58.06 W h kg^{-1} at 800 W kg^{-1}	10 000, 85.57%	164
NiCoFe-LDHs//AC	3 M KOH	207 F g^{-1}, 1 mA cm^{-2}	65 W h kg^{-1} at 83 W kg^{-1}	5000, 126%	167
EGP@NiCo-LDHs//AC	2 M KOH	124.63 F g^{-1}, 1 A g^{-1}	44.31 W h kg^{-1} at 799.98 W kg^{-1}	5000, 92.8%	168
O_v-NiCo-LDHs//O_v-NiCo-LDHs	3 M KOH	168.9 F g^{-1}, 2 A g^{-1}	216.19 W h kg^{-1} at 1.75 kW kg^{-1}	2000, 71.45%	169
MoO_{3-x}@NiCo-LDHs//MoO_{3-x}@NiCo-LDHs	0.5 M K_2SO_4	0.45 F cm^{-2}, 2 mA cm^{-2}	0.047 mW h cm^{-2} at 0.865 mW cm^{-2}	—	165
$MnCo_2O_4$@NiCo-LDHs/NF//AC	6 M KOH	60 F g^{-1}, 0.2 A g^{-1}	21.3 W h kg^{-1} at 160.0 W kg^{-1}	5000, 86.6%	170
NiCo-LDHs@Ni-NTNW//AC	1 M KOH	64.9 F g^{-1}, 1 mA cm^{-2}	14.7 mW h cm^{-2} at 4769 mW cm^{-2}	20 000, 120%	166
$FeCoSe_2$@NiCo-LDHs//PPC-2	2 M KOH	95.2 mA h g^{-1}, 1 A g^{-1}	1.248 kW kg^{-1} at 65.9 W h kg^{-1}	10 000, 87.6%	171
NCW-2//rGO	2 M KOH	120 F g^{-1}, 2 A g^{-1}	43 W h kg^{-1} at 1.3 kW kg^{-1}	10 000, 89%	185
NTA18//AC	1 M KOH	126 F g^{-1}, 1 A g^{-1}	45.1 W h kg^{-1} at 16000 W kg^{-1}	5000, 59%	186
Ni-Co LDHs//AC	1 M KOH	68.1 F g^{-1}, 0.5 A g^{-1}	21.28 W h kg^{-1} at 375.09 W kg^{-1}	10 000, 83.6%	187
CuCo-LDHs//AC	1 M KOH	76 F g^{-1}, 1 A g^{-1}	22 W h kg^{-1} at 23200 W kg^{-1}	10 000, 91.3%	188

phosphides have higher metallic properties than LDHs, and LDHs can be modified with them to form composites.[198,199] In general, the improved performances of the hybrid nanostructures result from the synergistic effect of the heterogeneous interface formed between LDHs and other objects. In this chapter the modification methods for hybridized LDH nanostructures are divided into four categories: addition of components, construction of defects, generation of heterogeneous structures and direct generation on the substrate.[200,201] All these methods provide a larger surface area and expose a greater number of active sites. It is important to note, however, that each method provides different structural effects, which have a different impact on the electrochemical properties of the hybridized LDHs.

3.1 Addition of components

The addition of other components to the original LDHs can change the composition and structure of the material.[202] This behavior during the synthesis processes can increase the synergy between the substances and can also modify the structure of materials, and some intercalation substances can also improve the electrochemical properties.[203–207] However, the application of this modification method needs to consider the force between raw materials. A certain theoretical study for this method can have an unexpected effect.[208] The preparation of composites with different components is a meaningful route to obtain new and efficient electrode materials.[209] Ma *et al.*[210] prepared Ni-embedded carbon nanofibers/NiAl-LDH hybrids. First, Ni-containing carbon nanofibers were skillfully fabricated *via* electrostatic spinning and thermal treatment, which provided many active sites and increased the space for ion transport. Subsequently, Ni-embedded carbon nanofibers were combined with nanostructured NiAl-LDHs by the hydrothermal method (Fig. 12(a)). The results showed that the former could optimize the microstructure of NiAl-LDHs, alleviate their aggregation and improve the multiplicative performances of NiAl-LDHs. 3% Ni-embedded carbon nanofibers/NiAl-LDHs (3%-Ni-C/NiAl-LDHs) achieved a 1228.2 C g^{-1} specific capacitance at 1 A g^{-1} (Fig. 12(b)). Besides, an asymmetric supercapacitor device was assembled with an energy density of 74.9 W h kg^{-1} at 800 W kg^{-1}. Notably, the device achieved a 91.4% capacity after 10 000 cycles at 6 A g^{-1} (Fig. 12(c)).

NiCo-LDHs have layer spacing and a high ion exchange capacity, but poor electrical conductivity, severe agglomeration and structural defects limit their energy storage capacity. Wu *et al.*[88] prepared zeolite imidazole framework-67 (ZIF-67) sulfur-doped NiCo-LDHs and polypyrrole nanotube composites (NiCo-LDHs-S/PNTs) for the first time by electrospinning and hydrothermal methods (Fig. 12(d)). The 1D hollow polypyrrole with a high aspect ratio provides straight charge-transfer routes and abundant contacts with the electrolyte. When the sulfur content is 7%, the specific capacitance of NiCo-LDH-S/PNTs is 1936.3 F g^{-1}. The device assembled by the graphene anode and the NiCo-LDH-S/PNT cathode achieves an energy density of 16.28 W h kg^{-1} at 650 W kg^{-1}. And the capacity retention rate reaches 74% after 8000 cycles.

Changes in the anions between the layers also influence the resulting performances. The layer spacing of different anion intercalated LDHs can vary, while a larger layer spacing

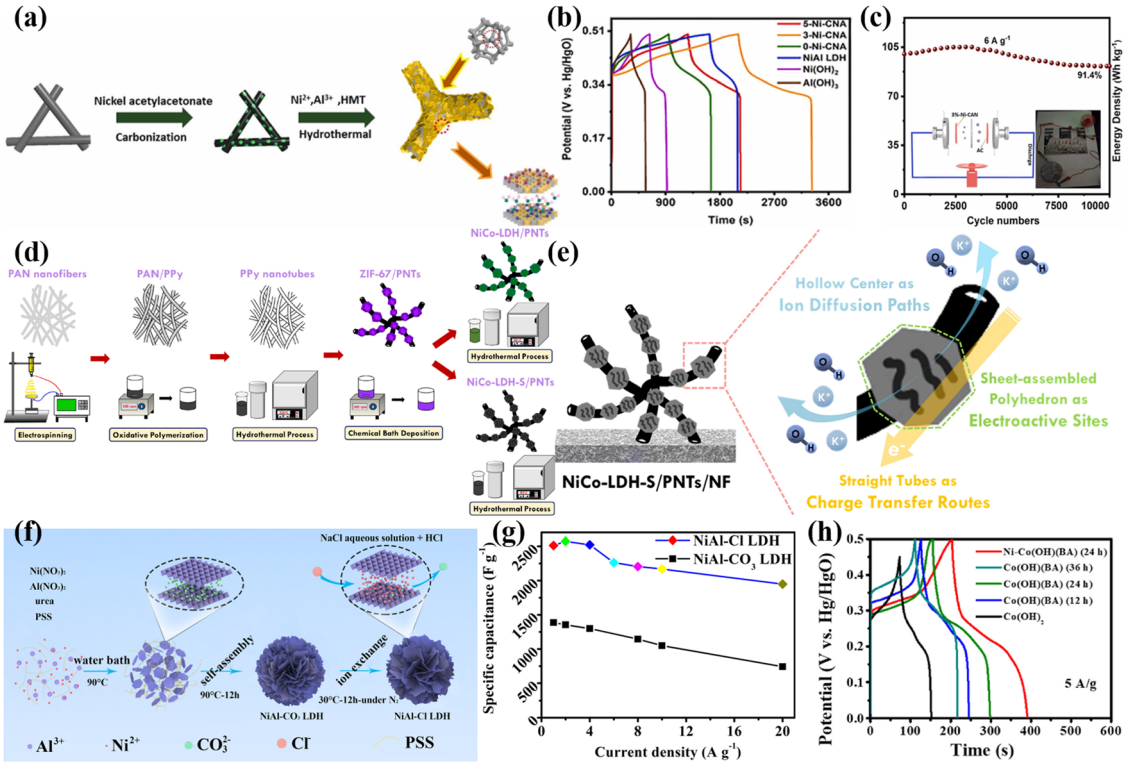

Fig. 12 (a) Detailed preparation strategy for obtaining hierarchical structure Ni-CAN, (b) the GCD curves of the as-obtained samples at 1 A g^{-1} with the potential window of 0–0.5 V, (c) cycling performance of 3%-Ni-C/NiAl-LDHs//AC at 10 A g^{-1}. Adapted with permission from ref. 210 Copyright 2022, Elsevier B.V. (d) Illustration of the synthesis processes of NiCo-LDHs/PNTs and NiCo-LDHs-S/PNTs, (e) illustration of morphology features of NiCo-LDHs-S/PNTs/NF. Adapted with permission from ref. 88 Copyright 2022, Elsevier Inc. (f) Specific capacitance of NiAl-CO_3 LDH and NiAl-Cl LDH electrodes at a variety of current densities. (g) Specific capacitance of two electrodes at different current densities. Adapted with permission from ref. 211 Copyright 2022, Elsevier Ltd. (h) GCD curves of those electrodes at a current density of 5 A g^{-1}. Adapted with permission from ref. 212 Copyright 2022, Elsevier Ltd.

facilitates the contact between the active atoms on the LDH plate layer and OH^-, resulting in improved electrochemical properties. A spherical NiAl-Cl LDH with chloride ions as interlayer anions was prepared by Lv *et al.*[211] with a specific capacitance of 2512 F g^{-1} at 1 A g^{-1}. NiAl-Cl LDHs have a wider interlayer spacing, which promotes contact between the active atoms of the hydro magnesite-like layers and OH^-, improves electron transport kinetics, increase the utilization of the active material and exhibit better multiplicative performance (the specific capacitance at 20 A g^{-1} is 77.5% of that at 1 A g^{-1}). At the same time, the gaps between the interlaced hierarchical structures facilitate the buffering of volume changes during the reaction, ensuring the structural stability of NiAl-Cl LDHs during the redox reaction. They were also compared to materials with carbonate ions as interlayer anions, and the results showed superior performances of NiAl-Cl LDHs (Fig. 12(g)). The energy density of the prepared NiAl-Cl LDHs//AC asymmetric supercapacitor was 53.9 W h kg^{-1} at 1540 W kg^{-1} and maintained 94.1% specific capacitance after 1000 cycles.

Deng *et al.*[212] used the hydrothermal method to prepare benzoate anion intercalated nickel-doped inorganic organic cobalt hydroxide ultrathin nanoribbons Ni-Co(OH)(BA) without the use of binders and surfactants, and the electrochemical performance was effectively improved due to the large interlayer distance and enhanced ion flow efficiency. The results show a 1664 F g^{-1} specific capacitance at 5 A g^{-1} (Fig. 12(h)) and an 83% capacity retention after 8000 cycles. At the same time, the composed Ni-Co(OH)(BA)//AC asymmetric supercapacitor device was able to provide a 47.5 W h kg^{-1} energy density at 850 W kg^{-1} and a 91% capacity retention after 8000 cycles. Saber *et al.*[213] inserted silicon into Co-LDH nanospheres to form Si/Co-LDH nanofibers by inserting cyanate anions as the backbone for building the nanospheres. The structure can be tuned through controlling the preparation conditions and Si content to further improve the properties. The results show that morphological changes from nanoparticles or flat plates to nanofibers enhance the specific capacitive performances of Si/Co-LDHs. The specific capacitance was increased to 621.5 F g^{-1} and the cycling stability was 84.5%. The outcomes can be explained by the properties of the nanofiber morphology and the cooperation effect from capacitive properties of Si and pseudocapacitive properties of C.

The size of the layer spacing of LDHs is one of the key factors affecting their electrochemical properties, and increasing the layer spacing by suitable methods can greatly improve the performances. The composites based on Ni-Cr-LDHs and polyoxotungstate nanoclusters (Ni-Cr-LDHs-POW) were fabricated by Padalkar *et al.*[185] using exfoliative recombination. The interlayer intercalation hybridization of POW nanoclusters in

Ni-Cr-LDHs forms the cumulate frame (Fig. 13(a)) and significantly enlarges the spacing between layers. An NCW-2//rGO AHSC device (Fig. 13(b)) was assembled with the Ni-Cr-LDHs-POW nanohybrid material as the positive electrode. The energy density at 1.32 kW kg^{-1} is 34 W h kg^{-1}, and the capacitance retention after 10 000 charge–discharge cycles is 86%. Mahmood *et al.*[214] designed a unique synthesis strategy based on polyaniline-doped 2D cobalt–iron LDH (CoFe-LDHs/P) nanomaterials. The results showed that PANI was combined with CoFe-LDHs nanoparticle to form nanopore structure. The ordered pores increase the redox sites and promote the efficient movement of ions. The optimized CoFe-LDHs/P2 displays a 1686 F g^{-1} specific capacitance at 1 A g^{-1} (Fig. 13(d)) and exhibits excellent cycling stability (98% over 10 000 cycles). Furthermore, an asymmetric aqueous device (CoFe-LDHs/P2//AC) was prepared with an energy density of 75.9 W h kg^{-1} at 1124 W kg^{-1}, as well as 97.5% stability after 10 000 cycles.

Deng *et al.*[215] synthesized a hierarchical array of scaled trimetallic hydroxides (CuCoNi-OH) under a moderate alkaline hydrolysis strategy through rational nanostructure design using a bimetallic 2D zeolite imidazole framework (CuCo-ZIF-L) as a template (Fig. 13(g)). The hierarchical porous structure provides large active sites and promotes rapid ion diffusion, and the synergistic multi-metal effect provides high electrical conductivity and favors redox conversion, facilitating the electrochemical kinetics of the supercapacitor. As a battery-type electrode, the CuCoNi-OH electrode possesses a specific capacitance of 821.6 C g^{-1} at 1 A g^{-1} and a capacity retention of 89.8% at 20 A g^{-1} (Fig. 13(e)). The assembled device has a remarkable energy density and power density. The strategy is universal in the preparation of bimetallic ZIF-L and the corresponding metal hydroxides and provides an effective approach to rationally design electrochemical storage and conversion materials. Wang *et al.*[186] synthesized NiTiAl-LDHs by adding a trace amount of Al to the NiTi-LDH substrate layer and then etching some Al with sodium hydroxide solution, resulting in higher specific surface area, specific capacitance and rate properties. The specific surface area of the samples after 18 h of etching reached 203 m^2 g^{-1} and the specific capacitance at 5 mA cm^{-2} was up to 3483 mF cm^{-2} (Fig. 13(f)), and better structural stability than that of the NiTi-LDHs. The hybrid devices assembled from the etched samples exhibited an energy

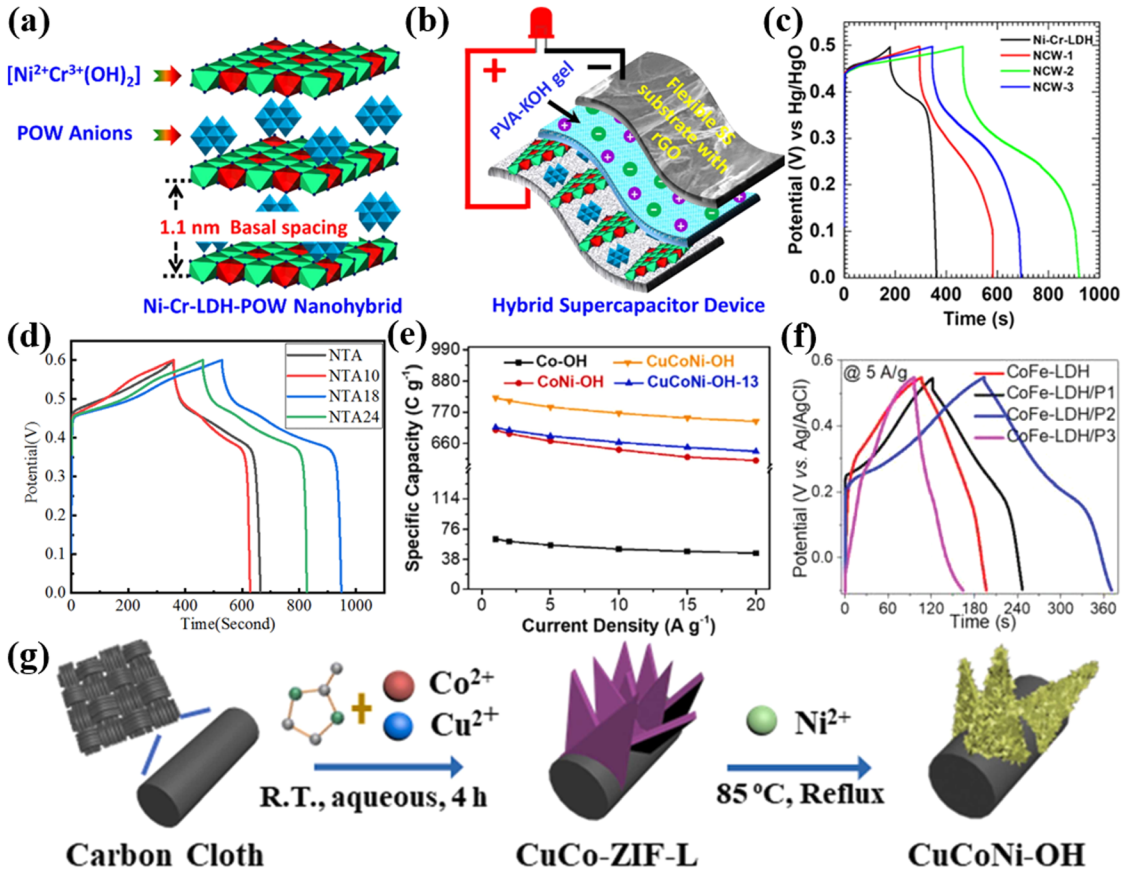

Fig. 13 (a) Structural schematic model of the NCW nanohybrid, (b) NCW-2//rGO AHSC assembly diagram, (c) GCD curves of pristine Ni-Cr-LDHs and NCW nanohybrids at 1 A g^{-1}. Adapted with permission from ref. 185 Copyright 2022, Elsevier Inc. (d) GCD curves of different materials at 5 mA cm^{-2}. Adapted with permission from ref. 186 Copyright 2021, Elsevier B.V. (e) Corresponding specific capacitance of hydroxide electrodes at 1–20 A g^{-1}. Adapted with permission from ref. 215 Copyright 2022, Elsevier B.V. (f) GCD curves of CoFe-LDHs/P2 electrode. Adapted with permission from ref. 214 Copyright 2022, Wiley-VCH GmbH. (g) Schematic of the synthesis procedures of CuCo-ZIF-L and CuCoNi-OH. Adapted with permission from ref. 215Copyright 2022, Elsevier B.V.

density of 45.1 W h kg^{-1} at 16 000 W kg^{-1}. This alkaline etching method can improve the porosity of aluminum-containing layered dihydroxy talc, promote the specific capacitance and rate performance, and has a more promising application.

The rational design of highly porous structures with large specific surface areas to facilitate ion/electron transport and insertion/de-insertion is an effective route to improve electrochemical redox reactions in materials. However, challenges such as unsatisfactory energy storage exist due to the simplicity of the porous structure and severe performance degradation during long-term electrochemical cycling occurs. Inspired by the natural geographical structure of forests, Liu *et al.*[216] designed Ni/Co-LDHs on a metal-organic framework of ZnO nanotubes grown on transparent conducting substrates with different porous structures to simulate a "rock-soil-tree-leaf" system (Fig. 14(a)). Due to the high specific surface area of 3D ZnO@Ni/Co-LDHs, the enhanced OH^- trapping ability of ZnO, the enhanced electrochemical activity due to Ni/Co doping, and the hybrid charge storage behavior, excellent specific capacitance and durability are achieved. Of the five ZnO@Ni/Co-LDH films, LDH-3 exhibits remarkable conductivity and energy storage performances, with a charge capacity of 507.2 C g^{-1} at 0.1 mA cm^{-2} and a capacity retention of 72.1% after 10 000 cycles, and LDH-3-based devices have excellent durability, with an energy density of 7.7 μW h cm^{-2} at 375.0 pW cm^{-2}. The prepared ZnO@Ni/Co-LDH device allows for automatic optical switching through solar energy harvesting and charge storage/release. These new insights will pave the way for the next generation of smart technologies towards a sustainable and habitable future.

Zhou *et al.*[217] synthesized ultrathin cobalt–nickel–magnesium LDH (CoNiMg-LDH) nanosheets with abundant oxygen vacancies at room temperature through a sacrificial magnesium-based replacement reaction (Fig. 14(b)). The self-doping and the mild reduction of magnesium improve the concentration of oxygen vacancies, improve the electrochemical charge transfer efficiency, and enhance the adsorption capacity of the electrolyte. Density functional theory (DFT) calculations indicate that Mg^{2+} doping reduces the generation energy of oxygen vacancies, thereby increasing the concentration of oxygen vacancies. Moreover, the CoNiMg-LDH//AC device exhibits a specific capacitance of 333 C g^{-1} at 1 A g^{-1} and an energy density of 73.9 W h kg^{-1} at 0.8 kW kg^{-1}. After 5000 cycles, there is only 13% capacity loss. This finding highlights the positive role of Mg in regulating oxygen vacancies for enhanced supercapacitor performances, which is beneficial to expand the range of high-quality supercapacitor active materials. Wang *et al.*[218] achieved high loading and high capacitance performance by one-step hydrothermal loading of NiMn-LDHs on NF using sodium dodecyl sulfate (SDS) as an intercalator and soft template. The electrode added with 4 mM SDS had an area capacitance of up to 6311 mF cm^{-2} at 5 mA cm^{-2}. The hybrid supercapacitor assembled with this electrode had an energy density of 34.61 W h kg^{-1} at 831 W kg^{-1} and a capacitance retention of 129% at 4 A g^{-1} after 5000 cycles and 85% after 10 000 cycles at 10 A g^{-1}. Li *et al.*[219] successfully fabricated soluble graphite nitride (SCN) nanosheets NiFe-LDHs by electrostatic self-assembly (Fig. 14(d)) as a one-layer high performance electrode (NiFe-LDHs@SCN) for supercapacitors. The optimized structure has a specific capacitance of 1060.4 F g^{-1} at 1 A g^{-1}. The prepared hybrid supercapacitor has an energy density of 68.7 W h kg^{-1} at 827.5 W kg^{-1} and has a 83.3% capacitance after 8000 cycles.

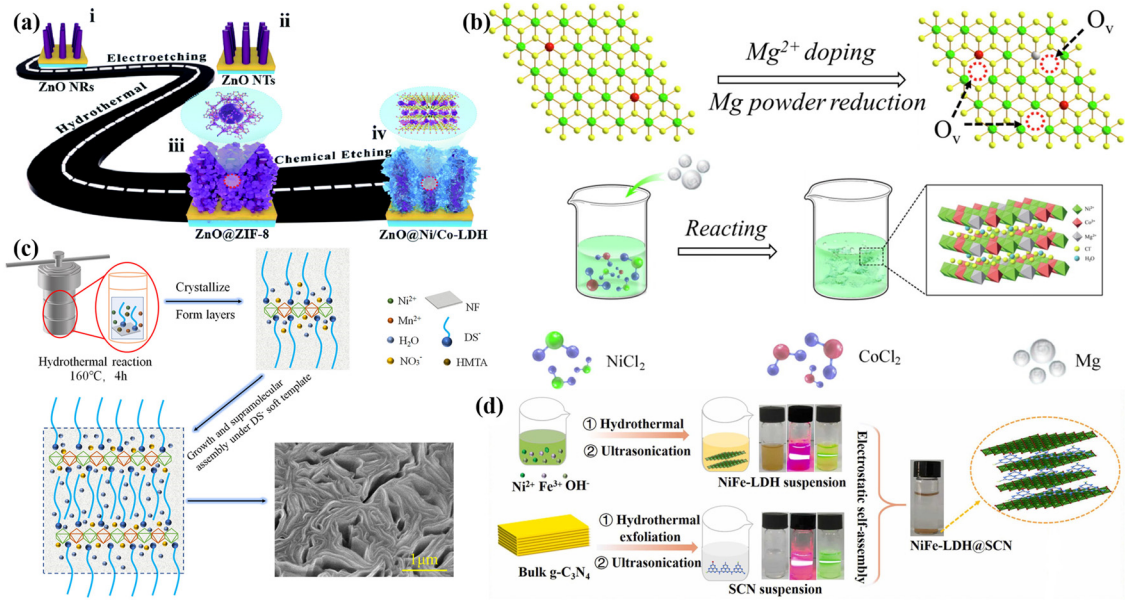

Fig. 14 (a) Synthesis scheme of the ZnO@Ni/Co-LDH film. Adapted with permission from ref. 216 Copyright 2022, Royal Society of Chemistry. (b) Schematic illustration of the fabrication strategy of oxygen-vacancy abundant CoNiMg-LDHs. Adapted with permission from ref. 217 Copyright 2021, Elsevier Inc. (c) Growth mechanism of LDH with SDS as a soft template. Adapted with permission from ref. 218 Copyright 2022, Elsevier Ltd. (d) The synthetic process of the NiFe-LDH@SCN. Adapted with permission from ref. 219 Copyright 2022, Elsevier B.V.

3.2 Constructing defects in materials

Constructing defects is another promising approach to improve the electrochemical properties of LDHs as it modulates the electronic structure and increases the active sites.[220] This method can endow the materials with more holes, facilitating the electrolyte to enter the electrode materials. However, the condition of this method is difficult to control, and it is prone to form excessive defects. Hence, it is used to construct material defects by selecting suitable raw materials and controlling conditions.[221] Chu *et al.*[188] chose Cu element as a dopant to prepare CuCo-LDHs. The prepared structure was grown onto NF by *in situ* hydrolysis. Electron images of CuCo-LDHs are shown in Fig. 15(a and b). The addition of Cu obviously increases the density of local electron density, thereby improving the electronic conductivity and facilitating the charge transfer. CuCo-LDH electrodes provide excellent capacitive performance (Fig. 15(c and d)). The CuCo-LDHs//AC device showed a 22 W h kg^{-1} energy density of 22 W h kg^{-1} and a 91.3% stability after 10 000 cycles. This study has structurally tuned the LDH material to construct lattice defects to modify their performances, which have a very positive effect on the preparation of superior supercapacitor electrode materials in the future.

Lei *et al.*[222] synthesized NiCo-LDHs/NF (D-NiCo-LDHs/NF) based on the memory effect (Fig. 15(e)). DFT calculations reveal that Co vacancies induce more electrons to approach the Fermi energy level, thereby improving the conductivity and favoring the transfer of charge. The SEM image in Fig. 15(f) shows the microscopic morphology of D-NiCo-LDHs/NF, and the surface of NF is uniformly covered by vertically aligned NiCo-LDH nanosheets. The synthesized D-NiCo-LDHw/NF has a 3200 F g^{-1}

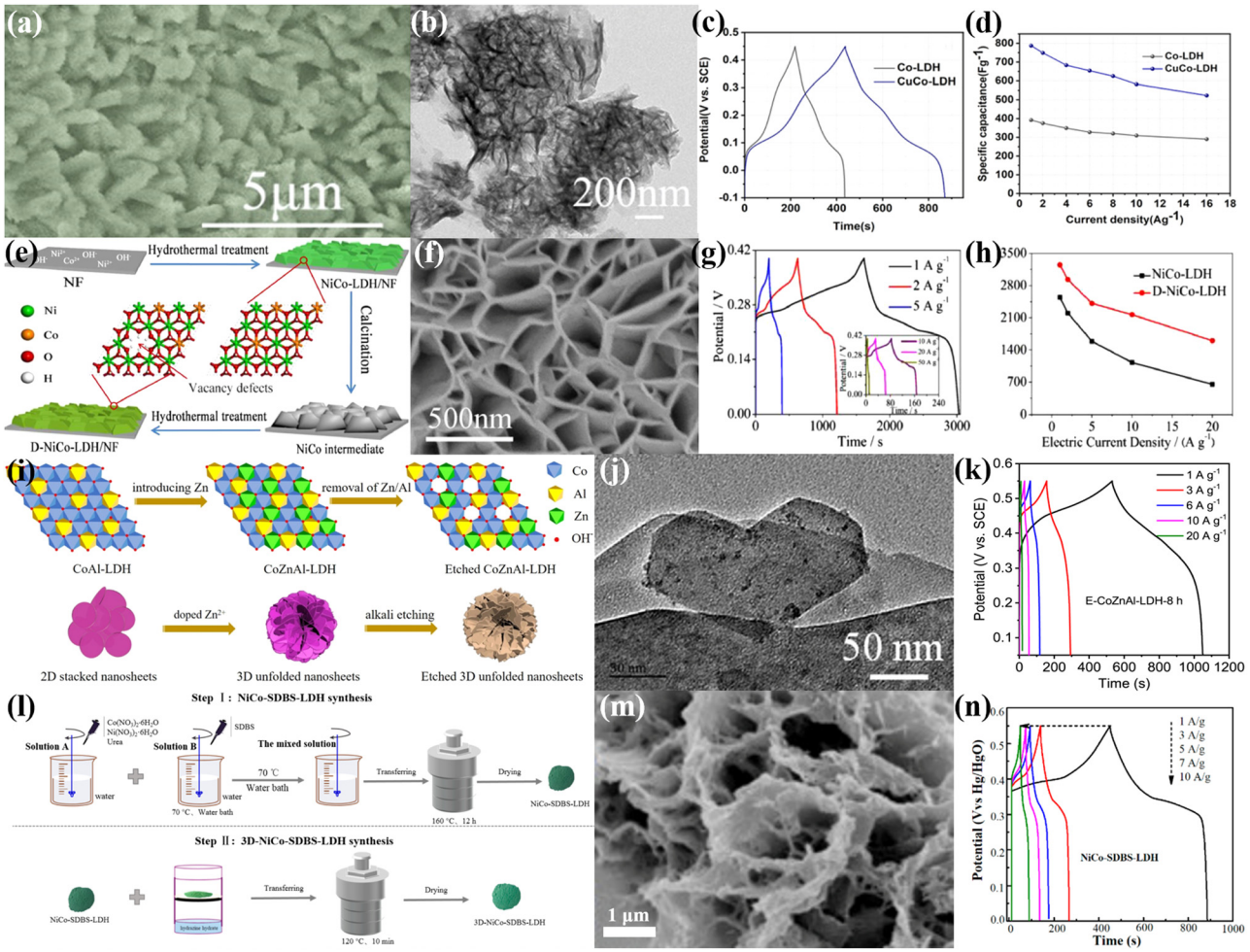

Fig. 15 (a) SEM image of CuCo-LDHs, (b) TEM image of CuCo-LDHs, (c) GCD curves, and (d) rate capability of Co-LDHs and CuCo-LDHs. Adapted with permission from ref. 188 Copyright 2022, American Chemical Society. (e) Schematic illustration of introducing vacancy defects to NiCo-LDHs through the memory effect, (f) SEM image of D-NiCo-LDHs/NF nanosheet arrays, (g) GCD curves of the D-NiCo-LDHs/NF electrode at different current densities, (h) capacitance retention of D-NiCo-LDHs/NF and NiCo-LDHs/NF electrodes at different current densities. Adapted with permission from ref. 222 Copyright 2022, Elsevier Ltd. (i) Zn^{2+} doped induced morphological change in CoAl-LDHs and Al/Zn dual ion etching of CoZnAl-LDHs in alkaline solution, (j) TEM image of E-CoZnAl-LDHs-8 h, (k) GCD curves of E-CoZnAl-LDHs-8 h at different scan rates and current densities. Adapted with permission from ref. 223 Copyright 2022, Elsevier Ltd. (l) Diagram of the synthesis of 3D-NiCo-SDBS-LDHs, (m) SEM image of 3D-NiCo-SDBS-LDHs at different magnifications, (n) GCD curves of NiCo-SDBS-LDHs at different scan rates and current densities. Adapted with permission from ref. 224 Copyright 2022, MDPI.

specific capacitance at 1 A g^{-1} (Fig. 15(g and h)). The asymmetric supercapacitor achieved an energy density of 53 W h kg^{-1} at 752 W kg^{-1} and a retention rate of 94.7% after 5000 cycles. Yang *et al.*[223] first transformed 2D dense CoAl-LDHs to 3D loosely stacked CoZnAl-LDHs using Zn^{2+} doping to induce morphological changes in LDHs (Fig. 15(i and j)). In addition, the partial dissolution of Zn/Al double ions between the LDH lamellae in alkaline solution resulted in a large change in the electronic environment of the Co surface and the generation of a certain concentration of oxygen defects in CoZnAl-LDHs. This case improves the multiplicative performance and cycling stability of CoZnAl-LDH nanosheets. Compared to unetched CoZnAl-LDHs, E-CoZnAl-LDHs-8 h has a 946 F g^{-1} specific capacitance at 1 A g^{-1} (Fig. 15(k)) and a 92.3% cycle life after (4000 cycles) The E-CoZnAl-LDHs-8 h//AC asymmetric supercapacitor was prepared with an energy density of 36.75 W h kg^{-1} at 400 W kg^{-1} and a 72.7% cycle life after 8000 cycles. The ''doping'' and ''double ion etching'' strategies proposed in this study provide theoretical guidance and experimental basis to develop supercapacitors with excellent properties.

Porous structures and surface defects are important factors in improving the performance of supercapacitors. Zhong *et al.*[224] prepared NiCo-SDBS-LDHs by a one-step hydrothermal method using sodium dodecylbenzene sulfonate (SDBS) as the anionic surfactant. Then, 3D connected porous flower-like 3D-NiCo-SDBS-LDH microspheres were designed and synthesized using the gas-phase hydrazine hydrate reduction method (Fig. 15(l)). The results show that hydrazine hydrate reduction not only introduces many pores, giving rise to the formation of oxygen vacancies, but also roughens up the surface of the microspheres (Fig. 15(m)). All these changes contribute to the electrochemical activity of 3D-NiCo-SDBS-LDHs, and the specific capacitance is 1148 F g^{-1} at 1 A g^{-1} (Fig. 15(n)) (about 1.46 times that of NiCo-SDBS-LDHs), and the retention rate after 4000 cycles is 94%. In addition, the assembled 3D-NiCo-SDBS-LDHs//AC device has an energy density of 800 W kg^{-1} at 73.14 W h kg^{-1} and a cycle life of 95.5% after 10 000 cycles.

For electrochemical materials, domain boundaries are considered to work as active sites because of their defect enrichment. Nevertheless, LDHs are easy to form single-crystal nanosheets caused by the 2D lattice.[225] Many research studies have been performed on designing layered structures for providing abundant active sites and speeding up mass transfer.[226] Ban *et al.*[226] proposed a method to introduce low-angle grain boundaries (LAGBs) in NiCo-LDH flakes. Construction of nanosheets is as cage-like structures with hollow structures by manufacturing defects (Fig. 16(a)). Both the hierarchical structure and the formation of grain boundaries are explained using the Ni^{2+}/Co^{2+} ratio during ''etch growth''. Domain boundary defects also lead to the preferential formation of oxygen vacancies. In addition, DFT calculations show that Co substitution plays a decisive role in fabricating lattice defects and forming domain boundaries. The prepared NiCo-LDHs-2 electrode material showed a significant increase in specific capacitance to 899 C g^{-1} at 1 A g^{-1}. The maximum energy density of the NiCo-LDHs-2//AC asymmetric capacitor was 101.1 W h kg^{-1} at 1.5 kW kg^{-1}.

Designing metal cation defects with a desired structure is a major challenge to improve the electrochemical performances. Wu *et al.*[220] designed ultrathin ZnNi-LDH nanosheets with Zn-rich vacancies uniformly anchored on a CuO nanowire backbone as high-performance capacitive electrodes by a zeolite imidazolium salt framework-8 derivatization method (Fig. 16(b)). The optimized V_{Zn}-deficient electrode achieved an area capacity of 3967 mF cm^{-2} at 2.0 mA cm^{-2}. Moreover, the maximum energy density of the device composed of V_{Zn}-deficient samples and AC was 1.03 mW h cm^{-3} and the power density was 9.3 mW cm^{-3}. The mechanistic study showed that V_{Zn} modulated the electronic structure of the ZnNi-LDH nanosheets sheets, promoting the electronic conductivity and surface Faraday reaction. This work reveals the role of metal cation defects in influencing the electrochemical activity at the atomic level. Coincidentally, Kim *et al.*[227] developed a lattice engineering route for concurrently controlling the defect and the porosity *via* tuning the elastic deformation and the chemical interactions of the nanosheets in restacking. The increase in the intercalation size and reduction in charge density effectively increases the oxygen vacancy content and improves the porosity amount. The defect-rich Co-Al-LDHs-NO_3-nanohybrids exhibit excellent performances as electrodes with a 2230 F g^{-1} specific capacitance of 2230 F g^{-1} at 1 A g^{-1}. Combined with DFT calculations, the observed good correlation between overpotential (capacitance) and defect content (stacking) number highlights the significance of the defect (stacking) structure in the optimization of energy function. Zhang *et al.*[228] prepared oxygen-rich 3D $Co_{0.50}$-$Ga_{0.50}$-LDHs assembled in porous ultra-thin nanosheets using a simple one-step method (Fig. 16(c)). This synthetic strategy introduced many holes in the ultrathin LDH nanosheets, resulting in a high concentration of oxygen vacancies in $Co_{0.50}$-$Ga_{0.50}$-LDHs. The synergistic effect of the oxygen vacancies and the introduced Ga ions enhances the adsorption of OH^- by the LDH nanosheets, conferring $Co_{0.50}$-$Ga_{0.50}$-LDHs with excellent properties for supercapacitors. The prepared LDHs achieve a specific capacitance of 0.62 C cm^{-2} at 10 mV s^{-1}. The $Co_{0.50}$-$Ga_{0.50}$-LDHs//AC asymmetric supercapacitors have excellent energy density and service life. This discovery also promotes the wider application of porous ultra-thin LDH nanosheets in energy storage and other fields.

3.3 Generation of heterogeneous structures

The construction of heterogeneous structures is another important strategy to enhance the electrochemical properties of LDHs.[229] The interfacial regions of heterogeneous structures can provide opportunities to enrich the number of active sites[230] and promote electron transfer.[231,232] And strong electronic interactions in the heterogeneous interfaces facilitate the enhancement of electronic and ionic conductivity[233] and redox reaction kinetics.[234] However, the tightness of the heterogeneous interface is difficult to control, and the existence of voids between the interfaces affects the electrochemical properties. Adding certain ingredients such as binders in the synthesis process might solve the tightness problem. Luo *et al.*[235] successfully synthesized layered $NiCo_2O_4$@NiFe-LDH heterostructures by sequential hydrothermal methods, heat treatment and electrodeposition, as positive electrodes

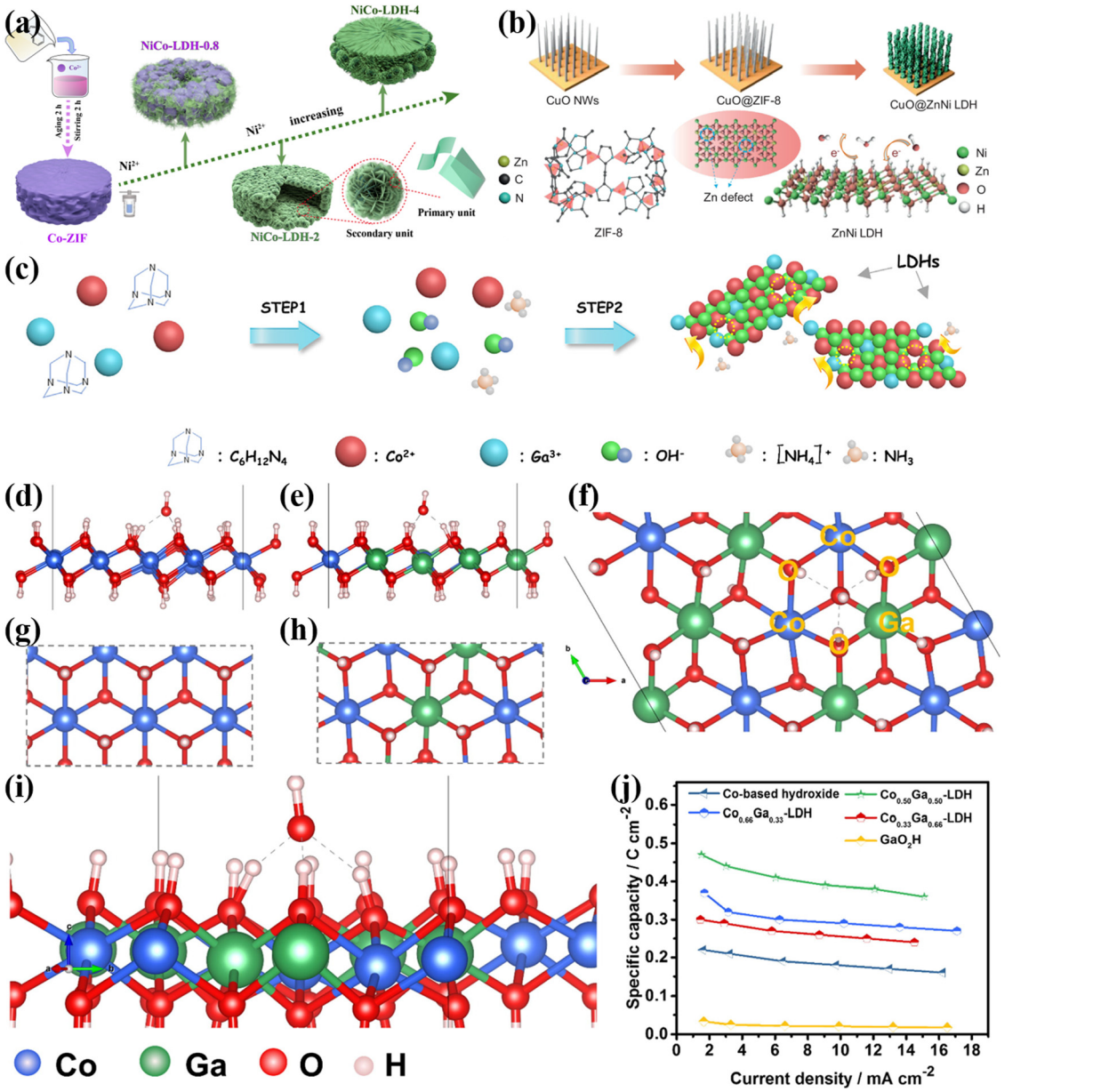

Fig. 16 (a) Synthesis strategy of NiCo-LDHs. Adapted with permission from ref. 226 Copyright 2022, Springer. (b) Schematic illustration of the fabrication procedures of the hierarchical ZnNi-LDHs architectures with rich V_{Zn} through the ZIF-derived method. Adapted with permission from ref. 220 Copyright 2021, Elsevier Ltd. (c) Synthesis mechanism of defect-rich porous ultrathin LDHs, the crystal structure and adsorption sites on the side and top views of (d and g) bulk Co-LDHs, (e and h) bulk Co-Ga-LDHs and (f and i) oxygen defect-rich $Co_{0.50}$-$Ga_{0.50}$-LDHs, (j) Rate performance of GaOOH, Co-based hydroxide and Co_x-Ga_y-LDHs electrodes. Adapted with permission from ref. 228 Copyright 2021, Elsevier Inc.

for high-performance supercapacitors. In this unique structure, on the one hand, $NiCo_2O_4$, which acts as a scaffold, provides high conductivity, thus accelerating transfer of electrons. On the other hand, the NiFe-LDH nanosheets have high surface area, providing an abundance of active sites for electrochemical reactions. The 3D layered structure is also more conducive to diffuse electrolyte ions, and the SEM images are displayed in Fig. 17(a). Thus, the synergistic effect between $NiCo_2O_4$ and NiFe-LDHs confers the best $NiCo_2O_4$@NiFe-LDHs-150/CC with excellent electrochemical performances including good area specific capacitance (1.09 F cm^{-2} at 1 mA cm^{-2}) (Fig. 17(b and c)), small charge transfer resistance (0.35 Ω) and excellent cycling stability.

Huang *et al.*[164] obtained a unique array of intercalated pseudocapacitive properties and battery-type electrode materials LDHs nanosheets by a simple and pollution-free two-step electrodeposition technique. The electrode material consists of MoO_3 and NiCo-LDHs grown directly on a 3D conductive NF substrate to form a binder-free 2D ultrathin cross-layered heterogeneous structure (NiCo-LDHs@MoO_3/NF). This heterojunction exhibited a 952.2 C g^{-1} specific capacitance at 1 A g^{-1} and a 86.42% capacity retention after 10 000 cycles at 20 A g^{-1}. Wang *et al.*[170] prepared a

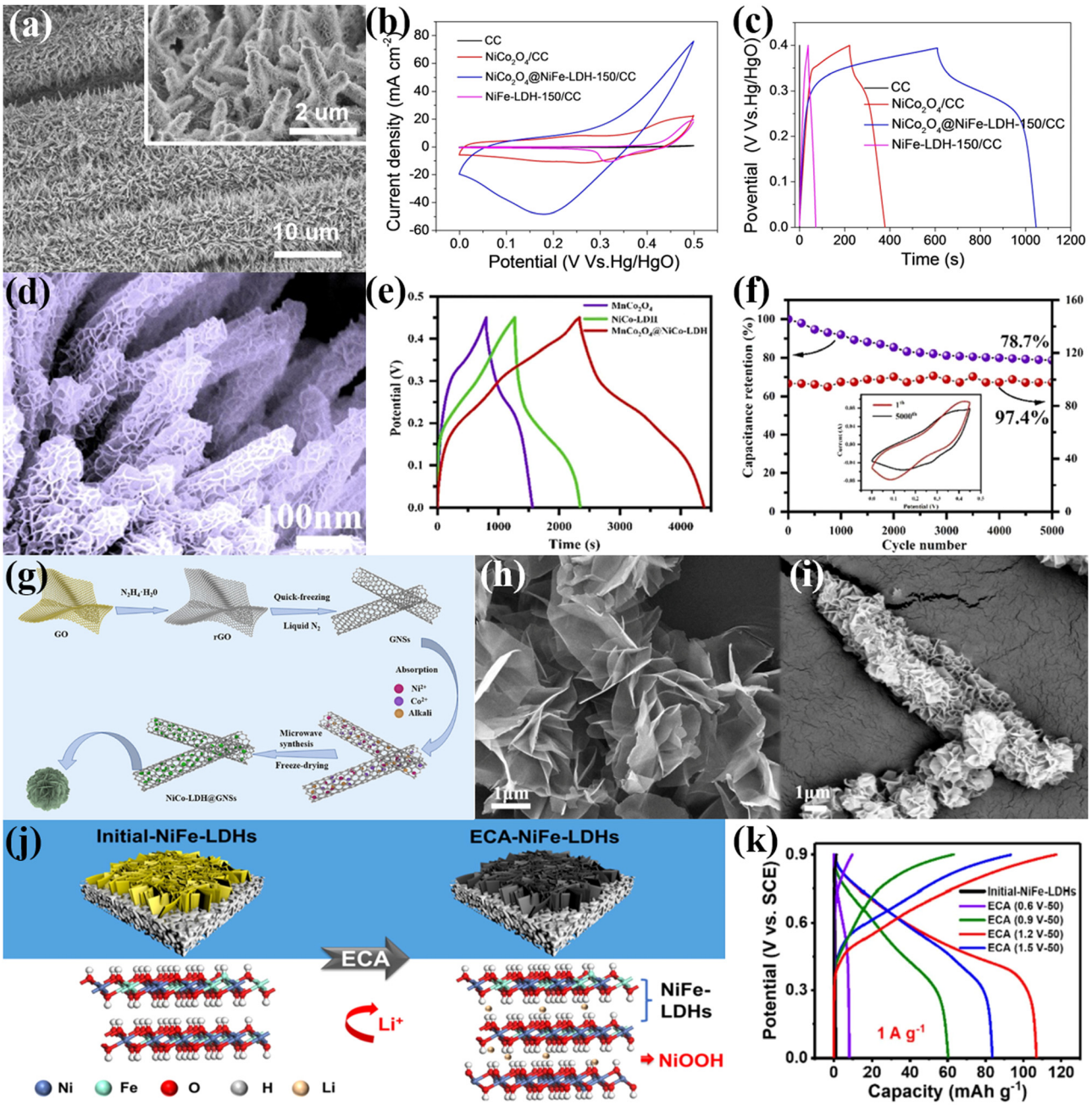

Fig. 17 (a) SEM image of $NiCo_2O_4$@NiFe-LDHs-150/CC, (b) CV curves of the CC, $NiCo_2O_4$/CC, $NiCo_2O_4$@NiFe-LDHs-150/CC and NiFe-LDHs-150/CC at 100 mV s^{-1}, (c) GCD curves of the CC, $NiCo_2O_4$/CC, $NiCo_2O_4$@NiFe-LDHs-150/CC and NiFe-LDHs-150/CC at 1 mA cm^{-2}. Adapted with permission from ref. 235 Copyright 2022, Wiley-VCH GmbH. (d) SEM image of $MnCo_2O_4$@NiCo-LDHs/NF, (e) GCD curves of $MnCo_2O_4$/NF, NiCo-LDHs/NF and $MnCo_2O_4$@NiCo-LDHs/NF at 1 A g^{-1}, and (f) the cycling performance at 10 A g^{-1} (the inset showing CV curves recorded at the 1 st and 5000th cycles measured at 10 mV s^{-1}). Adapted with permission from ref. 170 Copyright 2022, Elsevier B.V. (g) Schematic illustration of the synthesis procedures of NiCo-LDHs@GNSs, SEM images of (h) pristine NiCo-LDHs and (i) NiCo-LDHs@GNSs. Adapted with permission from ref. 236 Copyright 2022 Elsevier Ltd. (j) Schematic illustration of the fabrication processes of ECA (1.2 V-50), (K) GCD curves of ECA (1.2 V-50) at 1 A g^{-1}. Adapted with permission from ref. 238 Copyright 2022, Elsevier B.V.

core-sheath heterostructure ($MnCo_2O_4$@NiCo-LDHs/NF) consisting of NiCo-LDHs encapsulating $MnCo_2O_4$ nanowires on a NF substrate. As shown in Fig. 17(d), the core-sheath structure with a diameter of about 65 nm was anchored on the NF backbone. NiCo-LDH nanosheets act as the sheath material. This heterogeneous structure combines the advantages of the interconnection between NiCo-LDH nanosheets, the high electrical conductivity and mechanical strength of $MnCo_2O_4$. Moreover, the $MnCo_2O_4$@NiCo-LDHs/NF composite achieves a 4555.0 F g^{-1} specific capacitance at 1 A g^{-1} (Fig. 17(e)) and a 78.7% capacitance retention after 5000 cycles (Fig. 17(f)).

Exploiting the synergistic effect of bilayer capacitance and pseudo capacitance and modifying nanostructures are also

common strategies. Kuang *et al.*[236] designed and synthesized a core–shell heterostructure graphene nano scroll array composite, in which petal-like NiCo-LDH nanoflakes are vertically anchored to a 3D interconnected skeleton of GNSs, accomplished by a highly convenient microwave-assisted method (Fig. 17(g)). This design combines several advantages, for example more active sites, promoting electron and ion collection/transport and buffering the volume variation in the cycling process. Owing to its superior nanostructure (Fig. 17(h and i)), the prepared NiCo-LDH@GNS electrode has a 1470 F g^{-1} specific capacitance of 1470 F g^{-1} at 1 A g^{-1} and a 81.6% retention rate after 1000 cycles. A multilayer multi-walled carbon nanotube and graphene nanoribbon/CoNi-LDHs (MWGR/CoNi-LDHs) composite was prepared by Ma *et al.*[237] using a rapid microwave method. The synergistic effect between the MWCNTs-GONRs with high electrical conductivity, structural stability and electrochemical properties and the LDHs with a p-n junction structure facilitates the redox reaction. As a result, the MWGR/CoNi-LDHs have a unique heterogeneous structure and excellent electrochemical properties (1 A g^{-1}, specific capacitance of 1030.2 C g^{-1}) (Fig. 17(b and c)). The prepared MWGR/Co-Ni LDH//AC devices have an energy density of 47.2 W h kg^{-1} at 0.85 kW kg^{-1} and a 88.8% retention rate after 10 000 cycles at 10 A g^{-1}.

An intriguing heterostructure electrode material of NiFe-LDHs was fabricated by Zhang *et al.*[238] using a high-voltage electrochemical cycle activation (ECA) technique (Fig. 17(j)). During the high-voltage ECA process, the surface of NiFe-LDHs is reconstituted *in situ* into a low-crystalline NiOOH phase, which eventually evolves into a unique NiFe-LDHs/NiOOH heterostructure. This surface reconstruction process can generate abundant non-homogeneous interfaces, increase the active sites for reversible cation adsorption and intercalation, and significantly improve the electrochemical performances in neutral electrolytes. In a neutral electrolyte (2 M $LiNO_3$ solution), the ECA (1.2 V-50) electrode presented a 107 mA h g^{-1} specific capacitance at 1 A g^{-1} (Fig. 17(k)), which was 50 times higher than that of the initial NiFe-LDHs (2.1 mA h g^{-1} 1 A g^{-1}). By coupling with MoS_2/rGO electrodes, the assembled ECA (1.2 V-50)//MoS_2/rGO hybrid supercapacitor device has an energy density of 48.1 W h kg^{-1} at 432.9 W kg^{-1}.

Zeolite imidazolium skeletons (ZIFs) are excellent templates for the synthesis of functional materials and have extensive applications.[239] However, the direct use of ZIFs as electrode materials has limited exposure to electroactive sites, poor chemical stability, slow charging kinetics and unsatisfactory electrochemical performances.[240] How to combine their advantages and give full play to their performance becomes a key issue. Liao *et al.*[241] demonstrated the *in situ* transformation of ZnCo-ZIFs modified on ZnCo nanorod arrays (ZnCo-NA) into 3D spatially distributed ZnCo-LDHs/ZnCo-NA heterostructures (Fig. 18(a)). This structure has a huge specific surface area, and its SEM image is shown in Fig. 18(b). The electrochemical performances were improved due to its abundant electroactive sites and ion migration paths in all directions, reaching a 1576 F g^{-1} specific capacitance at 2 A g^{-1}. In Fig. 18(c), the ZnCo-LDHs/ZnCo-NA electrode has the longest discharge time of GCD curve, proving the best energy storage capacity among the three samples. A coin cell asymmetric supercapacitor (aSC) was assembled exhibiting a 88.1% capacitance retention after 5000 cycles. More importantly, this simple *in situ* mimetic transformation of the ZIF template into intriguing LDHs demonstrates the application of a new generation of bimetallic heterostructures in energy-related fields.

Wan *et al.*[171] have *in situ* modified arrays of highly porous $FeCoSe_2$@NiCo-LDH core–shell nanosheets on the surface of CC by an electrodeposition method and salinization treatment. The hierarchical heterogeneous structure consisting of two vertically aligned interconnected 2D nanosheets provided high surface area and an effective diffusion pathway for rapid electron/ion transport and generated a heterogeneous interface rich in electron structures. The results show that the well-designed $FeCoSe_2$@NiCo-LDH electrode has a much higher specific capacitance of 220.9 mA h g^{-1} at 1 A g^{-1} and a capacity retention of 83.5% at 20 A g^{-1}, with cycling stability better than that of the one-component electrode. In addition, the asymmetric supercapacitor assembled from $FeCoSe_2$@NiCo-LDH electrodes and layered porous carbon electrodes exhibits an energy density of 65.9 W h kg^{-1} at 1.248 kW kg^{-1} and a capacity retention of 87.6% after more than 10 000 cycles. These excellent performances indicate that the integrated electrodes have good prospects, and the idea of synthesizing heterostructures on the substrate surface for improving the resulting performances has good operability.

The MXene/graphene oxide/NiMn-LDH (MGL) material prepared by Chen *et al.*[242] also makes reasonable use of the advantages of the heterostructure (Fig. 18(d)). By utilizing the heterostructure, the MXene stacking problem can be effectively prevented. The SEM image of MGL show that nano-LDH aggregates on the surface of MXene flakes, forming blocky porous arrays (Fig. 18(e)). The structural stability of the matrix is ensured, which can inhibit the morphological collapse of LDHs and thus significantly increase the specific capacitance of LDHs. The presence of graphene oxide accelerates charge transfer and increases the electron density. The existence of the various components in this heterogeneous structure largely enhances the active sites and electrochemical capability. As an anode material, MGL achieves a 241.9 mA h g^{-1} specific capacitance and a 90.9% cycling stability at 1 A g^{-1} in the presence of multivalent (Mn, Ni) hydroxides and stabilized carbon materials. The combination of the conductivity of the surface graphene oxide and the substrate MXene increases the available electrons in the hydroxide root. The assembled asymmetric device can achieve a 2.0 V voltage window (Fig. 18(f)). This once again demonstrates the importance of constructing heterogeneous structures for enhancing the electrochemical properties and proves that the synergy between these three materials has a wide range of applications. Besides, Zhu *et al.*[243] prepared Co_2Mn bimetallic hydroxide nanofilms directly on NF by a hydrothermal method, and then prepared Co_2Al-LDH nanosheets on Co_2Mn nanofins by a hydrothermal method to obtain heterostructure nanocomposites (Co_2Al/Co_2Mn/NF)

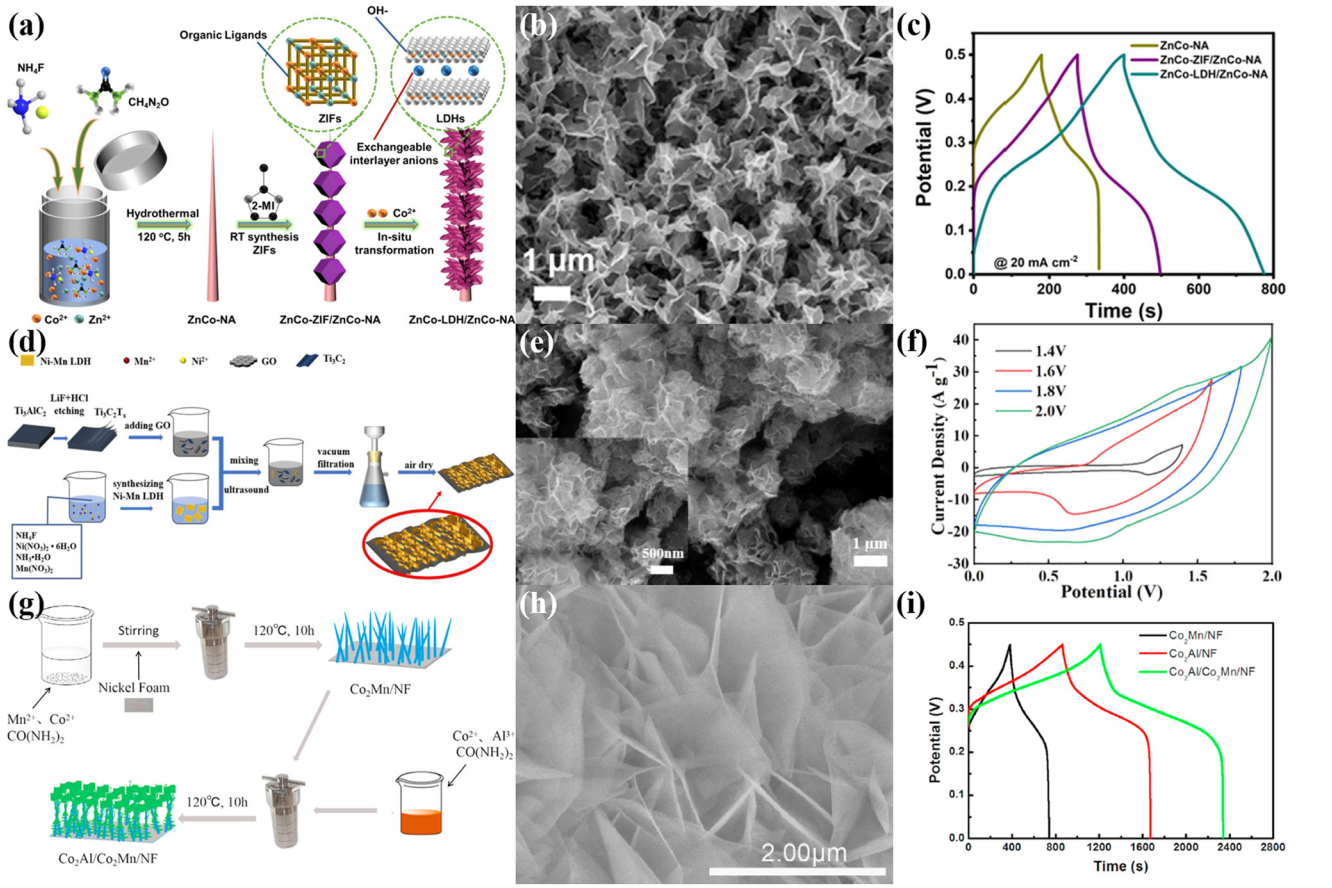

Fig. 18 (a) Schematic illustration of the synthesis processes of the ZnCo-LDHs/ZnCo-NA hybrid, (b) SEM image of ZnCo-LDHs/ZnCo-NA, (c) GCD curves of the ZnCo-NA, ZnCo-ZIF/ZnCo-NA and ZnCo-LDHs/ZnCo-NA electrodes. Adapted with permission from ref. 241 Copyright 2022, Elsevier Inc. (d) Schematic illustration of the fabrication of the MGL composite, (e) SEM image of the MGL composite, (f) CV curves of MGL//AC in different scan potential windows at a scan rate of 100 mV s^{-1}. Adapted with permission from ref. 242 Copyright 2021, Elsevier Ltd. (g) Schematic diagram of the synthesis of $Co_2Al/Co_2Mn/NF$, (h) SEM image of $Co_2Al/Co_2Mn/NF$, (i) GCD curves of the Co_2Mn/NF, Co_2Al/NF and $Co_2Al/Co_2Mn/NF$ at a current density of 1 A g^{-1}. Adapted with permission from ref. 243 Copyright 2020, Elsevier B.V.

(Fig. 18(g)). Fig. 18(h) shows the structure of $Co_2Al/Co_2Mn/NF$ surface nanosheets. The specific capacitance can reach 2502.0 F g^{-1} at 1 A g^{-1}. After 7000 cycles, the specific capacitance is maintained at 92.21%. The energy density at 412.73 W kg^{-1} is 64.58 W h kg^{-1}.

Stable MnO_2 nanowires@NiCo-LDHs heterostructures were fabricated *via* a liquid-phase way by Ma *et al.*[244] The NiCo-LDH nanosheets were grown uniformly in stable channels on the surface of the ultra-long MnO_2 nanowires, and the synthesis schematic is shown in Fig. 19(a). SEM images of the MnO_2@LDHs-2 sample in Fig. 19(b) show NiCo-LDH nanosheets evenly grown on the MnO_2 periphery, which favors the electron transfer and ion diffusion during the electrochemical reaction. Electrochemical testing revealed that the core–shell heterostructure displayed 708 C g^{-1} and 630 C g^{-1} specific capacitance at 1 A g^{-1} and 10 A g^{-1}, and a 82.3% capacitance retention rate after 2000 cycles. Characterization by Raman spectroscopy revealed that the prepared electrode has a transition from α phase to β phase during cycling in comparison with NiCo-LDHs, due to the heterogeneous structure buffering the collapse. Furthermore, the asymmetric supercapacitor assembled with this electrode exhibits a 72.4% capacitance retention rate after 10 000 cycles. Chen *et al.*[245] constructed a bilayer LDH nanosheet array through a hydrothermal method (Fig. 19(c)). The prepared bilayer electrode material with Ni, Co and Mn elements has a high surface area. As a result, this structure increases the contact between the electrolyte and the prepared material. The bilayer electrode showed excellent capacitive performance (2950 F g^{-1} at 1 A g^{-1}) (Fig. 19(d)) and good stability (79% retention after 10 000 cycles at 10 A g^{-1}). Besides, the asymmetric NiCo/NiMn-LDHs//AC devices were prepared, which had good capacity and 82.2% cycling stability after 10 000 cycles. The preparation of this double-LDHs array provides a new idea for increasing the active sites of electrode materials.

Two nanostructures of ZnO nanorods (NR) and nanosheets (NF) were prepared by a hydrothermal method on conductive flexible CC by Xiong *et al.*[246] Then NiCo-LDH nanosheets were formed on these nanostructures for preparing NiCo-LDHs/ZnO NR/CC and NiCo-LDHs/ZnO NF/CC heterostructures (Fig. 19(e)). The influences of ZnO morphology on electrochemical properties were studied in detail. The results show that the latter heterostructure is denser and more homogeneous than the former.

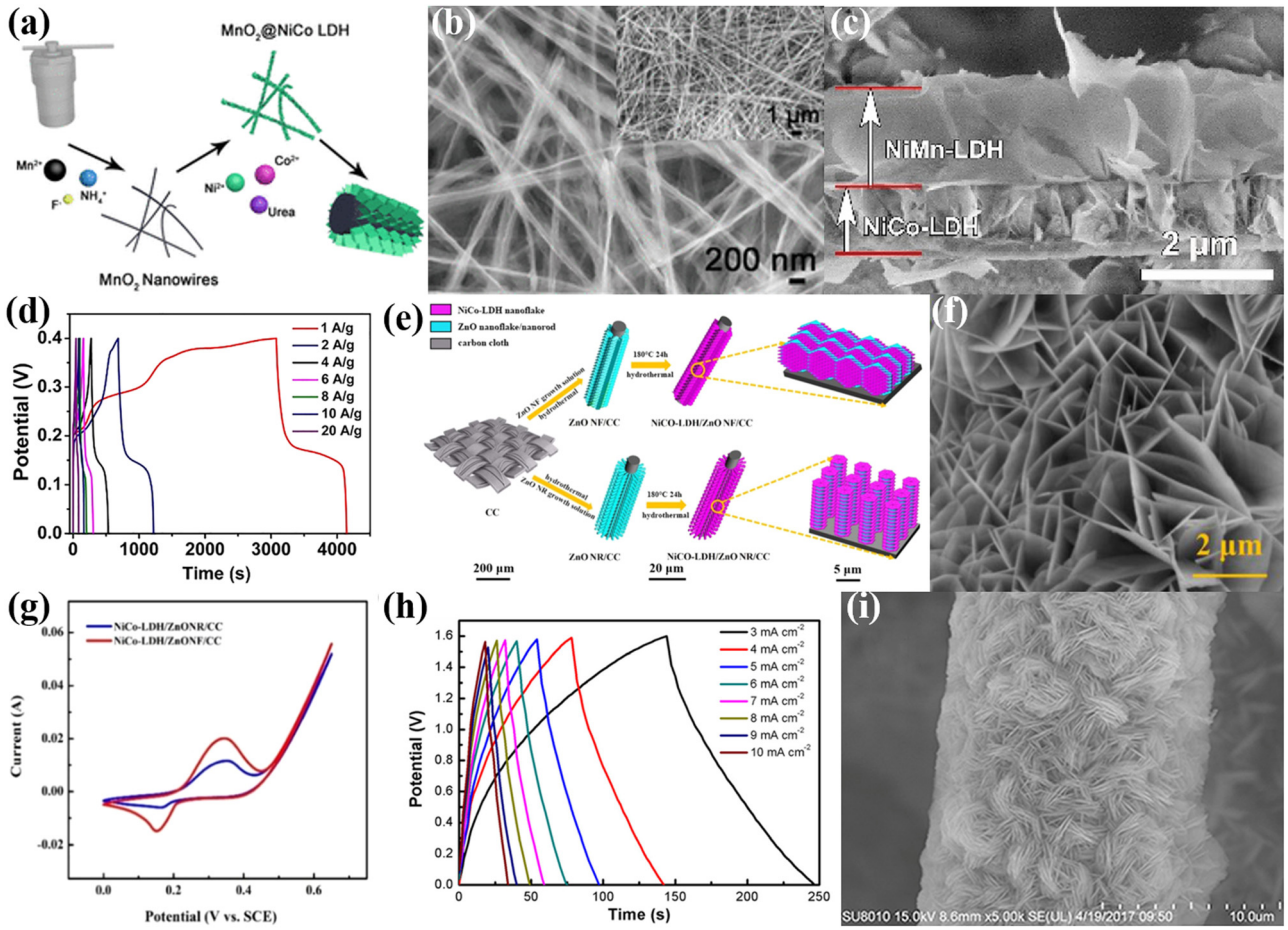

Fig. 19 (a) Schematic illustration of the formation processes of the stable MnO_2 nanowires@NiCo-LDH nanosheet core–shell heterostructure, (b) SEM image of MnO_2@LDHs-2 samples. Adapted with permission from ref. 244 Copyright 2021, American Chemical Society. (c) Cross-sectional diagram of NiCo-LDHs and NiCo/NiMn-LDHs, (d) GCD curves of the NiCo/NiMn-LDH electrode at various current densities, respectively. Adapted with permission from ref. 245 Copyright 2021, Elsevier Ltd. (e) The synthesis procedures of NiCo-LDH NF on ZnO NF/CC and ZnO NR/CC substrates, (f) SEM image of NiCo-LDHs/ZnO NF/CC, (g) CV profiles of NiCo-LDHs/ZnO NR/CC and NiCo-LDHs/ZnO NF/CC electrodes at a scanning speed of 5 mV s^{-1}. Adapted with permission from ref. 246 Copyright 2020, Elsevier B.V. (h) Galvanostatic current charge–discharge curves at different current densities, (i) SEM image of the $NiCo_2S_4$/NiCo-LDH sample. Adapted with permission from ref. 247 Copyright 2021, Springer.

The corresponding SEM image is shown in Fig. 19(f). The latter heterostructure displays more excellent electrochemical properties than the former heterostructure (Fig. 19(g)), with a 2.6-fold specific capacitance (1577.6 F g^{-1} at 1 A g^{-1}), a 2.2-fold higher multiplicative capacity and a 1.5-fold higher cycling stability. Moreover, the NiCo-LDHs/ZnO NFs//AC asymmetric solid-state flexible device has a maximum energy density of 51.39 W h kg^{-1} at 800 W kg^{-1} with 87.3% capacitance retention after 1000 cycles. Finally, the two packaged devices were successfully lit in series with a red 2.2 V LED, demonstrating the potential for practical applications. Zhou *et al.*[247] prepared porous heterostructure $NiCo_2S_4$/NiCo-LDHs on carbon fiber paper using a simple solvothermal method. The active material was deposited vertically on the carbon fiber paper and its SEM image is shown in Fig. 19(i). This composite was assembled from nanoflakes into an intertwined 3D structure with abundant microporous dimensions and excellent electrochemical properties. Its unique structure facilitates the acceleration of electron transfer and electrolyte transport during electrochemical processes. The specific capacitance was 1403 F g^{-1} at 10 mA cm^{-2}. At 30 mA cm^{-2}, the capacitance retention after 5000 cycles reached 111.1%, showing excellent cycling stability. Symmetric supercapacitors assembled from this material correspond to a 0.19 F cm^{-2} area capacitance at 3 mA cm^{-2} (Fig. 19(h)).

3.4 Preparation of binder-free materials

Growing metal precursors directly onto the surface of the current collector, such as NF, copper foam, stainless steel mesh and carbon-based materials, offers significant advantages.[248–250] This modification strategy reduces the mass of inactive materials such as conductive polymer binders, increasing the total energy density and allowing for lighter weight devices to be assembled.[251] In the process, charge transfer and internal resistance are reduced. Besides, the elimination of the polymer binder allows more electroactive sites to be exposed, which increases the electrical conductivity and speeds up the rate of electron transfer. Importantly, this strategy allows for the

combination of different types of active materials, which provides the opportunity for multi-component synergistic effects that improve electrochemical performance.[35] But a suitable base material needs to be selected. The pretreatment for the base material is beneficial to the growth of active material.

Li *et al.*[252] synthesized nickel iron sulfide nanosheets (NiFeSx) and carbon nanotubes (CNTs) on diatomite by chemical vapor deposition and a two-step hydrothermal method to overcome the application challenges of transition metal LDHs in the field of supercapacitors such as easy aggregation and low conductivity. The synthesis of this composite successfully exploited the cooperative effect of multicomponent materials for enhancing the electrochemical properties (Fig. 20(a)). The SEM image of NiFeSx@CNTs@MnS is shown in Fig. 20(b). After the simultaneous sulfidation process, NiFeSx also has *ortho*-hexagonal nanosheet morphology and shows the presence of CNTs on its surface. The diatomite as the matrix can provide a good environment for the uniform dispersion of nanomaterials on its surface, expands the active sites in contact with the electrolyte, and significantly improves the electrochemical performance. Combining high conductivity and the simultaneous sulfurization effect, the NiFeSx@CNTs@MnS@diatomite structure displays a 552 F g^{-1} specific capacitance at 1 A g^{-1} (Fig. 20(c)) and a retention rate of 68.4% at 10 A g^{-1}, maintaining a 89.8% cycling stability after 5000 cycles at 5 A g^{-1}. Furthermore, the asymmetric supercapacitor assembled by this composite and graphene achieves an energy density of 28.9 W h kg^{-1} at 9375 W kg^{-1}. Rajapriya *et al.*[253] synthesized laminated NiS nanoflowers on flexible CC substrates by a hydrothermal method, and then used electrodeposition to vertically immobilize Sr-Fe LDHs nanosheets on highly conductive and flexible NiS/CC electrodes without destroying the original structure. This abundant 3D hybridized NiS@Sr-Fe OH/CC nanostructure provides a large number of nucleation active sites. The excellent structural (Fig. 20(d)) and morphological advantages of the reticular flakes accelerate the activity of NiS/CC, Sr-Fe OH/CC and NiS@Sr-Fe OH/CC flexible electrodes having specific capacitances of 556, 1151 and 1553 F g^{-1} (Fig. 20(e and f)) at 1 A g^{-1},

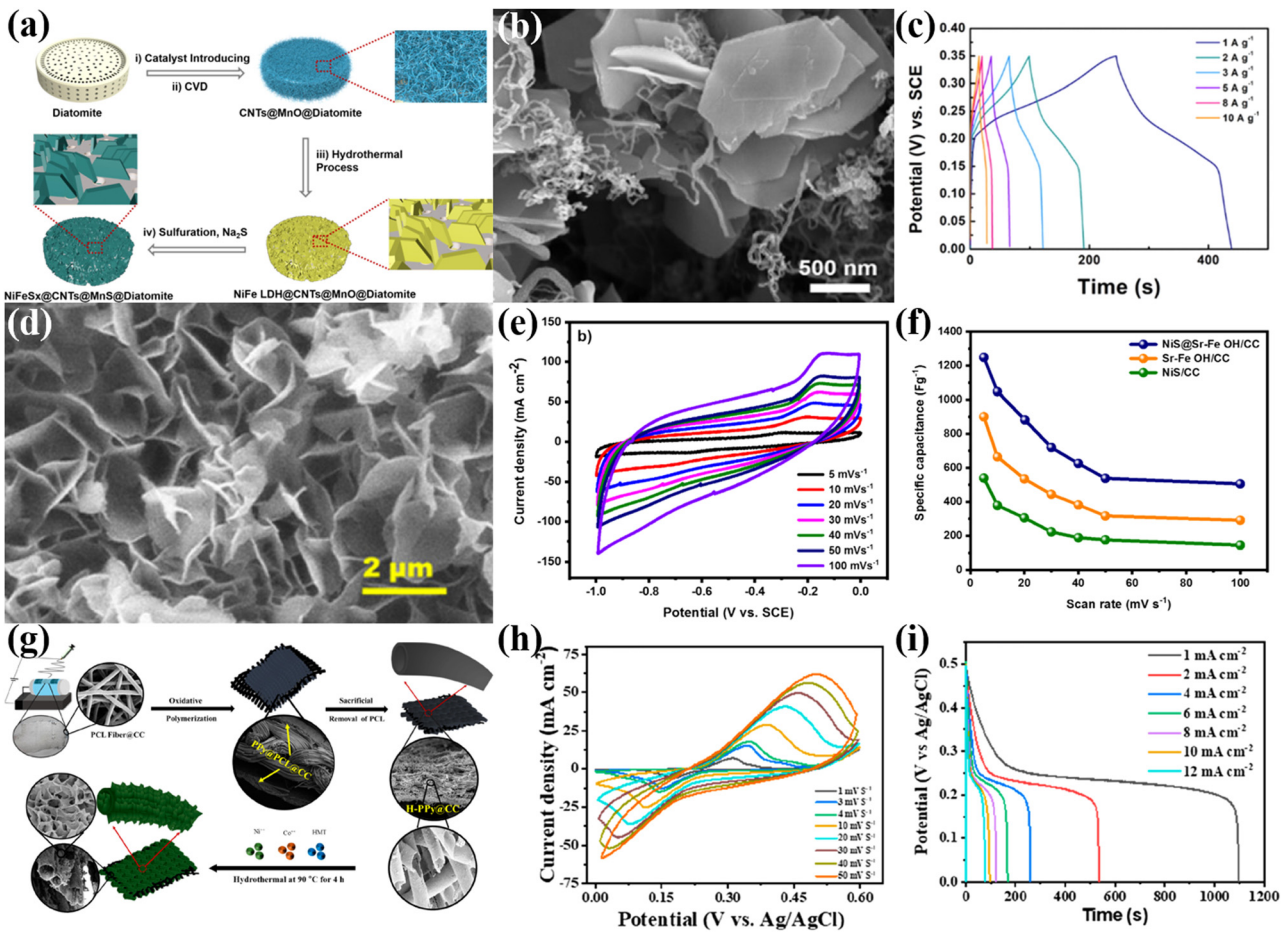

Fig. 20 (a) The schematic illustration of the preparation processes of NiFeSx@CNTs@MnS@Diatomite, (b) SEM image of NiFeSx@CNTs@MnS@Diatomite, (c) GCD curves with different current densities. Adapted with permission from ref. 252 Copyright 2021, Elsevier Inc. (d) SEM images of the NiS@Sr-Fe OH/CC nanostructure. (e) CV curves at different scan rates, (f) the calculated specific capacitance of Sr-Fe OH/CC, NiS/CC and NiS@Sr-Fe OH/CC at 5–100 mV s^{-1}. Adapted with permission from ref. 253 Copyright 2022, Elsevier Ltd. (g) Schematic representation of the step-by-step synthesis of NiCo-LDH@H-PPy@CC, (h) CV curves at different scan rates, (i) GCD profile for the NiCo-LDHs@H-PPy@CC electrode at different current densities. Adapted with permission from ref. 254 Copyright 2022, American Chemical Society.

respectively. The NiS@Sr-Fe OH/CC//AC/CC device has an energy density of 53.07 W h kg^{-1} at 4.4 kW kg^{-1}.

Lohani *et al.*[254] designed an assembly of thin-LDH nanosheets arranged in the lumen and luminal portions of a polypyrrole tunnel as an electrode material. The SEM images show that the NiCo-LDHs@H-PPy@CC electrodes are constructed by combining NiCo-LDHs nanosheets inside and outside the lumen on long polypyrrole tunnels on CC (Fig. 20(g)). The capacitance of the sample at 1.0 mA cm^{-2} was 149.16 mA h g^{-1} (Fig. 20(h and i)). Besides, the device consisting of NiCo-LDHs@H-PPy@CC and vanadium phosphate carbon nanofibers (VPO@CNFs900) has a specific energy density of 32.42 W h kg^{-1} at 3 mA cm^{-2}. Using the facile and feasible in-situ oxidation combined with the potential electrodeposition method, Wang *et al.*[255] constructed densely distributed, core–shell structured $Cu(OH)_2$@NiFe-LDHs nanoarrays (COH@NF-LDHs/CF) on copper foam. This unique core–shell structure and the synergy between $Cu(OH)_2$ and NiFe-LDHs provide great advantages such as sufficient chemically active sites, and electron and ion transfer pathways to enhance the electrochemical performances. In particular, at 5 mA cm^{-2}, the capacitance of the synthesized COH@NF-LDHs/CF can reach 4.139 F cm^{-2}, which is significantly better than those of single bare $Cu(OH)_2$ (198 mF cm^{-2} at the same current density) and NiFe-LDHs/CF (71 mF cm^{-2}). Furthermore, COH@NF-LDHs/CF exhibits remarkable stability (86.47% for 5000 cycles). The asymmetric supercapacitor possesses a high energy density of 65.56 W h kg^{-1} at 750 W kg^{-1}.

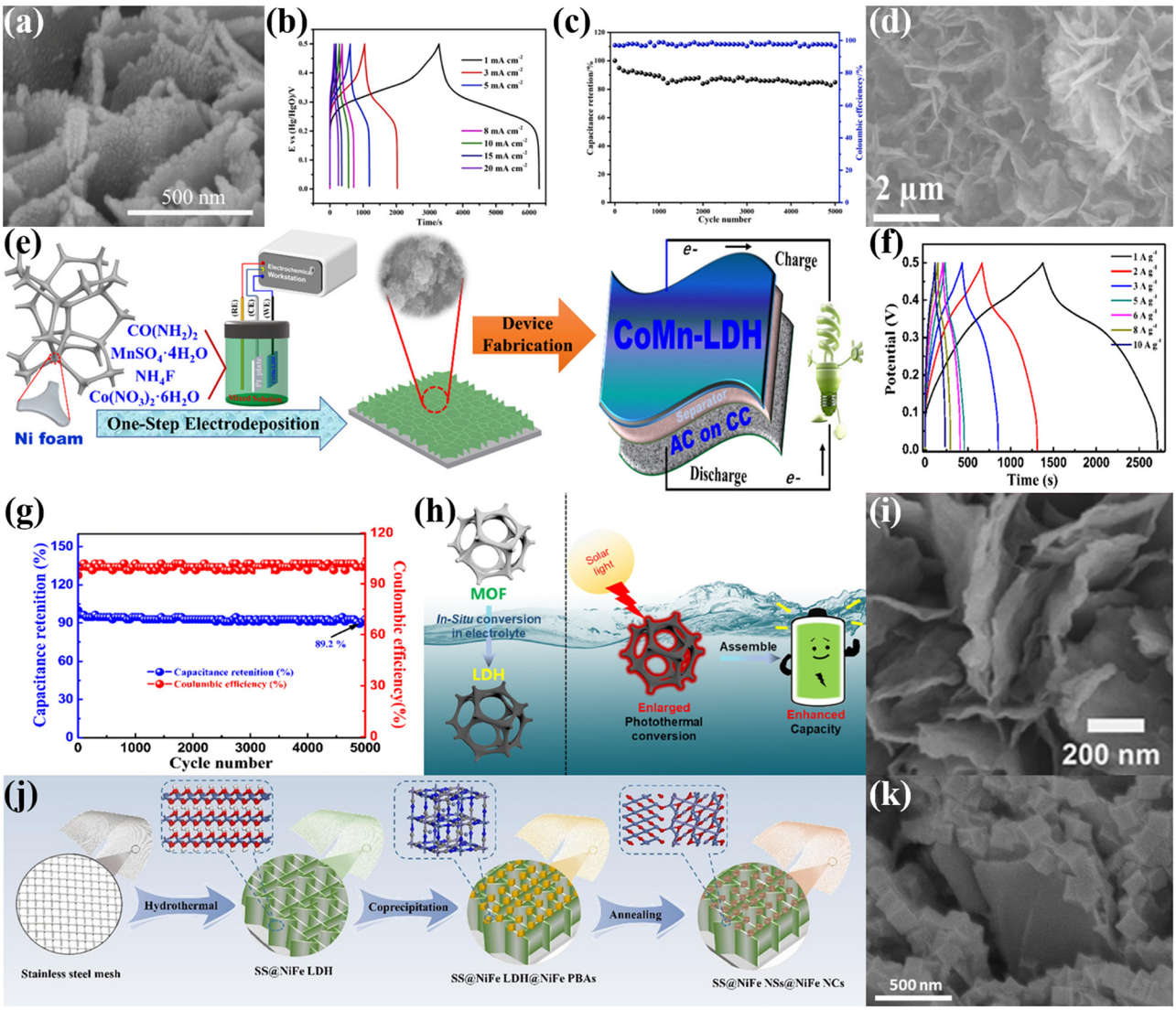

Fig. 21 (a) SEM image of NiCo-LDH hierarchical nanosheets on NF, (b) GCD curves of the Ni_1Co_2/NF electrode with current densities from 1 to 20 mA cm^{-2}, (c) cycling performance of the HSC device. Adapted with permission from ref. 256 Copyright 2022, Elsevier B.V. (d) SEM image of CoMn-LDHs, (e) Main fabrication procedures of the CoMn-LDH cathodes and AASCs, (f) GCD curves at various current densities of 1–10 A g^{-1}, (g) cycling performance and coulombic efficiency for 5000 cycles at 5 A g^{-1}. Adapted with permission from ref. 257 Copyright 2022, Elsevier Ltd. (h) Synthesis and working process diagram, (i) SEM image of NC37. Adapted with permission from ref. 258 Copyright 2022, Elsevier B.V. (j) Schematic illustration of the formation of SS@NiFe-LDHs@NiFe NCs, (k) SEM image of SS@NiFe NSs@NiFe NCs. Adapted with permission from ref. 259 Copyright 2021, Elsevier B.V.

NF is also commonly used as a substrate material in supercapacitors, mainly because of the porous structure, low density and excellent conductivity. The growth of LDHs on its surface as supercapacitor electrode materials has several advantages: the 3D mesh structure of the NF substrate enables the effective deposition of active materials and promotes the transfer of charges. Direct deposition of LDH material on NF eliminates the need for pressing during electrochemical performance testing and eliminates the need for adhesive, making the test results more representative. Cao *et al.*[256] chemically etched NF with transition metal (NiCo-based) nitric acid solutions of different Ni and Co ratios. And after rinsing and drying, the etched NF was used as the anode and the platinum mesh as the cathode in an alkaline solution. By constant voltage action, NiCo-LDHs will self-grow on the NF (Fig. 21(a)). The Ni_1Co_2/NF monolithic electrode exhibited the best electrochemical performances with a specific capacitance of 3.01 C cm^{-2} at 1 mA cm^{-2} (Fig. 21(b)). A hybrid device showed an energy density of 97.4 pW h cm^{-2} at 800.5 μW cm^{-2}, and an initial capacity of 85.0% after 5000 cycles (Fig. 21(c)).

A CoMn-LDH nanostructured high-performance self-contained supercapacitor electrode was prepared on NF surface by Emin *et al.*[257] by employing electrochemical deposition, as shown in Fig. 21(e). The electrode has an open interconnected thin layered structure (Fig. 21(d)) with a high capacitance of 2673.6 F g^{-1} at 1 A g^{-1} (Fig. 21(f)) and good cycling stability (86.7% for 5000 cycles at 12 A g^{-1}). The asymmetric device has an energy density of 97.5 W h kg^{-1} at 800.0 W kg^{-1}, a capacitance retention of 89.2% for 5000 cycles at 5 A g^{-1}, and a coulombic efficiency of about 100% (Fig. 21(g)). Lu *et al.*[258] constructed binder-free NiCo-LDHs high-performance energy storage device on NF by *in situ* electrochemically triggered MOF hydrolysis, which has remarkable energy storage capacity under solar irradiation (Fig. 21(h)). Through electrochemically controlled hydrolysis, the ligands in the MOFs are replaced by OH^- and the resulting NiCo-LDHs retained the original layered porous structure of the MOFs. The NiCo-LDH electrode has ample oxygen vacancies and a large surface area (Fig. 21(i)), reaching a capacity of 5.4 C cm^{-2} at 1.25 mA cm^{-2}, 64.3 times that of the MOF template. Importantly, the electrode material also has excellent photothermal conversion capabilities (52.9 °C temperature increase in only 30 s). Furthermore, the energy density of the asymmetric supercapacitor prepared using NiCo-LDH increased by 329.2% after 15 min of sunlight irradiation at low temperatures (−4 °C).

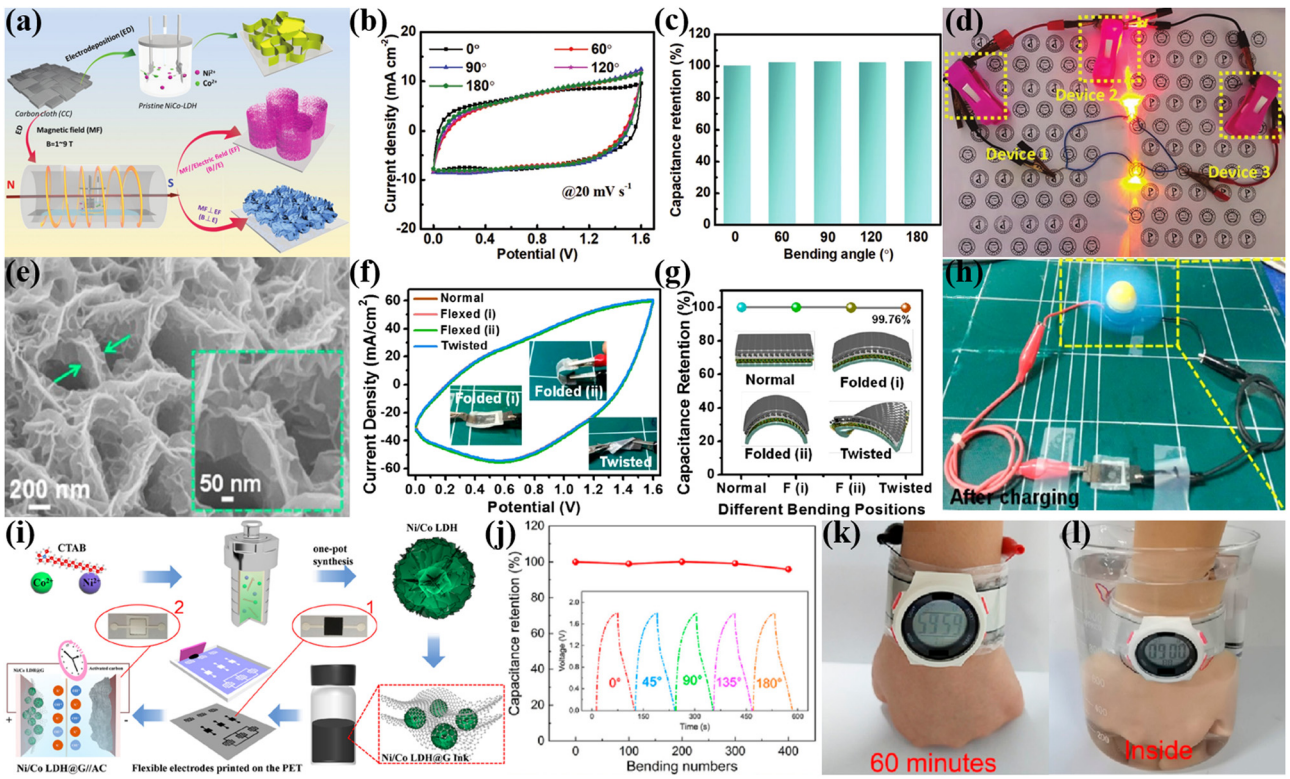

Fig. 22 (a) Schematic illustration of the preparation of NiCo-LDHs on CC, (b) CV curves and (c) capacitance retention of the device with bending at different angles, (d) digital picture of three devices connected in series lighting up the red and yellow LED lights connected in parallel. Adapted with permission from ref. 260 Copyright 2022 Wiley-VCH GmbH. (e) Core–shell-like NC-LDH NFAs@NSs/Ni fabric, (f) CV curves and (g) capacitance retention of the flexible hybrid SC under various bending conditions, and the corresponding insets show the photograph and schematic diagrams of the device under various bending states, (h) the potential suitability of the device for wearable electronic applications. Adapted with permission from ref. 261 Copyright 2017 American Chemical Society. (i) Schematic diagram of the preparation of screen-printed flexible NiCo LDH-based electrodes, (j) capacitance retention of the flexible Ni_3Co_1 LDH@G//AC ASC under different bending cycles, inset of GCD curves tested under different bending angles, (k) two devices connected in series to power the electronic watch, (l) two devices connected in series in water to power the electronic watch. Adapted with permission from ref. 262 Copyright 2022 American Chemical Society.

Table 4 Properties of devices consisting of LDHs and their composites mentioned in this manuscript

Devices	Electrolyte	Capacitance	Energy density at power density	Cycles	Ref.
3%-Ni-C/NiAl-LDHs//AC	6 M KOH	210.8 C g^{-1}, 1 A g^{-1}	74.9 W h kg^{-1} at 800 W kg^{-1}	10 000, 91.4%	210
NiCo-LDHs-S/PNT//GF-LDHs@NF	3 M KOH	98 F g^{-1}, 1 A g^{-1}	16.28 W h kg^{-1} at 650 W kg^{-1}	8000, 74%	88
CoFe-LDHs/P2//AC	6 M KOH	1686 F g^{-1}, 1 A g^{-1}	75.9 W h kg^{-1} at 1124 W kg^{-1}	10 000, 97.5%	214
CoNiMg-LDHs//AC	—	333 C g^{-1}, 1 A g^{-1}	73.9 W h kg^{-1} at 0.8 kW kg^{-1}	5000, 87%	217
NCW-2//rGO	PVA-KOH	98 F g^{-1}, 2 A g^{-1}	34 W h kg^{-1} at 1.32 kW kg^{-1}	10 000, 86%	185
Ni-Co(OH)(BA)//AC	—	118 F g^{-1}, 1 A g^{-1}	47.5 W h kg^{-1} at 850 W kg^{-1}	8000, 91%	212
ECA(1.2 V-50)//MoS_2/rGO	—	134 F g^{-1}, 0.5 A g^{-1}	48.1 W h kg^{-1} at 432.9 W kg^{-1}	—	238
NiAl-Cl LDHs//AC	6 M KOH	81.82 F g^{-1}, 1 A g^{-1}	53.9 W h kg^{-1} at 1540 W kg^{-1}	1000, 94.1%	211
NMHS-4//AC	1 M KOH	97.3 F g^{-1}, 1 A g^{-1}	34.61 W h kg^{-1} at 831 W kg^{-1}	10 000, 85%	218
ZnO@Ni/Co-LDHs//AC	PVA-KOH	24.6 mF cm^{-2}, 0.5 mA cm^{-2}	7.7 uW h cm^{-2} at 375.0 pW cm^{-2}	—	216
CuCoNi-OH//HPC	3 M KOH	180 C g^{-1}, 0.5 A g^{-1}	39.67 W h kg^{-1} at 400 W kg^{-1}	—	215
NiFe-LDHs@SCN-32//AC	6 M KOH	386 F g^{-1}, 1 A g^{-1}	68.7 W h kg^{-1} at 827.5 W kg^{-1}	8000, 83.3%	219
NTA18//AC	1 M KOH	126 F g^{-1}, 1 A g^{-1}	45.1 W h kg^{-1} at 16000 W kg^{-1}	5000, 59%	186
CuCo-LDHs//AC	1 M KOH	76 F g^{-1}, 1 A g^{-1}	22 W h kg^{-1} at 23200 W kg^{-1}	10 000, 91.3%	188
D-NiCo-LDHs/NF//AC	3 M KOH	267 F g^{-1}, 1 A g^{-1}	53 W h kg^{-1} at 752 W kg^{-1}	5000, 94.7%	222
3D-NiCo-SDBS-LDHs//AC	1 M KOH	205.7 F g^{-1}, 1 A g^{-1}	73.14 W h kg^{-1} at 800 W kg^{-1}	10 000, 95.5%	224
NiCo-LDHs-2//AC	6 M KOH	559 C g^{-1}, 1 A g^{-1}	101.1 W h kg^{-1} at 1500 W kg^{-1}	5000, 87.8%	226
V_{Zn}-defect sample//AC	1.2 M LiOH	528.5 mF cm^{-2}, 2 mA cm^{-2}	1.03 mW h cm^{-3} at 9.35 mW cm^{-3}	2000, 85.6%	220
$Co_{0.50}$-$Ga_{0.50}$-LDHs//AC	6 M KOH	187 mF cm^{-2}, 3.15 mA cm^{-2}	33.38 W h kg^{-1} at 920 W kg^{-1}	10 000, 95.8%	228
E-CoZnAl-LDHs-8 h//AC	1 M KOH	114 F g^{-1}, 1 A g^{-1}	36.75 W h kg^{-1} at 400 W kg^{-1}	8000, 72.7%	223
NiCo-LDHs@MoO_3/NF//AC	2 M KOH	952.2 C g^{-1}, 1 A g^{-1}	58.06 W h kg^{-1} at 800 W kg^{-1}	10 000, 86.42%	164
NiCo-LDHs@GNSs//AC	3 M KOH	102.6 F g^{-1}, 1 A g^{-1}	32.1 W h kg^{-1} at 750.4 W kg^{-1}	—	236
MWGR/CoNi-LDHs//AC	6 M KOH	132.9 F g^{-1}, 1 A g^{-1}	47.2 W h kg^{-1} at 850 W kg^{-1}	10 000, 88.8%	237
$MnCo_2O_4$@NiCo-LDHs/NF//AC	6 M KOH	60 F g^{-1}, 1 A g^{-1}	21.3 W h kg^{-1} at 160 W kg^{-1}	5000, 86.6%	170
ZnCo-LDHs/ZnCo-NA//AC	6 M KOH	68.4 F g^{-1}, 0.2 A g^{-1}	21.3 W h kg^{-1} at 900 W kg^{-1}	5000, 88.1%	241
$FeCoSe_2$@NiCo-LDHs//PPC-2	2 M KOH	95.2 mA h g^{-1}, 1 A g^{-1}	1.248 kW kg^{-1} at 65.9 W h kg^{-1}	10 000, 87.6%	171
MXene/GO/Ni-Mn LDHs//AC	PVA-KOH	69.1 mA h g^{-1}, 1 A g^{-1}	55.3 W h kg^{-1} at 800 W kg^{-1}	4000, 94.7%	242
Co_2Al/Co_2Mn/NF//AC	6 M KOH	281.7 C g^{-1}, 0.5 A g^{-1}	64.58 W h kg^{-1} at 412.7 W kg^{-1}	7000, 92.21%	243
MnO_2@LDHs-2//AC	6 M KOH	95.5 F g^{-1}, 0.5 A g^{-1}	31.9 W h kg^{-1} at 502.7 W kg^{-1}	10 000, 72.4%	244
NiCo/NiMn-LDHs//AC	6 M KOH	185.1 F g^{-1}, 1 A g^{-1}	45.16 W h kg^{-1} at 1400 W kg^{-1}	10 000, 82.2%	245
NiCo-LDHs/ZnO NFs//AC	1 M KOH	144.5 F g^{-1}, 1 A g^{-1}	51.39 W h kg^{-1} at 800 W kg^{-1}	1000, 87.3%	246
NiFeSx@CNTs@MnS@diatomite// graphene	6 M KOH	92.3 F g^{-1}, 0.5 A g^{-1}	28.9 W h kg^{-1} at 9375 W kg^{-1}	5000, 80.8%	252
NiS@Sr-Fe OH/CC//AC	1 M KOH	146.21 F g^{-1}, 1 A g^{-1}	53.07 W h kg^{-1} at 4.4 kW kg^{-1}	—	253
NiCo-LDHs@H-PPy@CC//VPO@CNFs900	2 M KOH	40.53 mA h g^{-1}, 3 mA cm^{-2}	32.42 W h kg^{-1} at 359.16 W kg^{-1}	10 000, 94.09%	254
COH@NF-LDHs/CF//AC	6 M KOH	195.7 F g^{-1}, 1 A g^{-1}	65.56 W h kg^{-1} at 750 W kg^{-1}	5000, 88.93%	255
Ni_1Co_2/NF//AC	1 M KOH	273.8 mF cm^{-2}, 1 mA cm^{-2}	97.4 pW h cm^{-2} at 800.5 μw cm^{-2}	5000, 85%	256
CoMn-LDHs//AC	2 M KOH	274.26 F g^{-1}, 1 A g^{-1}	97.5 W h kg^{-1} at 800 W kg^{-1}	5000, 89.2%	257
NiCo-LDHs//GO/AC	1 M KOH	1.4 C cm^{-2}, 1.25 mA cm^{-2}	1.06 mW h cm^{-2} at 1.03 mW cm^{-2}	—	258
NSs@NiFe NCs//SS@Fe_2O_3	1 M Na_2SO_4	102 F g^{-1}, 1 A g^{-1}	45.9 W h kg^{-1} at 902.7 W kg^{-1}	2000, 89.7%	259
$Ti_3C_2T_x$/NiCo-LDH-3 T (B//E)//AC	PVA-KOH	3.12 C cm^{-2}, 1 mA cm^{-2}	0.134 mW h cm^{-2} at 1.61 mW cm^{-2}	6000, 82.3%	260
NC LDH NFAs@NSs/Ni fabric//AC@CF	1 M KOH	1147.23 mF cm^{-2}, 3 mA cm^{-2}	46.15 W h kg^{-2} at 2604.42 W kg^{-1}	2000, 86.49%	261
Ni_3Co_1 LDH@G//AC	PVA-KOH	599 mF cm^{-2}, 1 mA cm^{-2}	0.27 mW h cm^{-2} at 0.9 mW cm^{-2}	10 000, 123%	262

Stainless steel mesh (SS) is also a suitable substrate material for the growth of LDHs. Wang *et al.*[259] prepared uniformly distributed 3D NiFe Prussian blue analogue (NiFe PBAs) nanocubes on SS and transformed them into 3D oxide arrays (SS@NiFe NSs@NiFe NCs) by penetrating 2D NiFe-LDHs and thermally annealing them in air (Fig. 21(j)). This 3D array shows a nanocubic structure (Fig. 21(k)) with high specific surface area and good electrochemical properties. In addition, hybrid supercapacitor (HSC) SS@NiFe NSs@NiFe NCs//SS@Fe_2O_3 devices were assembled and showed impressive electrochemical performance.

3.5 Application of LDH-based supercapacitors

LHD-based supercapacitors are widely used in flexible wearable devices or other integrated intelligent devices. Li *et al.*[260] prepared NiCo-LDHs on flexible CC and $Ti_3C_2T_x$ functional CC by high magnetic field electrodeposition (Fig. 22(a)). The flexible hybrid supercapacitor has excellent energy density and cyclic stability. The device exhibits slight polarization during bending and the total capacitance remains almost constant, further confirming the great flexibility (Fig. 22(b) and (c)). Three devices connected in series lighting up the red and yellow LED lights connected in parallel prove the potential application (Fig. 22(d)). Nagaraju *et al.*[261] used a hot-air oven-based method to grow aligned NC LDH NFAs on Ni fabric and a simple electrochemical deposition method to further decorate fluffy NC LDH NS branches on NC LDH NFAs (Fig. 22(e)). The shape of the CV curves measured under various bending conditions at 50 mV s^{-1} is almost similar to normal without any distortion (Fig. 22(f) and (g)), which shows that the device has good capacitance and flexibility. Fig. 22(h) demonstrates its potential suitability for wearable electronic applications. By adjusting the ratio of Ni and Co, Liu *et al.*[262] obtained the optimized porous nanoflower-like NiCo LDH (Fig. 22(i)). A flexible Ni_3Co_1 LDH@graphene//AC asymmetric supercapacitor is prepared by using screen printing, and the device exhibits excellent flexibility by maintaining 95.8% capacitance after bending at different angles and 400 bends (Fig. 22(j)). When the two devices are connected in series, they can power the watch for more than 60 minutes after

only 50 seconds of charging and can power the watch normally even when it is worn on the hand and fully submerged in water (Fig. 22(k) and (l)). In order to show the performances in this manuscript, Table 4 displays the properties of the device based on LDHs and their composite electrodes.

4. Summary and outlook

Supercapacitors are one of the most promising energy storage devices, because of the advantages of fast charging and discharging speed, large temperature range and long cycle life. The large specific surface area of layered structures can substantially increase the double layer capacitance, and the redox reaction of transition metal elements can provide pseudocapacitance. LDHs can be used for energy storage in supercapacitors by both double layer capacitance and pseudocapacitance mechanisms. Meanwhile, the anions between the layers give rich options for modification and compounding of LDHs.

The advantages and disadvantages of each method can be considered after a broad understanding of the various synthesis methods. The appropriate method can be reasonably selected to prepare electrode materials with better performances. However, the prepared electrode materials in many cases still do not meet the actual requirements. Thus, the modification of the materials is particularly important. For instance, other components can be added during the preparation process or compounded with other materials for performance optimization. The defects can be constructed by etching and heat treatment for increasing the number of active sites. The heterogeneous structures can be generated on LDHs by electrochemical deposition to promote electron transfer. The electrode materials can be grown directly on the substrate to generate binder-free electrodes to reduce the internal resistance and mass, as well as enhance the ability of charge transfer.

This paper reviews the recent progress and the results of preparation methods and modification methods of hybrid LDHs, providing a cutting-edge reference for supercapacitor applications based on LDHs. A comprehensive understanding of the characteristics of various synthesis and modification methods can help to further synthesize materials with outstanding performances. There are both connections and distinctions between different synthesis and modification methods, and adequate mastery of these methods facilitates further research.

However, LDHs still have poor electrical conductivity, which inevitably leads to blocked electron transfer in the redox process and further affects the capacitance performances. Specifically, the CV curve deviates from the rectangular shape and the current–voltage is correspondingly poor during constant GCD processes. Moreover, the existing methods for the synthesis and modification of LDHs still have the disadvantages of complex reaction conditions and environmental pollution, which should be combined with the actual conditions in the subsequent research process to select the appropriate synthesis and modification methods.

It is a very meaningful work to further enhance the conductivity and the structure stability in order to expand the application fields while making full use of the structural advantages of the LDHs. As the research progresses, the preparation of LDHs evolves from simply using the synthesized LDHs directly as electrode materials to composite materials, and the continuous optimization of properties can enable a wider range of applications in the future. It is believed that with the efforts of many researchers, LDHs have great development prospects in the future and it can be expected that LDHs can contribute more to the development of science and technology.

Conflicts of interest

The authors declare that they have no conflict of interest.

Acknowledgements

We gratefully appreciate the support from the Natural Science Foundation of Shandong Province (ZR2019BB063). The author thanks the environmental and function material team, supported by the Project of Shandong Province Higher Educational Young Innovative Talent Introduction and Cultivation.

References

1 J. Wang, R. Fu, S. Wen, P. Ning, M. H. Helal, M. A. Salem, B. Xu, Z. El-Bahy, M. Huang, Z. Guo, L. Huang and Q. Wang, Progress and current challenges for CO_2 capture materials from ambient air, *Adv. Compos. Hybrid Mater.*, 2022, **5**, 2721–2759.

2 Z. Wang, M. Yang, X. Xie, C. Yu, Q. Jiang, M. Huang, H. Algadi, Z. Guo and H. Zhang, Applications of machine learning in perovskite materials, *Adv. Compos. Hybrid Mater.*, 2022, **5**, 2700–2720.

3 R. Kottayi, D. K. Maurya, R. Sittaramane and S. Angaiah, Recent developments in metal chalcogenides based quantum dot sensitized solar cells, *ES Energy Environ.*, 2022, **18**, 1–40.

4 C. T. Sarr, M. B. Camara and B. Dakyo, Supercapacitors aging assessment in wind/tidal intermittent energies application with variable temperature, *J. Energy Storage*, 2022, **46**, 103790.

5 N. Li, C. Y. Jia, Z. Fang, Z. J. Jiang, A. Ahmed, D. N. Hao, Z. T. Zhang and D. B. Luo, A U-shaped kinetic energy harvester for application in a near-zero energy parking system, *Sustain Cities Soc.*, 2022, **81**, 103866.

6 B. R. Ravada, N. R. Tummuru and B. N. L. Ande, Photovoltaic-Wind and Hybrid Energy Storage Integrated Multi-Source Converter Configuration for DC Microgrid Applications, *IEEE Trans. Sustain. Energy*, 2021, **12**, 83–91.

7 M. Eqi, C. Shi, J. Xie, F. Kang, H. Qi, X. Tan, Z. Huang, J. Liu and J. Guo, Synergetic effect of Ni-Au bimetal nanoparticles on urchin-like TiO_2 for hydrogen and arabinose co-production by glucose photoreforming, *Adv. Compos. Hybrid Mater.*, 2023, **6**, 5.

8 S. L. Hamukwaya, Z. Zhao, H. Hao, H. Abo-Dief, K. M. Abualnaja, A. K. Alanazi, M. M. Mashingaidze, S. M. El-Bahy, M. Huang and Z. Guo, Enhanced photocatalytic performance for hydrogen production and carbon dioxide reduction by a mesoporous single-crystal-like TiO_2 composite catalyst, *Adv. Compos. Hybrid Mater.*, 2022, **5**, 2620–2630.
9 W. Qiu, Q. Hao, S. H. K. Annamareddy, B. Xu, Z. Guo and Q. Jiang, Electric vehicle revolution and implications: ion battery and energy, *Eng. Sci.*, 2022, **20**, 100–109.
10 W. Yang, D. Peng, H. Kimura, X. Zhang, X. Sun, R. A. Pashameah, E. Alzahrani, B. Wang, Z. Guo, W. Du and C. Hou, Honeycomb-like nitrogen-doped porous carbon decorated with Co_3O_4 nanoparticles for superior electrochemical performance pseudo-capacitive lithium storage and supercapacitors, *Adv. Compos. Hybrid Mater.*, 2022, **5**, 3146–3157.
11 R. Wang, Z. H. Meng, X. M. Yan, T. Tian, M. Lei, R. A. Pashameah, H. M. Abo-Dief, H. Algadi, N. N. Huang, Z. H. Guo and H. L. Tang, Tellurium intervened Fe–N codoped carbon for improved oxygen reduction reaction and high-performance Zn-air batteries, *J. Mater. Sci. Technol.*, 2023, **137**, 215–222.
12 H. Li, Y. Fu, D. Alhashmialameer, H. K. Thabet, P. Zhang, C. Wang, K. Zhu, M. Huang, Z. Guo and F. Dang, Lattice distortion embedded core–shell nanoparticle through epitaxial growth barium titanate shell on the strontium titanate core with enhanced dielectric response, *Adv. Compos. Hybrid Mater.*, 2022, **5**, 2631–2641.
13 T. Ma, H. X. Yang and L. Lu, Development of hybrid battery-supercapacitor energy storage for remote area renewable energy systems, *Appl. Energy*, 2015, **153**, 56–62.
14 S. Liu, H. Du, M. Ma, Y. Kwon, C. Si, X. Ji, S. Choi and X. Zhang, Flexible and porous Co_3O_4-carbon nanofibers as binder-free electrodes for supercapacitors, *Adv. Compos. Hybrid Mater.*, 2021, **4**, 1367–1383.
15 H. Cheng, L. Xing, Y. Zuo, Y. Pan, M. Huang, A. Alhadhrami, M. M. Ilrahim, Z. M. El-Bahy, C. Liu, C. Shen and X. Liu, Constructing nickel chain/MXene networks in melamine foam towards phase change materials for thermal energy management and absorption-dominated electromagnetic interference shielding, *Adv. Compos. Hybrid Mater.*, 2022, **5**, 755–765.
16 C. Ding, N. Zhu, X. Wang, A. Alhadhrami, M. H. H. Mahmoud, M. M. Ibrahim, Q. Huang, C. Liu, M. Huang and J. Wang, Experimental study on the burning behaviors of 21 700 lithium-ion batteries with high specific energy after different immersion duration, *Adv. Compos. Hybrid Mater.*, 2022, **5**, 2575–2588.
17 S. Yang, K. Qu and Z. Huang, Optimizing hierarchical porous carbon from biomass waste for high-performance supercapacitors, *ES Food Agrofor.*, 2022, **10**, 39–50.
18 J. A. Lopez-Villanueva and S. R. Bolivar, Constant Phase Element in the Time Domain: The Problem of Initialization, *Energies*, 2022, **15**, 792.
19 H. J. Liu, J. C. Zhu, Z. Li, Z. C. Shi, J. L. Zhu and H. Mei, Fe_2O_3/N doped rGO anode hybridized with NiCo LDH/Co(OH)(2) cathode for battery-like supercapacitor, *Chem. Eng. J.*, 2021, **403**, 126325.
20 P. Xie, Z. Shi, M. Feng, K. Sun, Y. Liu, K. Yan, C. Liu, T. A. A. Moussa, M. Huang, S. Meng, G. Liang, H. Hou, R. Fan and Z. Guo, Recent advances in radio-frequency negative dielectric metamaterials by designing heterogeneous composites, *Adv. Compos. Hybrid Mater.*, 2022, **5**, 679–695.
21 Y. Tong, W. Zhao, W. Wu, D. Zhang, G. He and Z. Yang, Realizing enhanced dielectric and mechanical performance of polyvinylidene fluoride/SiC nanocomposites through a bio-inspired interface design, *Adv. Compos. Hybrid Mater.*, 2022, **5**, 263–277.
22 P. Wang, T. Song, H. M. Abo-Dief, J. Song, A. K. Alanazi, B. Fan, M. Huang, Z. Lin, A. A. Altalhi, S. Gao, L. Yang, J. Liu, S. Feng and T. Cao, Effect of carbon nanotubes on the interface evolution and dielectric properties of polylactic acid/ethylene–vinyl acetate copolymer nanocomposites, *Adv. Compos. Hybrid Mater.*, 2022, **5**, 1100–1110.
23 P. Wang, L. Yang, S. Gao, X. Chen, T. Cao, C. Wang, H. Liu, X. Hu, X. Wu and S. Feng, Enhanced dielectric properties of high glass transition temperature PDCPD/CNT composites by frontal ring-opening metathesis polymerization, *Adv. Compos. Hybrid Mater.*, 2021, **5**(4), 639–646.
24 Z. Zhuang, W. Wang, Y. Wei, T. Li, M. Ma and Y. Ma, Preparation of polyaniline nanorods/manganese dioxide nanoflowers core/shell nanostructure and investigation of electrochemical performances, *Adv. Compos. Hybrid Mater.*, 2021, **4**, 938–945.
25 R. Ma, C. Cui, D. Hu, S. M. El-Bahy, Y. Wang, I. H. El Azab, A. Elnaggar, H. Gu, G. A. M. Mersal, M. Huang and V. Murugadoss, Enhanced energy storage of lead-free mixed oxide core double-shell barium strontium zirconate titanate@magnesium aluminate@zinc oxide-boron trioxide-silica ceramic nanocomposites, *Adv. Compos. Hybrid Mater.*, 2022, **5**, 1477–1489.
26 C. D. Ma, J. L. Bai, M. Demir, X. Hu, S. F. Liu and L. L. Wang, Water chestnut shell-derived N/S-doped porous carbons and their applications in CO_2 adsorption and supercapacitor, *Fuel*, 2022, **326**, 125119.
27 Y. Ma, C. P. Hou, H. Zhang, M. T. Qiao, Y. H. Chen, H. P. Zhang, Q. Y. Zhang and Z. H. Guo, Morphology-dependent electrochemical supercapacitors in multi-dimensional polyaniline nanostructures, *J. Mater. Chem. A*, 2017, **5**, 14041–14052.
28 B. Dai, Y. Ma, S. X. Feng, H. W. Wang, M. L. Ma, J. X. Ding, X. Q. Yin and T. X. Li, Fabrication of one-dimensional M (Co, Ni)@polyaniline nanochains with adjustable thickness for excellent microwave absorption properties, *J. Colloid Interface Sci.*, 2022, **627**, 113–125.
29 L. A. Chen, X. W. Zheng, C. Y. Hao, Q. D. Sun, P. C. Si, L. J. Ci and J. Wei, Enhanced ions and electrons transmission enables high-performance KxMnO@C cathode for hybrid supercapacitors, *Ceram. Int.*, 2022, **48**, 16516–16521.
30 Y. Yang, M. T. Hoang, A. Bhardwaj, M. Wilhelm, S. Mathur and H. Wang, Perovskite solar cells based self-charging power packs: fundamentals, applications and challenges, *Nano Energy*, 2022, **94**, 106910.

31 Q. Wu, P. F. Li, Y. H. Wang and F. F. Wu, Construction and electrochemical energy storage performance of free-standing hexagonal Ti_3C_2 film for flexible supercapacitor, *Appl. Surf. Sci.*, 2022, **593**, 153380.
32 J. L. Shang, Y. D. Zhang, Q. Zhang, Y. Li, F. Y. Deng, R. J. Gao and J. B. Wang, A novel interlaced NiCoFe hydrotalcite assembled by nanorods and nanosheets with enhanced electrochemical performance for supercapacitor, *J. Alloys Compd.*, 2022, **925**, 166668.
33 M. A. Aziz, S. S. Shah, S. M. Abu Nayem, M. N. Shaikh, A. S. Hakeem and I. A. Bakare, Peat soil-derived silica doped porous graphitic carbon with high yield for high-performance all-solid-state symmetric supercapacitors, *J. Energy Storage*, 2022, **50**, 104278.
34 E. Cevik, S. M. M. Asiri, T. F. Qahtan and A. Bozkurt, Fabrication of high mechanical stability electrodes and bio-electrolytes for high-performance supercapacitor application, *J. Alloys Compd.*, 2022, **913**, 165230.
35 Y. S. Chen, Z. Yin, D. L. Huang, L. Lei, S. Chen, M. Yan, L. Du, R. H. Xiao and M. Cheng, Uniform polypyrrole electrodeposition triggered by phytic acid-guided interface engineering for high energy density flexible supercapacitor, *J. Colloid Interface Sci.*, 2022, **611**, 356–365.
36 J. D. Afroze, L. Tong, M. J. Abden and Y. Chen, Multifunctional hierarchical graphene-carbon fiber hybrid aerogels for strain sensing and energy storage, *Adv. Compos. Hybrid Mater.*, 2023, **6**, 18.
37 K. Dericiler, A. Kocanali, M. Buldu-Akturk, E. Erdem and B. Saner Okan, Upcycling process of transforming waste coffee into spherical graphene by flash pyrolysis for sustainable supercapacitor manufacturing with virgin graphene electrodes and its comparative life cycle assessment, *Biomass Convers. Biorefin.*, 2022, DOI: **10.1007/s13399-022-02447-8**.
38 X. Li, Z. Lin, Y. Wei, W. Luo, J. Ding, T. Li and Y. Ma, MXene-MnO_2–CoNi layered double hydroxides//activated carbon flexible asymmetric supercapacitor, *J. Energy Storage*, 2022, **55**, 105668.
39 H. Wei, A. Li, D. Kong, Z. Li, D. Cui, T. Li, B. Dong and Z. Guo, Polypyrrole/reduced graphene aerogel film for wearable piezoresisitic sensors with high sensing performances, *Adv. Compos. Hybrid Mater.*, 2021, **4**, 86–95.
40 S. Islam, M. M. Mia, S. S. Shah, S. Naher, M. N. Shaikh, M. A. Aziz and A. J. S. Ahammad, Recent Advancements in Electrochemical Deposition of Metal-Based Electrode Materials for Electrochemical Supercapacitors, *Chem. Rec.-Age*, 2022, **22**, e202200013.
41 C. L. Liu, Q. Li and K. Wang, State-of-charge estimation and remaining useful life prediction of supercapacitors, *Renewable Sustainable Energy Rev.*, 2021, **150**, 111408.
42 H. Liu, H. B. Wang, X. H. Lu, V. Murugadoss, M. N. Huang, H. S. Yang, F. X. Wan, D. G. Yu and Z. H. Guo, Electrospun structural nanohybrids combining three composites for fast helicide delivery, *Adv. Compos. Hybrid Mater.*, 2022, **5**, 1017–1029.
43 D. Wei, M. M. Weng, M. H. H. Mahmoud, A. Y. Elnaggar, I. H. El Azab, X. X. Sheng, M. N. Huang, Z. M. El-Bahy and J. T. Huang, Development of novel biomass hybrid aerogel supported composite phase change materials with improved light-thermal conversion and thermal energy storage capacity, *Adv. Compos. Hybrid Mater.*, 2022, **5**, 1910–1921.
44 P. Huo, S. Ni, P. Hou, Z. Xun, Y. Liu and J. Gu, A Cross-linked Soybean Protein Isolate Gel Polymer Electrolyte Based on Neutral Aqueous Electrolyte for a High-Energy-Density Supercapacitor, *Polymers*, 2019, **11**, 31086006.
45 D. S. Kong, Z. M. El-Bahy, H. Algadi, T. Li, S. M. El-Bahy, M. A. Nassan, J. R. Li, A. A. Faheim, A. Li, C. X. Xu, M. N. Huang, D. P. Cui and H. G. Wei, Highly sensitive strain sensors with wide operation range from strong MXene-composited polyvinyl alcohol/sodium carboxymethylcellulose double network hydrogel, *Adv. Compos. Hybrid Mater.*, 2022, **5**, 1976–1987.
46 X. Jin, L. Song, C. Dai, H. Ma, Y. Xiao, X. Zhang, Y. Han, X. Li, J. Zhang, Y. Zhao, Z. Zhang, L. Duan and L. Qu, A self-healing zinc ion battery under −20 °C, *Energy Storage Mater.*, 2022, **44**, 517–526.
47 X. Jin, L. Song, C. Dai, Y. Xiao, Y. Han, X. Li, Y. Wang, J. Zhang, Y. Zhao, Z. Zhang, N. Chen, L. Jiang and L. Qu, A Flexible Aqueous Zinc-Iodine Microbattery with Unprecedented Energy Density, *Adv. Mater.*, 2022, **34**, 2109450.
48 X. Jin, L. Song, H. Yang, C. Dai, Y. Xiao, X. Zhang, Y. Han, C. Bai, B. Lu, Q. Liu, Y. Zhao, J. Zhang, Z. Zhang and L. Qu, Stretchable supercapacitor at −30 °C, *Energy Environ. Sci.*, 2021, **14**, 3075–3085.
49 X. Jin, L. Song, C. Dai, Y. Xiao, Y. Han, X. Zhang, X. Li, C. Bai, J. Zhang, Y. Zhao, Z. Zhang, L. Jiang and L. Qu, An Aqueous Anti-Freezing and Heat-Tolerant Symmetric Microsupercapacitor with 2.3 V Output Voltage, *Adv. Energy Mater.*, 2021, **11**, 2101523.
50 L. Song, C. Dai, X. Jin, Y. Xiao, Y. Han, Y. Wang, X. Zhang, X. Li, S. Zhang, J. Zhang, Y. Zhao, Z. Zhang and L. Qu, Pure Aqueous Planar Microsupercapacitors with Ultrahigh Energy Density under Wide Temperature Ranges, *Adv. Funct. Mater.*, 2022, **32**, 2203270.
51 S. Kumar, G. Saeed, L. Zhu, K. N. Hui, N. H. Kim and J. H. Lee, 0D to 3D carbon-based networks combined with pseudocapacitive electrode material for high energy density supercapacitor: a review, *Chem. Eng. J.*, 2021, **403**, 126352.
52 X. J. Liu, M. Gao, J. Y. Chen, S. Guo, W. Zhu, L. C. Bai, W. Z. Zhai, H. J. Du, H. Wu, C. Z. Yan, Y. S. Shi, J. W. Gu, H. J. Qi and K. Zhou, Recent Advances in Stimuli-Responsive Shape-Morphing Hydrogels, *Adv. Funct. Mater.*, 2022, **32**, 2203323.
53 T. Z. Guo, D. Zhou, L. X. Pang, S. K. Sun, T. Zhou and J. Z. Su, Perspectives on Working Voltage of Aqueous Supercapacitors, *Small*, 2022, **18**, e2106360.
54 Y. Wei, W. Luo, Z. Zhuang, B. Dai, J. Ding, T. Li, M. Ma, X. Yin and Y. Ma, Fabrication of ternary MXene/MnO_2/polyaniline nanostructure with good electrochemical performances, *Adv. Compos. Hybrid Mater.*, 2021, **4**, 1082–1091.
55 M. Athanasiou, S. N. Yannopoulos and T. Ioannides, Biomass-derived graphene-like materials as active

electrodes for supercapacitor applications: a critical review, *Chem. Eng. J.*, 2022, **446**, 137191.
56 K. Krishnamoorthy, P. Pazhamalai, S. Manoharan, N. U. L. Ali and S. J. Kim, Recent trends, challenges, and perspectives in piezoelectric-driven self-chargeable electrochemical supercapacitors, *Carbon Energy*, 2022, **4**, 833–855.
57 S. P. Ega and P. Srinivasan, Quinone materials for supercapacitor: current status, approaches, and future directions, *J. Energy Storage*, 2022, **47**, 103700.
58 M. Dhanda, R. Arora, S. Ahlawat, S. P. Nehra and S. Lata, Electrolyte as a panacea to contemporary scientific world of super-capacitive energy: a condense report, *J. Energy Storage*, 2022, **52**, 104740.
59 K. P. Ruan and J. W. Gu, Ordered Alignment of Liquid Crystalline Graphene Fluoride for Significantly Enhancing Thermal Conductivities of Liquid Crystalline Polyimide Composite Films, *Macromolecules*, 2022, **55**, 4134–4145.
60 D. Mohanadas and Y. Sulaiman, Recent advances in development of electroactive composite materials for electrochromic and supercapacitor applications, *J. Power Sources*, 2022, **523**, 231029.
61 N. N. Loganathan, V. Perumal, B. R. Pandian, R. Atchudan, T. Edison and M. Ovinis, Recent studies on polymeric materials for supercapacitor development, *J. Energy Storage*, 2022, **49**, 104937.
62 M. M. Amaral, R. Venancio, A. C. Peterlevitz and H. Zanin, Recent advances on quasi-solid-state electrolytes for supercapacitors, *J. Energy Chem.*, 2022, **67**, 697–717.
63 H. Wei, H. Gu, J. Guo, D. Cui, X. Yan, J. Liu, D. Cao, X. Wang, S. Wei and Z. Guo, Significantly enhanced energy density of magnetite/polypyrrole nanocomposite capacitors at high rates by low magnetic fields, *Adv. Compos. Hybrid Mater.*, 2017, **1**, 127–134.
64 J. Kumar, H. J. Jung, R. R. Neiber, R. A. Soomro, Y. J. Kwon, N. Ul Hassan, M. Shon, J. H. Lee, K. Y. Baek and K. Y. Cho, Recent advances in oxygen deficient metal oxides: opportunities as supercapacitor electrodes, *Int. J. Energy Res.*, 2022, **46**, 7055–7081.
65 Y. Wei, M. Zheng, W. Luo, B. Dai, J. Ren, M. Ma, T. Li and Y. Ma, All pseudocapacitive MXene-MnO_2 flexible asymmetric supercapacitor, *J. Energy Storage*, 2022, **45**, 103715.
66 J. Chen, Y. Huang, X. Ma and Y. Lei, Functional self-healing materials and their potential applications in biomedical engineering, *Adv. Compos. Hybrid Mater.*, 2018, **1**, 94–113.
67 F. F. Xing, Z. H. Bi, F. Su, F. Y. Liu and Z. S. Wu, Unraveling the Design Principles of Battery-Supercapacitor Hybrid Devices: From Fundamental Mechanisms to Microstructure Engineering and Challenging Perspectives, *Adv. Energy Mater.*, 2022, **12**, 2200594.
68 B. Joshi, E. Samuel, Y. I. Kim, A. L. Yarin, M. T. Swihart and S. S. Yoon, Review of recent progress in electrospinning-derived freestanding and binder-free electrodes for supercapacitors, *Coordin. Chem. Rev.*, 2022, **460**, 214466.
69 R. Vinodh, R. S. Babu, S. Sambasivam, C. Gopi, S. Alzahmi, H. J. Kim, A. L. F. de Barros and I. M. Obaidat, Recent Advancements of Polyaniline/Metal Organic Framework (PANI/MOF) Composite Electrodes for Supercapacitor Applications: A Critical Review, *Nanomaterials*, 2022, **12**, 1511.
70 R. Bi, D. Mao, J. Wang, R. Yu and D. Wang, Hollow Nanostructures for Surface/Interface Chemical Energy Storage Application, *Acta Chim. Sin.*, 2020, **78**, 1200.
71 N. R. Chodankar, H. D. Pham, A. K. Nanjundan, J. F. S. Fernando, K. Jayaramulu, D. Golberg, Y. K. Han and D. P. Dubal, True Meaning of Pseudocapacitors and Their Performance Metrics: Asymmetric versus Hybrid Supercapacitors, *Small*, 2020, **16**, e2002806.
72 C. Li, L. Sha, K. Yang, F. Kong, P. Li, Y. Tao, X. Zhao and H. Chen, Effects of ultrafiltration on Co-Metal Organic Framework/pre-hydrolysis solution carbon materials for supercapacitor energy storage, *Front. Chem.*, 2022, **10**, 991230.
73 Y. Guo, H. Liu, D. D. Wang, Z. M. El-Bahy, J. T. Althakafy, H. M. Abo-Dief, Z. H. Guo, B. B. Xu, C. T. Liu and C. Y. Shen, Engineering hierarchical heterostructure material based on metal-organic frameworks and cotton fiber for high-efficient microwave absorber, *Nano Res.*, 2022, **15**, 6841–6850.
74 Z. Fahimi, O. Moradlou, A. Sabbah, K. H. Chen, L. C. Chen and M. Qorbani, $Co_3V_2O_8$ hollow spheres with mesoporous walls as high-capacitance electrode for hybrid supercapacitor device, *Chem. Eng. J.*, 2022, **436**, 135225.
75 Y. Tian, X. Yang, A. Nautiyal, Y. Zheng, Q. Guo, J. Luo and X. Zhang, One-step microwave synthesis of MoS_2/MoO_3@-graphite nanocomposite as an excellent electrode material for supercapacitors, *Adv. Compos. Hybrid Mater.*, 2019, **2**, 151–161.
76 B. Jain, A. Hashmi, S. Sanwaria, A. K. Singh, M. A. B. H. Susan and A. Singh, Zinc oxide nanoparticle incorporated on graphene oxide: an efficient and stable photocatalyst for water treatment through the Fenton process, *Adv. Compos. Hybrid Mater.*, 2020, **3**, 231–242.
77 O. Gerard, A. Numan, S. Krishnan, M. Khalid, R. Subramaniam and R. Kasi, A review on the recent advances in binder-free electrodes for electrochemical energy storage application, *J. Energy Storage*, 2022, **50**, 104283.
78 Y. T. Wang, X. F. He, G. Y. He, C. Meng, X. M. Chen, F. T. Li and Y. Zhou, A critical review on nickel sulfide-based electrode materials for supercapacitors, *Crit. Rev. Solid State*, 2022, DOI: **10.1080/10408436.2022.2078276**.
79 T. Wang, J. Q. Lei, Y. Wang, L. Pang, F. P. Pan, K. J. Chen and H. X. Wang, Approaches to Enhancing Electrical Conductivity of Pristine Metal–Organic Frameworks for Supercapacitor Applications, *Small*, 2022, **18**, e2203307.
80 K. Y. Zhang, Z. Y. Ma, H. Deng and Q. Fu, Improving high-temperature energy storage performance of PI dielectric capacitor films through boron nitride interlayer, *Adv. Compos. Hybrid Mater.*, 2022, **5**, 238–249.
81 Y. Wang, Y.-J. Hu, X. Hao, P. Peng, J.-Y. Shi, F. Peng and R.-C. Sun, Hydrothermal synthesis and applications of advanced carbonaceous materials from biomass: a review, *Adv. Compos. Hybrid Mater.*, 2020, **3**, 267–284.

82 S. Li, C. Yang, S. Sarwar, A. Nautiyal, P. Zhang, H. Du, N. Liu, J. Yin, K. Deng and X. Zhang, Facile synthesis of nanostructured polyaniline in ionic liquids for high solubility and enhanced electrochemical properties, *Adv. Compos. Hybrid Mater.*, 2019, **2**, 279–288.
83 S. V. Sadavar, N. S. Padalkar, R. B. Shinde, S. T. Kochuveedu, U. M. Patil, A. S. Patil, R. N. Bulakhe, C. D. Lokhande, I. In, R. R. Salunkhe and J. L. Gunjakar, Mesoporous nanohybrids of 2-D Cobalt-Chromium layered double hydroxide and polyoxovanadate anions for high performance hybrid asymmetric supercapacitors, *J. Power Sources*, 2022, **524**, 231065.
84 J. Zhao, Y. Guo, Y. Q. Yang, Z. Shen, Q. Wu, L. J. Yang, X. Z. Wang and Z. Hu, Insight into the decay mechanism of cycling capacitance for layered double hydroxides at sub-nanometer scale, *Chem. Commun.*, 2022, **58**, 9124–9127.
85 L. Xiao, H. Qi, K. Qu, C. Shi, Y. Cheng, Z. Sun, B. Yuan, Z. Huang, D. Pan and Z. Guo, Layer-by-layer assembled free-standing and flexible nanocellulose/porous Co_3O_4 polyhedron hybrid film as supercapacitor electrodes, *Adv. Compos. Hybrid Mater.*, 2021, **4**, 306–316.
86 L. Pu, J. Zhang, N. K. L. Jiresse, Y. Gao, H. Zhou, N. Naik, P. Gao and Z. Guo, N-doped MXene derived from chitosan for the highly effective electrochemical properties as supercapacitor, *Adv. Compos. Hybrid Mater.*, 2022, **5**, 356–369.
87 C. Z. Yin, C. Wang and Q. Hu, Selective removal of As(V) from wastewater with high efficiency by glycine-modified Fe/Zn-layered double hydroxides, *Adv. Compos. Hybrid Mater.*, 2021, **4**, 360–370.
88 Y. F. Wu, Y. C. Hsiao, C. H. Liao, C. S. Hsu, S. Yougbare and L. Y. Lin, Novel design of Sulfur-doped nickel cobalt layered double hydroxide and polypyrrole nanotube composites from zeolitic imidazolate Framework-67 as efficient active material of battery supercapacitor hybrids, *J. Colloid Interface Sci.*, 2022, **628**, 540–552.
89 Y. F. Wu, Y. C. Hsiao, C. H. Liao, C. S. Hsu, S. Yougbare and L. Y. Lin, Novel design of Sulfur-doped nickel cobalt layered double hydroxide and polypyrrole nanotube composites from zeolitic imidazolate Framework-67 as efficient active material of battery supercapacitor hybrids, *J. Colloid Interface Sci.*, 2022, **628**, 540–552.
90 X. Ge, C. D. Gu, X. L. Wang and J. P. Tu, Ionothermal synthesis of cobalt iron layered double hydroxides (LDHs) with expanded interlayer spacing as advanced electrochemical materials, *J. Mater. Chem. A*, 2014, **2**, 17066–17076.
91 R. B. Tang, P. Xu, J. W. Dong, H. G. Gui, T. Zhang, Y. S. Ding, V. Murugadoss, N. Naik, D. Pan, M. N. Huang and Z. H. Guo, Carbon foams derived from emulsion-templated porous polymeric composites for electromagnetic interference shielding, *Carbon*, 2022, **188**, 492–502.
92 L. H. Wang, D. D. Jia, L. J. Yue, K. Zheng, A. T. Zhang, Q. Jia and J. Q. Liu, In Situ Fabrication of a Uniform Co-MOF Shell Coordinated with $CoNiO_2$ to Enhance the Energy Storage Capability of NiCo-LDH via Vapor-Phase Growth, *ACS Appl. Mater. Interfaces*, 2020, **12**, 47526–47538.
93 S. Jamil, A. Rahat Alvi, H. Rauf Khan and M. R. S. A. Janjua, Layered Double Hydroxides(LDHs): Synthesis & Applications, *Prog. Chem.*, 2018, **31**, 394–412.
94 L. Hui, Y. R. Xue, B. L. Huang, H. D. Yu, C. Zhang, D. Y. Zhang, D. Z. Jia, Y. J. Zhao, Y. J. Li, H. B. Liu and Y. L. Li, Overall water splitting by graphdiyne-exfoliated and -sandwiched layered double-hydroxide nanosheet arrays, *Nat. Commun.*, 2018, **9**, 5309.
95 L. Wang, Z. L. Ma, H. Qiu, Y. L. Zhang, Z. Yu and J. W. Gu, Significantly Enhanced Electromagnetic Interference Shielding Performances of Epoxy Nanocomposites with Long-Range Aligned Lamellar Structures, *Nano-Micro Lett.*, 2022, **14**, 224.
96 B. Zhao, Z. L. Ma, Y. Y. Sun, Y. X. Han and J. W. Gu, Flexible and Robust $Ti_3C_2T_x$/(ANF (R) FeNi) Composite Films with Outstanding Electromagnetic Interference Shielding and Electrothermal Conversion Performances, *Small Struct.*, 2022, **3**, 2200162.
97 P. F. Li, X. Q. Liu, M. Arif, H. L. Yan, C. Y. Hu, S. M. Chen and X. H. Liu, In situ growth of glucose-intercalated LDHs on $NiCo_2S_4$ hollow nanospheres to enhance energy storage capacity for hybrid supercapacitors, *Colloids Surf., A*, 2022, **644**, 128823.
98 Z. Y. Xiao, Y. J. Mei, S. Yuan, H. Mei, B. Xu, Y. X. Bao, L. L. Fan, W. P. Kang, F. N. Dai, R. M. Wang, L. Wang, S. Q. Hu, D. F. Sun and H. C. Zhou, Controlled Hydrolysis of Metal-Organic Frameworks: Hierarchical Ni/Co-Layered Double Hydroxide Microspheres for High-Performance Supercapacitors, *ACS Nano*, 2019, **13**, 7024–7030.
99 J. Ni, X. Huang, Y. Bai, B. Zhao, Y. Han, S. Han, T. Xu, C. Si and C. Zhang, Resistance to aggregation-caused quenching: chitosan-based solid carbon dots for white light-emitting diode and 3D printing, *Adv. Compos. Hybrid Mater.*, 2022, **5**, 1865–1875.
100 C. Jing, B. Dong and Y. Zhang, Chemical Modifications of Layered Double Hydroxides in the Supercapacitor, *Energy Environ. Mater.*, 2020, **3**, 346–379.
101 G. Li, Y. Ji, D. Zuo, J. Xu and H. Zhang, Carbon electrodes with double conductive networks for high-performance electrical double-layer capacitors, *Adv. Compos. Hybrid Mater.*, 2019, **2**, 456–461.
102 Y. Guo, D. Wang, T. Bai, H. Liu, Y. Zheng, C. Liu and C. Shen, Electrostatic self-assembled $NiFe_2O_4/Ti_3C_2T_x$ MXene nanocomposites for efficient electromagnetic wave absorption at ultralow loading level, *Adv. Compos. Hybrid Mater.*, 2021, **4**, 602–613.
103 K. Qu, Z. Sun, C. Shi, W. Wang, L. Xiao, J. Tian, Z. Huang and Z. Guo, Dual-acting cellulose nanocomposites filled with carbon nanotubes and zeolitic imidazolate framework-67 (ZIF-67)-derived polyhedral porous Co_3O_4 for symmetric supercapacitors, *Adv. Compos. Hybrid Mater.*, 2021, **4**, 670–683.
104 P. Wang, T. Song, H. M. Abo-Dief, J. Song, A. K. Alanazi, B. Fan, M. Huang, Z. Lin, A. A. Altalhi, S. Gao, L. Yang, J. Liu, S. Feng and T. Cao, Effect of carbon nanotubes on the interface evolution and dielectric properties of

polylactic acid/ethylene-vinyl acetate copolymer nanocomposites, *Adv. Compos. Hybrid Mater.*, 2022, **5**, 1100–1110.
105 Q. X. Wu, Z. P. Feng, Z. M. Cai, C. W. Lan, J. C. Xu, K. Bi and Y. N. Hao, Poly(methyl methacrylate)-based ferroelectric/dielectric laminated films with enhanced energy storage performances, *Adv. Compos. Hybrid Mater.*, 2022, **5**, 1137–1144.
106 H. Liu, T. Xu, Q. Liang, Q. Zhao, D. Zhao and C. Si, Compressible cellulose nanofibrils/reduced graphene oxide composite carbon aerogel for solid-state supercapacitor, *Adv. Compos. Hybrid Mater.*, 2022, **5**, 1168–1179.
107 M. Xu and M. Wei, Layered Double Hydroxide-Based Catalysts: Recent Advances in Preparation, Structure, and Applications, *Adv. Funct. Mater.*, 2018, **28**, 1802943.
108 H. Zhang, X. B. Liang, Y. L. Hu, P. Zhang, L. W. Yang, D. Y. He, M. Y. Hua and Y. G. Tong, Correlation of C/C preform density and microstructure and mechanical properties of C/C-ZrC-based ultra-high-temperature ceramic matrix composites, *Adv. Compos. Hybrid Mater.*, 2021, **4**, 743–750.
109 H. Y. Du, Y. L. An, Y. H. Wei, X. D. Liu, L. F. Hou, B. S. Liu, M. M. Liu and P. K. Liaw, Experimental and numerical studies on strength and ductility of gradient-structured iron plate obtained by surface mechanical-attrition treatment, *Mater. Sci. Eng., A*, 2019, **744**, 471–480.
110 Y. Y. Wang, D. F. Yan, S. El Hankari, Y. Q. Zou and S. Y. Wang, Recent Progress on Layered Double Hydroxides and Their Derivatives for Electrocatalytic Water Splitting, *Adv. Sci.*, 2018, **5**, 1800064.
111 G. L. Fan, F. Li, D. G. Evans and X. Duan, Catalytic applications of layered double hydroxides: recent advances and perspectives, *Chem. Soc. Rev.*, 2014, **43**, 7040–7066.
112 Y. T. Guo, N. Meng, J. Xu, K. N. Zhang, Q. Q. Zhang, E. Pawlikowska, M. Szafran and F. Gao, Microstructure and dielectric properties of $Ba_{0.6}Sr_{0.4}TiO_3$/(acrylonitrile-butadiene-styrene)-poly(vinylidene fluoride) composites, *Adv. Compos. Hybrid Mater.*, 2019, **2**, 681–689.
113 L. Guo, Y. F. Zhang, J. J. Zheng, L. Q. Shang, Y. J. Shi, Q. Wu, X. X. Liu, Y. M. Wang, L. Q. Shi and Q. Shao, Synthesis and characterization of ZnNiCr-layered double hydroxides with high adsorption activities for Cr(VI), *Adv. Compos. Hybrid Mater.*, 2021, **4**, 819–829.
114 G. Li, L. Wang, X. Lei, Z. Peng, T. Wan, S. Maganti, M. Huang, V. Murugadoss, I. Seok, Q. Jiang, D. Cui, A. Alhadhrami, M. M. Ibrahim and H. Wei, Flexible, yet robust polyaniline coated foamed polylactic acid composite electrodes for high-performance supercapacitors, *Adv. Compos. Hybrid Mater.*, 2022, **5**, 853–863.
115 Z. Chen, Q. Fan, M. Huang and H. Cölfen, Synthesis of two-dimensional layered double hydroxides: a systematic overview, *CrystEngComm*, 2022, **24**, 4639–4655.
116 M. Khorshidi, S. Asadpour, N. Sarmast and M. Dinari, A review of the synthesis methods, properties, and applications of layered double hydroxides/carbon nanocomposites, *J. Mol. Liq.*, 2022, **348**, 118399.
117 A. Kim, I. Varga, A. Adhikari and R. Patel, Recent Advances in Layered Double Hydroxide-Based Electrochemical and Optical Sensors, *Nanomaterials*, 2021, **11**, 2809.
118 G. Wei, J. M. Zhang, M. Usuelli, X. F. Zhang, B. Liu and R. Mezzenga, Biomass vs inorganic and plastic-based aerogels: structural design, functional tailoring, resource-efficient applications and sustainability analysis, *Prog. Mater. Sci.*, 2022, **125**, 100915.
119 Y. Ma, X. Xie, W. Yang, Z. Yu, X. Sun, Y. Zhang, X. Yang, H. Kimura, C. Hou, Z. Guo and W. Du, Recent advances in transition metal oxides with different dimensions as electrodes for high-performance supercapacitors, *Adv. Compos. Hybrid Mater.*, 2021, **4**, 906–924.
120 N. S. Padalkar, S. V. Sadavar, R. B. Shinde, A. S. Patil, U. M. Patil, V. V. Magdum, Y. M. Chitare, S. P. Kulkarni, R. N. Bulakhe, V. G. Parale and J. L. Gunjakar, 2D-2D nanohybrids of Ni-Cr-layered double hydroxide and graphene oxide nanosheets: electrode for hybrid asymmetric supercapacitors, *Electrochim. Acta*, 2022, **424**, 140615.
121 N. Wang, H. W. Pang, S. J. Yu, P. C. Gu, S. Song, H. Q. Wang and X. K. Wang, Investigation of Adsorption Mechanism of Layered Double Hydroxides and Their Composites on Radioactive Uranium: A Review, *Acta Chim. Sin.*, 2019, **77**, 143–152.
122 Z. Yang, L. Han, X. Fu, Y. Wang, H. Huang and M. Xu, Double-safety flexible supercapacitor basing on zwitterionic hydrogel: over-heat alarm and flame-retardant electrolyte, *Adv. Compos. Hybrid Mater.*, 2022, **5**, 1876–1887.
123 Y. Wang, D. Yang, M. M. Hessien, K. Du, M. M. Ibrahim, Y. Su, G. A. M. Mersal, R. Ma, S. M. El-Bahy, M. Huang, Q. Yuan, B. Cui and D. Hu, Flexible barium titanate@polydopamine/polyvinylidene fluoride/polymethyl methacrylate nanocomposite films with high performance energy storage, *Adv. Compos. Hybrid Mater.*, 2022, **5**, 2106–2115.
124 B. Li, M. Guo, X. Chen and Y. Miao, Hydrothermally synthesized N and S co-doped mesoporous carbon microspheres from poplar powder for supercapacitors with enhanced performance, *Adv. Compos. Hybrid Mater.*, 2022, **5**, 2306–2316.
125 Y. Wen, Y. Zhao, L. Lu, S. J. Zhang and B. Xu, Electrochemical Performance of Zn-Al Double Layered Hydroxide for Supercapacitor Application, *3rd Annual International Workshop on Materials Science and Engineering (Iwmse2017)*, 2017, **250**, 012055.
126 B. R. Wiston, P. Prabhakaran and M. Ashok, Bimetallic NiFe hydroxide coated onto commercial graphite foil as efficient supercapacitor electrode, *J. Energy Storage*, 2022, **50**, 104226.
127 Q. Xiao, Y. Yuan, J. Zhu, Z. Shi, Z. Li and J. Zhu, Carbonate doped nickel-cobalt layered double hydroxide for high performance asymmetric supercapacitors, *J. Alloys Compd.*, 2022, **916**, 165391.
128 G. Wang, Y. Li, T. Zhao and Z. Jin, Phosphatized mild-prepared-NiCo LDHs cabbage-like spheres exhibit excellent performance as a supercapacitor electrode, *New J. Chem.*, 2021, **45**, 251–261.
129 Z. Wang, K. Yin, Y. Zhang, K. Sun, L. Xie, M. Cong, S. Cao, Y. Lei, X. Li and R. Fan, Two-dimensional $Ti_3C_2T_x$/carbonized wood metacomposites with weakly negative permittivity, *Adv. Compos. Hybrid Mater.*, 2022, **5**, 2369–2377.

130 Y. Li, B. Huang, X. Zhao and Z. Luo, Zeolitic imidazolate framework-L-assisted synthesis of inorganic and organic anion-intercalated hetero-trimetallic layered double hydroxide sheets as advanced electrode materials for aqueous asymmetric super-capacitor battery, *J. Power Sources*, 2022, **527**, 231149.

131 J. Wang, Z. Wang, N. Liu, C. Liu, J. Yan, C. C. Li, J. Cui, J. Liu, X. Hu and Y. Wu, Al doped Ni-Co layered double hydroxides with surface-sulphuration for highly stable flexible supercapacitors, *J. Colloid Interface Sci.*, 2022, **615**, 173–183.

132 W. Zhang, H. Fan, Q. Liu, N. Ta, Y. Pu, X. Chen, Y. Sui, E. Wang and P. Cao, Nickel-rich NiCo LDHs supported on hollow carbon shells for hybrid supercapacitors, *Electrochim. Acta*, 2021, **395**, 139167.

133 L. Wan, Y. M. Wang, C. Du, J. Chen, M. J. Xie, Y. P. Wu and Y. Zhang, NiAlP@Cobalt substituted nickel carbonate hydroxide heterostructure engineered for enhanced supercapacitor performance, *J. Colloid Interface Sci.*, 2022, **609**, 1–11.

134 F. B. M. Ahmed, D. Khalafallah, M. Zhi and Z. Hong, Porous nanoframes of sulfurized NiAl layered double hydroxides and ternary bismuth cerium sulfide for supercapacitor electrodes, *Adv. Compos. Hybrid Mater.*, 2022, **5**, 2500–2514.

135 F. Z. Janani, N. Taoufik, H. Khiar, W. Boumya, A. Elhalil, M. Sadiq, A. V. Puga and N. Barka, Nanostructured layered double hydroxides based photocatalysts: insight on synthesis methods, application in water decontamination/splitting and antibacterial activity, *Surf. Interfaces*, 2021, **25**, 101263.

136 F. Yang, J. Chu, Y. Cheng, J. Gong, X. Wang and S. Xiong, Hydrothermal Synthesis of NiCo-layered Double Hydroxide Nanosheets Decorated on Biomass Carbon Skeleton for High Performance Supercapacitor, *Chem. Res. Chin. Univ.*, 2021, **37**, 772–777.

137 M. Chen, J. Wang, H. Tang, Y. Yang, B. Wang, H. Zhao and D. Wang, Synthesis of multi-shelled MnO_2 hollow microspheres via an anion-adsorption process of hydrothermal intensification, *Inorg. Chem. Front.*, 2016, **3**, 1065–1070.

138 C. Y. Li, Y. J. Zhou, X. Li, H. Q. Wang, P. W. Huo and X. K. Wang, Ni dopping Co_2Al ternary layered double hydroxides for improving electrochemical performance of high-performance hybrid supercapacitors, *Appl. Surf. Sci.*, 2021, **536**, 147780.

139 D. A. Reddy, K. A. J. Reddy, M. Gopannagari, Y. Kim, A. P. Rangappa, D. P. Kumar and T. K. Kim, Exposure of NiFe-LDH active sites by cation-exchange to promote photoelectrochemical water splitting performance, *Appl. Surf. Sci.*, 2021, **570**, 151134.

140 R. Aladpoosh and M. Montazer, Functionalization of cellulose fibers alongside growth of 2D LDH platelets through urea hydrolysis inspired Taro wettability, *Carbohydr. Polym.*, 2022, **275**, 118584.

141 Nikhil, G. P. Ji and R. Prakash, Hydrothermal synthesis of Zn–Mg-based layered double hydroxide coatings for the corrosion protection of copper in chloride and hydroxide media, *Int. J. Min. Met. Mater.*, 2021, **28**, 1991–2000.

142 Z. Q. Liu, Y. X. Zhong, Y. L. Qiu, L. Cui, W. R. Yang, J. M. Razal, C. J. Barrow and J. Q. Liu, Multilayered and hierarchical structured NiCo double hydroxide nanosheets generated on porous $MgCo_2O_4$ nanowire arrays for high performance supercapacitors, *Appl. Surf. Sci.*, 2021, **546**, 149133.

143 Z. Meng, W. Yan, M. Zou, H. Miao, F. Ma, A. B. Patil, R. Yu, X. Yang Liu and N. Lin, Tailoring NiCoAl layered double hydroxide nanosheets for assembly of high-performance asymmetric supercapacitors, *J. Colloid Interface Sci.*, 2021, **583**, 722–733.

144 C. Lai, Y. Guo, H. Zhao, H. Song, X. Qu, M. Huang, S. W. Hong and K. Lee, High-performance double ''ion-buffering reservoirs'' of asymmetric supercapacitors enabled by battery-type hierarchical porous sandwich-like Co_3O_4 and 3D graphene aerogels, *Adv. Compos. Hybrid Mater.*, 2022, **5**, 2557–2574.

145 Y. Li, X. Yan, W. Zhang, W. Zhou, Y. Zhu, M. Zhang, W. Zhu and X. Cheng, Hierarchical micro-nano structure based NiCoAl-LDH nanosheets reinforced by $NiCo_2S_4$ on carbon cloth for asymmetric supercapacitor, *J. Electroanal. Chem.*, 2022, **905**, 115982.

146 T. T. Nguyen, D. Mohapatra, D. R. Kumar, M. Baynosa, S. Sahoo, J. Lee and J.-J. Shim, Direct growth of nickel cobalt layered double hydroxide on nickel foam via redox reaction between nitrate ion and ethanol for hybrid supercapacitors, *Electrochim. Acta*, 2021, **367**, 137226.

147 Y. Xue, X. Liu, L. Han, Z. Xie, L. Liu, Y. Li, Y. Hua, C. Wang, X. Zhao and X. Liu, Fabrication of hierarchical $NiCo_2S_4$ nanotubes@NiMn-LDH nanosheets core–shell hybrid arrays on Ni foam for high-performance asymmetric supercapacitors, *J. Alloys Compd.*, 2022, **900**, 163495.

148 W. Yan, Y. Zhang, T. Zeng, Y. Zhang, Q. Wan and N. Yang, A high-performance asymmetric supercapacitor using composite electrodes of layered double hydroxides and holey reduced graphene oxide, *J. Energy Storage*, 2022, **52**, 104899.

149 X. Wang, Y. Sun, W. Zhang, J. Liu and X. Wu, Hierarchical $Cu_{0.92}Co_{2.08}O_4$@NiCo-layered double hydroxide nanoarchitecture for asymmetric flexible storage device, *Mater. Today Sustain.*, 2022, **17**, 100097.

150 H. Fu, A. Zhang, F. Jin, H. Guo and J. Liu, Ternary NiCeCo-Layered Double Hydroxides Grown on $CuBr_2$@ZIF-67 Nanowire Arrays for High-Performance Supercapacitors, *ACS Appl. Mater. Interfaces*, 2022, **14**, 16165–16177.

151 L. Wang and N. Zhou, Construction of sulfide nanoparticles on hydrangea-like nickel–cobalt hydroxide for enhanced pseudocapacitance, *J. Energy Storage*, 2022, **53**, 105097.

152 G. Liu, G. Wang, X. Guo, X. Hao and Z. Jin, Toilless sulfuration route to enhance the supercapacitor performance of nanoflower-like NiAl-layered double hydroxide, *J. Electroanal. Chem.*, 2022, **916**, 116368.

153 G. Liu, G. Wang, X. Guo, X. Hao, K. Wang and Z. Jin, Toilless selenylation route to enhance the supercapacitor

conductive performance of nanoflower-like NiAl-layered double hydroxide, *J. Energy Storage*, 2022, **52**, 104968.

154 Y. Liu, C. Yu, H. Che, Z. Guo, J. Mu, X. Zhang and A. Liu, Ag nanoparticles-decorated CoAl-layered double hydroxide flower-like hollow microspheres for enhanced energy storage performance, *J. Colloid Interface Sci.*, 2021, **581**, 485–495.

155 S. Islam, M. M. Mia, S. S. Shah, S. Naher, M. N. Shaikh, M. A. Aziz and A. J. S. Ahammad, Recent Advancements in Electrochemical Deposition of Metal-Based Electrode Materials for Electrochemical Supercapacitors, *Chem. Rec.-Age*, 2022, **22**, e202200013.

156 F. C. Yao, W. H. Xie, C. Ma, D. D. Wang, Z. M. El-Bahy, M. H. Helal, H. Liu, A. Du, Z. H. Guo and H. B. Gu, Superb electromagnetic shielding polymer nanocomposites filled with 3-dimensional *p*-phenylenediamine/aniline copolymer nanofibers@copper foam hybrid nanofillers, *Composites, Part B*, 2022, **245**, 110236.

157 J. Liu, Z. Wang, Q. Liu, S. R. Li, D. C. Wang and Z. F. Zheng, Rational design of freestanding and high-performance thick electrode from carbon foam modified with polypyrrole/polydopamine for supercapacitors, *Chem. Eng. J.*, 2022, **447**, 137562.

158 J. El Nady, A. Shokry, M. Khalil, S. Ebrahim, A. M. Elshaer and M. Anas, One-step electrodeposition of a polypyrrole/NiO nanocomposite as a supercapacitor electrode, *Sci. Rep.*, 2022, **12**, 3611.

159 A. L. Chen, C. Y. Wang, O. A. A. Ali, S. F. Mahmoud, Y. T. Shi, Y. X. Ji, H. Algadi, S. M. El-Bahy, M. A. Huang, Z. H. Guo, D. P. Cui and H. G. Wei, MXene@nitrogen-doped carbon films for supercapacitor and piezoresistive sensing applications, *Composites, Part A*, 2022, **163**, 107174.

160 S. Normohammadi, F. Bahmani, L. Fotouhi and M. Khoshfetrat, Electrodeposited nickel nanocone/$NiMoO_4$ nanocomposite designed as superior electrode materials for high performance supercapacitor, *Int. J. Hydrogen Energy*, 2022, **47**, 5220–5229.

161 M. Y. Lian, J. X. Sun, D. W. Jiang, M. J. Xu, Z. J. Wu, B. B. Xu, H. Algadi, M. N. Huang and Z. H. Guo, Waterwheel-inspired high-performance hybrid electromagnetic-triboelectric nanogenerators based on fluid pipeline energy harvesting for power supply systems and data monitoring, *Nanotechnology*, 2023, **34**, 025401.

162 S. L. Gao, X. H. Zhao, Q. Fu, T. C. Zhang, J. Zhu, F. H. Hou, J. Ni, C. J. Zhu, T. T. Li, Y. L. Wang, V. Murugadoss, G. A. M. Mersal, M. M. Ibrahim, Z. M. El-Bahy, M. N. Huang and Z. H. Guo, Highly transmitted silver nanowires-SWCNTs conductive flexible film by nested density structure and aluminum-doped zinc oxide capping layer for flexible amorphous silicon solar cells, *J. Mater. Sci. Technol.*, 2022, **126**, 152–160.

163 E. Samuel, A. Aldalbahi, M. El-Newehy, H. El-Hamshary and S. S. Yoon, Flexible and freestanding manganese/iron oxide carbon nanofibers for supercapacitor electrodes, *Ceram. Int.*, 2022, **48**, 18374–18383.

164 X. Huang, R. Sun, Y. Li, J. Jiang, W. X. Mingjing Li, Y. Wang, J. T. Haishan Cong and S. Han, Two-step electrodeposition synthesis of heterogeneous NiCo-layered double hydroxides@MoO_3 nanocomposites on nickel foam with high performance for hybrid supercapacitors, *Electrochim. Acta*, 2022, **403**, 139680.

165 H. B. Zhang, Y. Lv, X. Y. Wu, J. X. Guo and D. Z. Jia, Electrodeposition synthesis of high performance MoO_{3-x}@Ni-Co layered double hydroxide hierarchical nanorod arrays for flexible solid-state supercapacitors, *Chem. Eng. J.*, 2022, **431**, 133233.

166 K. M. Amin, K. Krois, F. Muench, B. J. M. Etzold and W. Ensinger, Hierarchical pipe cactus-like Ni/NiCo-LDH core–shell nanotube networks as a self-supported battery-type electrode for supercapacitors with high volumetric energy density, *J. Mater. Chem. A*, 2022, **10**, 12473–12488.

167 N. Zhao, Y. Feng, H. Zhao, H. Fan, S. Tian and B. Hu, Simple electrodeposition of 3D NiCoFe-layered double hydroxide nanosheet assembled nanospheres/nanoflowers on carbon cloth for high performance hybrid supercapacitors, *J. Alloys Compd.*, 2022, **901**, 163566.

168 L. Wang and X. Chen, NiCo layered double hydroxide on three-dimensional modified graphite paper for high-performance supercapacitors, *J. Alloys Compd.*, 2022, **907**, 164411.

169 T. Wang, K. Liu, Z. Gao, Z. Zeng, R. Mao, G. Zhu, J. Ni, X. Xu, R. Jia and S. Han, Oxygen vacancy-rich flower-like nickel cobalt layered double hydroxides for supercapacitors with ultrahigh capacity, *Ceram. Int.*, 2022, **48**, 19798–19805.

170 Y. Wang, Z. Wang, X. Zheng, X. Teng, L. Xu, Y. Yuan, X. Liu, A. Fu, Y. Li and H. Li, Core-sheath heterostructure of $MnCo_2O_4$ nanowires wrapped by NiCo-layered double hydroxide as cathode material for high-performance quasi-solid-state asymmetric supercapacitors, *J. Alloys Compd.*, 2022, **904**, 164047.

171 L. Wan, L. Chen, M. Xie, J. Chen, Y. Zhang and C. Du, Hierarchical $FeCoSe_2$@NiCo-layered double hydroxide nanosheet arrays with boosted performance for hybrid supercapacitors, *J. Alloys Compd.*, 2022, **901**, 163567.

172 S. Ban, J. Xie, Y. J. Wang, B. Jing, B. Liu and H. J. Zhou, Insight into the Nanoscale Mechanism of Rapid H_2O Transport within a Graphene Oxide Membrane: Impact of Oxygen Functional Group Clustering, *ACS Appl. Mater. Interfaces*, 2016, **8**, 321–332.

173 Y. L. Zhang, K. P. Ruan and J. W. Gu, Flexible Sandwich-Structured Electromagnetic Interference Shielding Nanocomposite Films with Excellent Thermal Conductivities, *Small*, 2021, **17**, 2101951.

174 B. Kirubasankar, M. Narayanasamy, J. Yang, M. Y. Han, W. H. Zhu, Y. J. Su, S. Angaiah and C. Yan, Construction of heterogeneous 2D layered MoS_2/MXene nanohybrid anode material via interstratification process and its synergetic effect for asymmetric supercapacitors, *Appl. Surf. Sci.*, 2020, **534**, 147644.

175 F. Q. Qi, L. Wang, Y. L. Zhang, Z. L. Ma, H. Qiu and J. W. Gu, Robust $Ti_3C_2T_x$ MXene/starch derived carbon foam composites for superior EMI shielding and thermal insulation, *Mater. Today Phys.*, 2021, **21**, 100512.

176 C. B. Liang, H. Qiu, P. Song, X. T. Shi, J. Kong and J. W. Gu, Ultra-light MXene aerogel/wood-derived porous carbon composites with wall-like ''mortar/brick'' structures for electromagnetic interference shielding, *Sci. Bull.*, 2020, **65**, 616–622.

177 L. Wang, L. X. Chen, P. Song, C. B. Liang, Y. J. Lu, H. Qiu, Y. L. Zhang, J. Kong and J. W. Gu, Fabrication on the annealed $Ti_3C_2T_x$ MXene/Epoxy nanocomposites for electromagnetic interference shielding application, *Composites, Part B*, 2019, **171**, 111–118.

178 B. Dai, Y. Ma, F. Dong, J. Yu, M. Ma, H. K. Thabet, S. M. El-Bahy, M. M. Ibrahim, M. Huang, I. Seok, G. Roymahapatra, N. Naik, B. B. Xu, J. Ding and T. Li, Overview of MXene and conducting polymer matrix composites for electromagnetic wave absorption, *Adv. Compos. Hybrid Mater.*, 2022, **5**, 704–754.

179 W. Luo, Y. Ma, T. Li, H. K. Thabet, C. Hou, M. M. Ibrahim, S. M. El-Bahy, B. B. Xu and Z. Guo, Overview of MXene/conducting polymer composites for supercapacitors, *J. Energy Storage*, 2022, **52**, 105008.

180 Y. L. Zhang, Y. Yan, H. Qiu, Z. L. Ma, K. P. Ruan and J. W. Gu, A mini-review of MXene porous films: preparation, mechanism and application, *J. Mater. Sci. Technol.*, 2022, **103**, 42–49.

181 P. Song, B. Liu, C. B. Liang, K. P. Ruan, H. Qiu, Z. L. Ma, Y. Q. Guo and J. W. Gu, Lightweight, Flexible Cellulose-Derived Carbon Aerogel@Reduced Graphene Oxide/PDMS Composites with Outstanding EMI Shielding Performances and Excellent Thermal Conductivities, *Nano-Micro Lett.*, 2021, **13**, 91.

182 C. B. Liang, H. Qiu, Y. Y. Han, H. B. Gu, P. Song, L. Wang, J. Kong, D. P. Cao and J. W. Gu, Superior electromagnetic interference shielding 3D graphene nanoplatelets/reduced graphene oxide foam/epoxy nanocomposites with high thermal conductivity, *J. Mater. Chem. C*, 2019, **7**, 2725–2733.

183 Z. Zhao, X. Wu, C. Luo, Y. Wang and W. Chen, Rational design of $Ti_3C_2Cl_2$ MXenes nanodots-interspersed MXene@NiAl-layered double hydroxides for enhanced pseudocapacitor storage, *J. Colloid Interface Sci.*, 2022, **609**, 393–402.

184 X. Wu, B. Huang, Q. Wang and Y. Wang, High energy density of two-dimensional MXene/NiCo-LDHs interstratification assembly electrode: understanding the role of interlayer ions and hydration, *Chem. Eng. J.*, 2020, **380**, 122456.

185 N. S. Padalkar, S. V. Sadavar, R. B. Shinde, A. S. Patil, U. M. Patil, D. S. Dhawale, R. N. Bulakhe, H. Kim, H. Im, A. Vinu, C. D. Lokhande and J. L. Gunjakar, Layer-by-layer nanohybrids of Ni-Cr-LDH intercalated with 0D polyoxotungstate for highly efficient hybrid supercapacitor, *J. Colloid Interface Sci.*, 2022, **616**, 548–559.

186 X. Wang, F. Wu, J. Fan, A. Tian, Y. Cheng and S. Yang, High specific surface area NiTiAl layered double hydroxide derived via alkali etching for high performance supercapacitor electrode, *J. Alloys Compd.*, 2021, **888**, 161502.

187 M. Wang, Y. Feng, Y. Zhang, S. Li, M. Wu, L. Xue, J. Zhao, W. Zhang, M. Ge, Y. Lai and J. Mi, Ion regulation of hollow nickel cobalt layered double hydroxide nanocages derived from ZIF-67 for High-Performance supercapacitors, *Appl. Surf. Sci.*, 2022, **596**, 153582.

188 X. Chu, F. Meng, H. Yang, W. Zhang, T. Qin, Z. Wang, S. Molin, P. Jasinski and W. Zheng, Cu-Doped Layered Double Hydroxide Constructs the Performance-Enhanced Supercapacitor Via Band Gap Reduction and Defect Triggering, *ACS Appl. Energy Mater.*, 2022, **5**, 2192–2201.

189 M. Xu, Y. Huang, R. Chen, Q. Huang, Y. Yang, L. Zhong, J. Ren and X. Wang, Green conversion of Ganoderma lucidum residues to electrode materials for supercapacitors, *Adv. Compos. Hybrid Mater.*, 2021, **4**, 1270–1280.

190 F. Liu, Y. Zhao, H. Hou, Y. Zhao, Z. Wang and Z. Huang, Synthesis of silicon-based nanosheets decorated with Pd/Li particles with enhanced hydrogen storage properties, *Adv. Compos. Hybrid Mater.*, 2021, **4**, 1343–1353.

191 M. Pathak and C. S. Rout, Hierarchical $NiCo_2S_4$ nanostructures anchored on nanocarbons and $Ti_3C_2T_x$ MXene for high-performance flexible solid-state asymmetric supercapacitors, *Adv. Compos. Hybrid Mater.*, 2022, **5**, 1404–1422.

192 Z. Sun, K. Qu, J. Li, S. Yang, B. Yuan, Z. Huang and Z. Guo, Self-template biomass-derived nitrogen and oxygen co-doped porous carbon for symmetrical supercapacitor and dye adsorption, *Adv. Compos. Hybrid Mater.*, 2021, **4**, 1413–1424.

193 Y. H. Zhao, K. X. Liu, H. Hou and L. Q. Chen, Role of interfacial energy anisotropy in dendrite orientation in Al–Zn alloys: a phase field study, *Mater. Des.*, 2022, **216**, 110555.

194 T. Z. Xin, S. Tang, F. Ji, L. Q. Cui, B. B. He, X. Lin, X. L. Tian, H. Hou, Y. H. Zhao and M. Ferry, Phase transformations in an ultralight BCC Mg alloy during anisothermal ageing, *Acta Mater.*, 2022, **239**, 118248.

195 J. C. Cai, V. Murugadoss, J. Y. Jiang, X. Gao, Z. P. Lin, M. A. Huang, J. Guo, S. A. Alsareii, H. Algadi and M. Kathiresan, Waterborne polyurethane and its nanocomposites: a mini-review for anti-corrosion coating, flame retardancy, and biomedical applications, *Adv. Compos. Hybrid Mater.*, 2022, **5**, 641–650.

196 Y. Lian, Y. Zheng, D. Wang, Y. Bai, H. Yan, Z. Wang, J. Zhao and H. Zhang, Ultrafast and stable ion/electron transport of $MnNb_2O_6$ in LIC/SC via interface protection and lattice defects, *J. Colloid Interface Sci.*, 2022, **606**, 77–86.

197 S. L. Huo, W. Ni, X. Song, M. T. Zhang, H. Wang and K. X. Li, Insight from the synergistic effect of dopant and defect interplay in carbons for high-performance capacitive deionization, *Sep. Purif. Technol.*, 2022, **281**, 119807.

198 G. S. S. Mamaril, M. D. G. de Luna, K. Bindumadhavan, D. C. Ong, J. A. I. Pimentel and R. A. Doong, Nitrogen and fluorine co-doped 3-dimensional reduced graphene oxide architectures as high-performance electrode material for capacitive deionization of copper ions, *Sep. Purif. Technol.*, 2021, **272**, 117559.

199 Y. F. Zhang, J. J. Zheng, J. J. Nan, C. J. Gai, Q. Shao, V. Murugadoss, S. Maganti, N. Naik, H. Algadi, M. A. Huang, B. B. Xu and Z. H. Guo, Influence of mass ratio and calcination temperature on physical and

photoelectrochemical properties of ZnFe-layered double oxide/cobalt oxide heterojunction semiconductor for dye degradation applications, *Particuology*, 2023, **74**, 141–155.

200 D. Pan, G. Yang, H. M. Abo-Dief, J. W. Dong, F. M. Su, C. T. Liu, Y. F. Li, B. B. Xu, V. Murugadoss, N. Naik, S. M. El-Bahy, Z. M. El-Bahy, M. A. Huang and Z. H. Guo, Vertically Aligned Silicon Carbide Nanowires/ Boron Nitride Cellulose Aerogel Networks Enhanced Thermal Conductivity and Electromagnetic Absorbing of Epoxy Composites, *Nano-Micro Lett.*, 2022, **14**, 118.

201 Y. Feng, Y. C. Li, X. M. Ye, Z. M. Li, W. S. Wang, T. Liu, I. H. El Azab, G. A. M. Mersal, M. M. Ibrahim, Z. M. El-Bahy, M. N. Huang and Z. H. Guo, Synthesis and characterization of 2,5-furandicarboxylic acid poly(butanediol sebacate-butanediol) terephthalate (PBSeT) segment copolyesters with excellent water vapor barrier and good mechanical properties, *J. Mater. Sci.*, 2022, **57**, 10997–11012.

202 L. Suryanti, S. E. I. Suryani, H. Nasikhudin, J. Utomo, A. Taufiq, R. Suryana, Z. Aspanut and M. Diantoro, The effect of Mn_2O_3 nanoparticles on its specific capacitance of symmetric supercapacitors FC-ZnO-x(Mn_2O_3), *7th International Conference of Advanced Materials Science and Technology (ICAMST)*, 2019, **44**, 3355–3360.

203 E. Taer, A. Putri, R. Farma, Awitdrus, R. Taslim, Apriwandi and D. A. Yusra, The effect of potassium iodide (KI) addition to aqueous-based electrolyte (sulfuric acid/ H_2SO_4) for increase the performance of supercapacitor cells, *7th International Conference of Advanced Materials Science and Technology (ICAMST)*, 2019, **44**, 3241–3244.

204 Y. Zhao, F. Liu, Z. Zhao, P. Bai, Y. Ma, A. Alhadhrami, G. A. M. Mersal, Z. Lin, M. M. Ibrahim and Z. M. El-Bahy, Direct ink printing reduced graphene oxide/KCu_7S_4 electrodes for high-performance supercapacitors, *Adv. Compos. Hybrid Mater.*, 2022, **5**, 1516–1526.

205 Y. Zhao, F. Liu, K. Zhu, S. Maganti, Z. Zhao and P. Bai, Three-dimensional printing of the copper sulfate hybrid composites for supercapacitor electrodes with ultra-high areal and volumetric capacitances, *Adv. Compos. Hybrid Mater.*, 2022, **5**, 1537–1547.

206 R. Xue, H. Guo, W. Yang, S.-L. Huang and G.-Y. Yang, Cooperation between covalent organic frameworks (COFs) and metal organic frameworks (MOFs): application of COFs-MOFs hybrids, *Adv. Compos. Hybrid Mater.*, 2022, **5**, 1595–1611.

207 M. Lian, Y. Huang, Y. Liu, D. Jiang, Z. Wu, B. Li, Q. Xu, V. Murugadoss, Q. Jiang, M. Huang and Z. Guo, An overview of regenerable wood-based composites: preparation and applications for flame retardancy, enhanced mechanical properties, biomimicry, and transparency energy saving, *Adv. Compos. Hybrid Mater.*, 2022, **5**, 1612–1657.

208 R. Wang, W. Lei, L. Wang, Z. Li, J. Chen and Z. Hu, N-Doped Carbon Nanofibrous Film with Unique Wettability, Enhanced Supercapacitive Property, and Facile Capacity to Demulsify Surfactant Free Oil-in-water Emulsions, *Chem. Res. Chin. Univ.*, 2021, **37**, 436–442.

209 J. Wang, H. Tang, H. Ren, R. Yu, J. Qi, D. Mao, H. Zhao and D. Wang, pH-Regulated Synthesis of Multi-Shelled Manganese Oxide Hollow Microspheres as Supercapacitor Electrodes Using Carbonaceous Microspheres as Templates, *Adv. Sci.*, 2014, **1**, 1400011.

210 Q. Ma, X. Han, J. Cui, Y. Zhang and W. He, Ni embedded carbon nanofibers/Ni–Al LDHs with multicomponent synergy for hybrid supercapacitor electrodes, *Colloids Surf., A*, 2022, **649**, 129270.

211 H. Lv, H. Rao, Z. Liu, Z. Zhou, Y. Zhao, H. Wei and Z. Chen, NiAl layered double hydroxides with enhanced interlayer spacing via ion-exchange as ultra-high performance supercapacitors electrode materials, *J. Energy Storage*, 2022, **52**, 104940.

212 H. Deng, T. Liu, W. Liao and D. Yang, Double metal ions synergistic effect in the Ni-doped Co(OH)(BA) nanobelts for enhanced supercapacitor performance, *J. Phys. Chem. Solids*, 2022, **164**, 110641.

213 O. Saber, S. A. Ansari, A. Osama and M. Osama, One-Dimensional Nanoscale Si/Co Based on Layered Double Hydroxides towards Electrochemical Supercapacitor Electrodes, *Nanomaterials*, 2022, **12**, 1404.

214 A. Mahmood, B. Zhao, M. S. Javed, D. He, W. C. Cheong, D. Han and L. Niu, Unprecedented Dual Role of Polyaniline for Enhanced Pseudocapacitance of Cobalt-Iron Layered Double Hydroxide, *Macromol. Rapid. Commun.*, 2022, **43**, e2100905.

215 X. Y. Deng, H. Y. Qin, X. Y. Liu, S. Zhu, J. J. Li, L. Y. Ma and N. Q. Zhao, Hierarchically porous trimetallic hydroxide arrays for aqueous energy storage and oxygen evolution with enhanced redox kinetics, *J. Alloys Compd.*, 2022, **918**, 165650.

216 X.-A. Liu, J. Wang, D. Tang, Z. Tong, H. Ji and H.-Y. Qu, A forest geotexture-inspired ZnO@Ni/Co layered double hydroxide-based device with superior electrochromic and energy storage performance, *J. Mater. Chem. A*, 2022, **10**, 12643–12655.

217 G. Zhou, X. Gao, S. Wen, X. Wu, L. Zhang, T. Wang, P. Zhao, J. Yin and W. Zhu, Magnesium-regulated oxygen vacancies of cobalt-nickel layered double hydroxide nanosheets for ultrahigh performance asymmetric supercapacitors, *J. Colloid Interface Sci.*, 2022, **612**, 772–781.

218 X. Wang, Y. Cheng, X. Qiao, D. Zhang, Y. Xia, J. Fan, C. Huang and S. Yang, High-loading and high-performance NiMn layered double hydroxide nanosheets supported on nickel foam for supercapacitor via sodium dodecyl sulfonate intercalation, *J. Energy Storage*, 2022, **52**, 104834.

219 Z. Li, M. Yao, Z. Hu, L. Zhang, S. Gou, H. Feng, Y. Yang and X. Lu, g-C_3N_4 promoted NiFe-LDH self-assemble high performance supercapacitor composites, *J. Alloys Compd.*, 2022, **919**, 165805.

220 H. Wu, X. Zhang, J. Xue, H. Zhang, L. Yang and S. Li, Engineering active sites on hierarchical ZnNi layered double hydroxide architectures with rich Zn vacancies boosting battery-type supercapacitor performances, *Electrochim. Acta*, 2021, **374**, 137932.

221 R. Bi, N. Xu, H. Ren, N. Yang, Y. Sun, A. Cao, R. Yu and D. Wang, A Hollow Multi-Shelled Structure for Charge

Transport and Active Sites in Lithium-Ion Capacitors, *Angew. Chem., Int. Ed. Engl.*, 2020, **59**, 4865–4868.

222 G. Lei, D. Chen, Q. Li, H. Liu, Q. Shi and C. Li, NiCo-layered double hydroxide with cation vacancy defects for high-performance supercapacitors, *Electrochim. Acta*, 2022, **413**, 140143.

223 Y. Caihong, B. Zhang, X. Xie, C. Li, Y. Xu, H. Wang and L. Wang, Three-dimensional independent CoZnAl-LDH nanosheets via asymmetric etching of Zn/Al dual ions for high-performance supercapacitors, *J. Alloys Compd.*, 2021, **861**, 157933.

224 L. Zhong, Z. Yan, H. Wang and L. Wang, Hydrazine Hydrate Induced Three-Dimensional Interconnected Porous Flower-like 3D-NiCo-SDBS-LDH Microspheres for High-Performance Supercapacitor, *Materials*, 2022, **15**, 1405.

225 J. B. Kim, S. H. Koo, I. H. Kim, J. T. Kim, J. G. Kim, B. Jayaraman, J. Lim and S. O. Kim, Characteristic dual-domain composite structure of reduced graphene oxide and its application to higher specific capacitance, *Chem. Eng. J.*, 2022, **446**, 137390.

226 J. J. Ban, X. H. Wen, H. H. Lei, G. Q. Cao, X. H. Liu, C. Y. Niu, G. S. Shao and J. H. Hu, In-plane grain boundary induced defect state in hierarchical NiCo-LDH and effect on battery-type charge storage, *Nano Res.*, 2022, DOI: 10.1007/s12274-022-4485-1.

227 N. Kim, T. H. Gu, D. Shin, X. Jin, H. Shin, M. G. Kim, H. Kim and S. J. Hwang, Lattice Engineering to Simultaneously Control the Defect/Stacking Structures of Layered Double Hydroxide Nanosheets to Optimize Their Energy Functionalities, *ACS Nano*, 2021, **15**, 8306–8318.

228 H. Zhang, Y. Bai, H. Chen, J. Wu, C. M. Li, X. Su and L. Zhang, Oxygen-defect-rich 3D porous cobalt-gallium layered double hydroxide for high-performance supercapacitor application, *J. Colloid Interface Sci.*, 2022, **608**, 1837–1845.

229 W. Gao, Y. Li, J. Zhao, Z. Zhang, W. Tang, J. Wang, Z. Wu and Z. Li, Design and Preparation of Graphene/Fe_2O_3 Nanocomposite as Negative Material for Supercapacitor, *Chem. Res. Chin. Univ.*, 2022, **38**, 1097–1104.

230 S. V. Sadavar, N. S. Padalkar, R. B. Shinde, A. S. Patil, U. M. Patil, V. V. Magdum, Y. M. Chitare, S. P. Kulkarni, S. B. Kale, R. N. Bulakhe, D. S. Bhange, S. T. Kochuveedu and J. L. Gunjakar, Lattice engineering exfoliation-restacking route for 2D layered double hydroxide hybridized with 0D polyoxotungstate anions: cathode for hybrid asymmetric supercapacitors, *Energy Storage Mater.*, 2022, **48**, 101–113.

231 S. D. D. Raut, N. M. M. Shinde, B. G. G. Ghule, S. Kim, J. J. J. Pak, Q. X. Xia and R. S. S. Mane, Room-temperature solution-processed sharp-edged nanoshapes of molybdenum oxide for supercapacitor and electrocatalysis applications, *Chem. Eng. J.*, 2022, **433**, 133627.

232 C. Ding, N. Zhu, X. Wang, A. Alhadhrami, M. H. H. Mahmoud, M. M. Ibrahim, Q. Huang, C. Liu, M. Huang and J. Wang, Experimental study on the burning behaviors of 21700 lithium-ion batteries with high specific energy after different immersion duration, *Adv. Compos. Hybrid Mater.*, 2022, **5**, 2575–2588.

233 J. Z. Feng, X. Q. Zhang, Y. T. Xu, H. Y. Ma, Y. Xue, L. J. Su, J. W. Lang, Y. Tang, S. R. Yang and X. B. Yan, Regulating the electrolyte ion types and exposed crystal facets for pseudocapacitive energy storage of transition metal nitrides, *Energy Storage Mater.*, 2022, **46**, 278–288.

234 A. Helal, S. S. Shah, M. Usman, M. Y. Khan, M. A. Aziz and M. M. Rahman, Potential Applications of Nickel-Based Metal-Organic Frameworks and their Derivatives, *Chem. Rec.-Age*, 2022, **22**, e202200055.

235 D. Luo, Y. Yong, J. Hou, W. Guo, H. Liu, X. Zhao, J. Xiang, N. ZongZong, Y. Han and M. Yan, Construction of Hierarchical $NiCo_2O_4$@NiFe-LDH Core–Shell Heterostructure for High-performance Positive Electrode for Supercapacitor, *Chemnanomat*, 2022, **8**, e202200086.

236 H. Kuang, H. Zhang, X. Liu, Y. Chen, W. Zhang, H. Chen and Q. Ling, Microwave-assisted synthesis of NiCo-LDH/graphene nanoscrolls composite for supercapacitor, *Carbon*, 2022, **190**, 57–67.

237 Q. Ma, S. Wang, X. Han, J. Cui, G. Jia, Y. Zhang and W. He, Construction of three-dimensional (3D) vertical nanosheets electrode with electrochemical capacity applied to micro-supercapattery, *Vacuum*, 2022, **198**, 110914.

238 P. Zhang, X. Deng, W. Li, Z. Ma and X. Wang, Electrochemical-induced surface reconstruction to NiFe-LDHs-based heterostructure as novel positive electrode for supercapacitors with enhanced performance in neutral electrolyte, *Chem. Eng. J.*, 2022, **449**, 137886.

239 L. Luo, Y. L. Zhou, W. Yan, G. B. Du, M. Z. Fan and W. G. Zhao, Construction of advanced zeolitic imidazolate framework derived cobalt sulfide/MXene composites as high-performance electrodes for supercapacitors, *J. Colloid Interface Sci.*, 2022, **615**, 282–292.

240 A. G. El-Deen, M. K. Abdel-Sattar and N. K. Allam, High-performance solid-state supercapacitor based on Ni–Co layered double hydroxide@Co_3O_4 nanocubes and spongy graphene electrodes, *Appl. Surf. Sci.*, 2022, **587**, 152548.

241 L. Liao, K. Zheng, Y. Zhang, X. Li, D. Jiang and J. Liu, Self-templated pseudomorphic transformation of ZIF into layered double hydroxides for improved supercapacitive performance, *J. Colloid Interface Sci.*, 2022, **622**, 309–318.

242 M. Chen, J. Chen, X. Tan, W. Yang, H. Zou and S. Chen, Facile self-assembly of sandwich-like MXene/graphene oxide/nickel-manganese layered double hydroxide nanocomposite for high performance supercapacitor, *J. Energy Storage*, 2021, **44**, 103456.

243 X. Zhu, X. Li, H. Tao and M. Li, Preparation of Co_2Al layered double hydroxide nanosheet/Co_2Mn bimetallic hydroxide nanoneedle nanocomposites on nickel foam for supercapacitors, *J. Alloys Compd.*, 2021, **851**, 156868.

244 Z. Ma, L. Fan, F. Jing, J. Zhao, Z. Liu, Q. Li, J. Li, Y. Fan, H. Dong, X. Qin and G. Shao, MnO_2 Nanowires@NiCo-LDH Nanosheet Core-Shell Heterostructure: A Slow Irreversible Transition of Hydrotalcite Phase for High-Performance Pseudocapacitance Electrode, *ACS Appl. Energy Mater.*, 2021, **4**, 3983–3992.

245 X. Chen, M. He, Y. Zhou, G. He, C. Meng, Q. Cheng and F. Li, Design of hierarchical double-layer NiCo/NiMn-layered double hydroxide nanosheet arrays on Ni foam as electrodes for supercapacitors, *Mater. Today Chem.*, 2021, **21**, 100507.

246 H. Xiong, L. Liu, L. Fang, F. Wu, S. Zhang, H. Luo, C. Tong, B. Hu and M. Zhou, 3D self-supporting heterostructure NiCo-LDH/ZnO/CC electrode for flexible high-performance supercapacitor, *J. Alloys Compd.*, 2021, **857**, 158275.

247 Z. Zhou, J. Tie, H. Yang, G. Cheng, M. Sun and L. Yu, 3D hierarchical $NiCo_2S_4$/Ni-Co LDH architecture for high-performance supercapacitor, *J. Mater. Sci.: Mater. El*, 2021, **32**, 3843–3853.

248 H. Wang, T. Shu, C. X. Lin, F. Sun, Z. Y. Wang, B. Lin, F. X. Wei, K. X. Yao, J. Q. Qi and Y. W. Sui, Hierarchical construction of Co_3S_4 nanosheet coated by 2D multi-layer MoS_2 as an electrode for high performance supercapacitor, *Appl. Surf. Sci.*, 2022, **578**, 151897.

249 Y. Q. Guo, H. Qiu, K. P. Ruan, S. S. Wang, Y. L. Zhang and J. W. Gu, Flexible and insulating silicone rubber composites with sandwich structure for thermal management and electromagnetic interference shielding, *Compos. Sci. Technol.*, 2022, **219**, 109253.

250 Q. S. Zhu, Y. Zhao, B. J. Miao, H. M. Abo-Dief, M. C. Qu, R. A. Pashameah, B. Bin Xu, M. A. Huang, H. Algadi, X. H. Liu and Z. H. Guo, Hydrothermally synthesized ZnO-RGO-PPy for water-borne epoxy nanocomposite coating with anticorrosive reinforcement, *Prog. Org. Coat.*, 2022, **172**, 107153.

251 D. Kumar, A. Joshi, G. Singh and R. K. Sharma, Polyoxometalate/ZIF-67 composite with exposed active sites as aqueous supercapacitor electrode, *Chem. Eng. J.*, 2022, **431**, 134085.

252 K. Li, Z. Hu, R. Zhao, J. Zhou, C. Jing, Q. Sun, J. Rao, K. Yao, B. Dong, X. Liu, H. Li, Y. Zhang and J. Ji, A multidimensional rational design of nickel-iron sulfide and carbon nanotubes on diatomite via synergistic modulation strategy for supercapacitors, *J. Colloid Interface Sci.*, 2021, **603**, 799–809.

253 A. Rajapriya, S. Keerthana, C. Viswanathan and N. Ponpandian, Three dimensional integrated architecture of Sr Fe LDH on hierarchical NiS framework as a flexible electrode for efficient energy storage and conversion applications, *J. Energy Storage*, 2022, **53**, 105091.

254 P. C. Lohani, A. P. Tiwari, K. Chhetri, A. Muthurasu, B. Dahal, S. H. Chae, T. H. Ko, J. Y. Lee, Y. S. Chung and H. Y. Kim, Polypyrrole Nanotunnels with Luminal and Abluminal Layered Double Hydroxide Nanosheets Grown on a Carbon Cloth for Energy Storage Applications, *ACS Appl. Mater. Interfaces*, 2022, **14**, 23285–23296.

255 Z. H. Wang, Z. Q. Liu, L. Wang, K. Zhao, X. L. Sun, D. D. Jia and J. Q. Liu, Construction of Core-Shell Heterostructured Nanoarrays of Cu(OH)(2)@NiFe-Layered Double Hydroxide through Facile Potentiostatic Electrodeposition for Highly Efficient Supercapacitors, *ChemElectroChem*, 2022, **9**, e202101711.

256 W. Cao, C. Xiong, Y. Liu, F. Xu, W. Zhao, Q. Xia, G. Du and N. Chen, Novel fabrication strategy of nanostructured NiCo-LDHs monolithic supercapacitor electrodes via inducing electrochemical in situ growth on etched nickel foams, *J. Alloys Compd.*, 2022, **902**, 163679.

257 A. Emin, X. Song, Y. Du, Y. Chen, M. Yang, S. Zou, Y. Fu, J. Li, Y. Li and D. He, One-step electrodeposited Co and Mn layered double hydroxides on Ni foam for high-performance aqueous asymmetric supercapacitors, *J. Energy Storage*, 2022, **50**, 104667.

258 Y. Lu, J. Guo, Z. He, Z. Gao and Y.-Y. Song, Direct access to NiCo-LDH nanosheets by electrochemical-scanning-mediated hydrolysis for photothermally enhanced energy storage capacity, *Energy Storage Mater.*, 2022, **48**, 487–496.

259 J. Wang, M. Li, Y. Zhai, F. Wang, X. Zhang, H. Lv, T. Yu and W. Zhang, Construction of three-dimensional nanocube-on-sheet arrays electrode derived from Prussian blue analogue with high electrochemical performance, *Appl. Surf. Sci.*, 2021, **556**, 149789.

260 H. Li, S. Lin, H. Li, Z. Wu, Q. Chen, L. Zhu, C. Li, X. Zhu and Y. Sun, Magneto-Electrodeposition of 3D Cross-Linked NiCo-LDH for Flexible High-Performance Supercapacitors, *Small Methods*, 2022, **6**, e2101320.

261 G. Nagaraju, S. Chandra Sekhar, L. Krishna Bharat and J. S. Yu, Wearable Fabrics with Self-Branched Bimetallic Layered Double Hydroxide Coaxial Nanostructures for Hybrid Supercapacitors, *ACS Nano*, 2017, **11**, 10860–10874.

262 Z. Liu, H. Zhou, F. Zeng, L. Hu, X. Wu, X. Song, C. Jiang and X. Zhang, All-Printed High-Performance Flexible Supercapacitors Using Hierarchical Porous Nickel–Cobalt Hydroxide Inks, *ACS Appl. Energy Mater.*, 2022, **5**, 9418–9428.